Theoretical study on second hyperpolarizabilities of nitroxide and related radical species

YAMADA Satoru

Department of Chemistry
Graduate School of Science
Osaka University

1999

Acknowledgments

The present thesis is a summary of the author's study from April 1994 to January 1999 at the Department of Chemistry of the Graduate School of Science of Osaka University.

The author wishes to express his sincere gratitude of Professor Kizashi YAMAGUCHI for his warm encouragement, guidance and discussion throughout the course of the author's study. The author is deeply grateful to Dr. Masayoshi NAKANO for his helpful suggestion and continuous severe discussions.

The author also thanks to Assistant Professor Yasunori YOSHIOKA for his helpful advices. The author is also thankful to Dr. Hidemi NAGAO for his interesting discussion.

The author also makes his acknowledgments to Professor Wasuke MORI in Kanagawa University and Assistant Professor Sadamu TAKEDA in Gunma University for their continuos encouragement.

Dr. Kohji OHTA and Dr. Kenji KAMADA in Osaka National Research Institute gave the author practical counsel on matters of experiment. The author is much obliged to them very cordially.

The author owes a lot to Messrs Isamu SHIGEMOTO, Shinji KIRIBAYASHI and Jun NAKAMURA. This thesis would not be completed without their cooperation.

The author had extensive discussions about the author's study and other many things with Messrs Takashi KAWAKAMI, Takao KOBAYASHI, Goro MARUTA, Daisuke YAMAKI and other members of YAMAGUCHI Laboratory. The author also appreciates for their generous cooperation and lasting friendships.

The numerical calculation were carried out on the super computers at the Institute for Molecular Science and work stations at YAMAGUCHI Laboratory. The author's work was supported by Research Fellowships of the Japan Society for the Promotion of Science for Young Scientist from April 1997 to March 1999.

Finally, the author blesses his parents, Mr. Yozo YAMADA and Mrs. Yasuko YAMADA for understanding of the author's study and their affections.

YAMADA Satoru

February, 1999

Contents

Introduction

The interaction between material and light is one of the most basic and important phenomena in nature. Therefore, a large number of studies on the interaction have been done experimentally and theoretically. Development of laser brings the powerful light source, and has made it possible to investigate nonlinear optical response properties. In theoretical chemistry, examples for the accurate calculation of molecular nonlinear optical response, *i.e.*, hyperpolarizabilities, were limited, though the basic perturbational formulation had been given in 1950's. The reason is that it is indispensable to calculate energies of ground and excited states, transition moments and transition energies with high precision in order to reproduce hyperpolarizabilities. However, a recent rapid progress of computer system makes it possible to begin full-dress of investigation on hyperpolarizabilities for molecules. In recent years, nonlinear optical properties have been studied actively both experimentally and theoretically for several materials. Above all, organic materials have attracted a great deal of attention because of their high-speed response originating in fluctuation of π electrons.

Although examples of investigation on hyperpolarizabilities of organic molecules increase, there are only a few theoretical and experimental investigations of molecular hyperpolarizabilities for organic radical species. One reason is that the most organic radical molecules are unstable and then experimental measurements of hyperpolarizabilities for radical species is difficult. The other reason is that in the calculation for the open-shell systems, response properties of radical species have large electron-correlation dependency in general. However, many stable radical molecules have been synthesized from the recent study on the organic magnetic molecules, *e.g.*, para-phenyl nitronyl nitroxide radical (p-NPNN). Therefore, the number of studies on the hyperpolarizabilities for radical molecules are expected to increase. Besides, higher-order electron-correlation methods can be applied in the theoretical calculation of nonlinear optical properties thanks to the recent progress in computer system. It is expected that response properties, especially for nonlinear optical response properties of radical species, are changed remarkably by slight physical and chemical perturbations. The reason is that radical species have some instability in their electronic states, so that the electronic states are changed easily by the slight perturbations. Such sensitivity of response properties for radical species is presumed to be useful for controlling the properties. Therefore, an importance of the study on nonlinear response properties for stable radical species is considered to increase in the near future.

It is well-known that almost organic compounds provide positive second hyperpolarizability (γ), which is the origin of the macroscopic third-order nonlinear optical response. The sign of γ is also known to be important in quantum optics: the positive value causes the self-focussing

effect of an incident beam, while the negative one causes the self-defocusing effects. We have proposed a classification rule of γ based on the time-dependent perturbation theory. By applying this rule, we have also proposed a structure-correlation rule of systems exhibiting negative γ. Namely, a system whose ground state has a large contribution from a symmetric resonance structure with inversible polarization (SRIP) tends to exhibit negative γ. In comparison with closed-shell systems, open-shell systems are expected to have fair possibilities of providing large contribution of SRIP to the ground states because of the instability in their electronic states.

Because of several reasons mentioned above, the author investigates the second hyperpolarizability of radical species, especially for nitroxide radical species, and elucidate the relationship between open-shell system and appearance of negative γ as one of the peculiarity of nonlinear optical properties for radical species based on our calcification rule of γ. An analysis method is introduced and applied in this study. This method, *i.e.*, hyperpolarizability density analysis, is first developed and implemented in ab initio calculations by the author, and is useful for obtaining pictorial and intuitive understanding of the spatial characteristics of hyperpolarizability.

In chapter 1, several basic matters of nonlinear optics and our calcification rule of γ is explained. In chapter 2, several calculation methods employed for the calculation of hyperpolarizabilities in this study are explained. In chapter 3, the definition of hyperpolarizability density and how to use of hyperpolarizability density are explained. In chapter 4, the second hyperpolarizabilities of a small closed-shell system, formaldehyde, and an open-shell system, nitroxide radical, are calculated in order to examine the difference in nonlinear optical properties between closed- and open-shell systems. In chapter 5, the second hyperpolarizabilities of small iso-electronic radical model systems are investigated in order to elucidate the character of γ for radical species. In this chapter, a possibility of negative γ in radical species is examined. In chapter 6, γ of nitronyl nitroxide radical, which is expected to have large negative γ, is examined. In chapter 7, structure-property correlation in γ for several radical species is investigated. These radical species, studied in this chapter, include a part corresponding to the nitronyl nitroxide radical structure and are also expected to have negative γ. In chapter 8, the second hyperpolarizabilities of p-NPNN are examined. The p-NPNN is a real molecule including nitronyl nitroxide radical structure in their flame. The macroscopic third-order nonlinear optical susceptibilities for the β-phase crystal of p-NPNN are also studied. In chapter 9, the present study is summarized and the future extensions of nonlinear optics for open-shell systems are expressed.

Chapter 1 *Nonlinear optical process and a classification rule of the second hyperpolarizability*

In the off-resonant regions, the time-dependent perturbation theory (TDPT) is used for the calculation of the response property of the system in the presence of external oscillating fields. Bloembergem [1], Orr and Ward [2] derived the perturbative expressions for various nonlinear optical phenomena. The transition energies, dipole moment differences and transition moments are included in the TDPT formulae. The dispersion effects of the polarizability and hyperpolarizabilities can be considered in the off-resonant region when the time-dependent external fields are applied. In quantum chemistry, the approach using these TDPT formulae is referred to as the sum-over-state (SOS) method [3-52]. In general, relatively small number of ab initio MO calculations are performed due to the problem of the convergence of the hyperpolarizability including the sum over the excited states and to the difficulty of the calculations of precise quantities relating to the excited states. In contrast, the TDPT with the semi empirical MO methods that can well reproduce the quantities relating to the excited states is performed to analyze the virtual excitation processes qualitatively. On the basis of the energy-time uncertainty relation, the linear and nonlinear polarizations are regarded as the virtual excitation processes starting from the ground state to the ground state through plural excited states. The virtual excitation processes are characterized by these transition quantities. Since the transition properties reflect the electronic structures of molecular systems, explicit criteria designing the nonlinear optical systems can be constructed based on the perturbative formulae. Actually many guidelines for molecular design of the nonlinear optical materials have been proposed [53-55].

In section 1.1, the relation between macroscopic linear and nonlinear optical susceptibilities ($\chi^{(n)}$) and microscopic polarizability (α) and hyperpolarizabilities (β, γ, etc.) is outlined. In section1.2, the TDPT formulae for α, β and γ are explained. In sections 1.3-1.5, the analytical formula for γ is partitioned to three types of virtual excitation processes. In section 1.6, a classification rule of systems with large γ is proposed based on the analysis of the virtual excitation processes.

1.1. Nonlinear optical process and hyperpolarizability

When an optical electric field $\boldsymbol{F}_0(\boldsymbol{r},t)$ is applied to the materials, *e.g.*, molecular crystals, the microscopic polarization $\boldsymbol{p}$ of a molecule constructing the materials is induced. The microscopic polarization induces the macroscopic polarization $\boldsymbol{P}$ whole over the crystal. As a result, new electric field $\boldsymbol{F}_n(\boldsymbol{r},t)$ is generated. This process is shown in Fig. 1.1. When the angular frequency of $\boldsymbol{F}_0(\boldsymbol{r},t)$ does not equal that of $\boldsymbol{F}_n(\boldsymbol{r},t)$, the process is referred to as the nonlinear optical process. In this case, various nonlinear optical effects such as the second harmonic generation (SHG) and the THG are observed. [34,53-59]

The macroscopic polarization $\boldsymbol{P}$ can be expanded by an electric field $\boldsymbol{F}$:

$$P^I(\omega) = \sum_J \chi^{(1)}_{IJ} F^J(\omega_1) + \sum_{JK} \chi^{(2)}_{IJK} F^J(\omega_1) F^K(\omega_2) + \sum_{JKL} \chi^{(3)}_{IJKL} F^J(\omega_1) F^K(\omega_2) F^L(\omega_3) + \cdots \tag{1.1.1}$$

The I, J, K and L denote the components in the laboratory coordinate system. Here F^I is the I component of the polarization and ω is the angular frequency of the polarization field. $\chi^{(1)}_{IJ}$ is the component of the linear susceptibility tensor of rank 2. $\chi^{(2)}_{IJK}$ and $\chi^{(3)}_{IJKL}$ are the components of the nonlinear susceptibility tensors of rank 3 and 4, respectively. $F^I(\omega_n)$ is the I component of the external field oscillating at angular frequency ω_n.

The microscopic polarization $\boldsymbol{p}$ can be similarly expanded as:

$$\begin{aligned} p^i(\omega) &= \mu^i_{tot} - \mu^i_0 \\ &= \sum_j \alpha_{ij} F'^j(\omega_1) + \sum_{jk} \beta_{ijk} F'^j(\omega_1) F'^k(\omega_2) + \sum_{jkl} \gamma_{ijkl} F'^j(\omega_1) F'^k(\omega_2) F'^l(\omega_3) + \cdots \end{aligned} \tag{1.1.2}$$

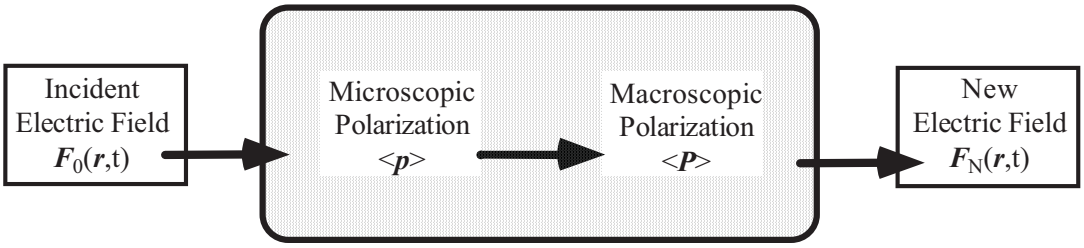

Frequency of $\boldsymbol{F}_0(\boldsymbol{r},t)$ ≠ Frequency of $\boldsymbol{F}_N(\boldsymbol{r},t)$

Frequency Mixing
Harmonic Generation

Fig.1.1 Nonlinear optical process

Here, $\boldsymbol{F'}$ represents the local electric field. The i, j, k and l represent the components in the molecular-fixed coordinate system. Here, μ^i_{tot} is the molecule-fixed i component of the total electric dipole moment and μ^i_0 is the i component of the permanent dipole moment (μ^i_0). In the case of the medium intense electric field $\boldsymbol{F'}$, the right-hand side of Eq.(1.1.2) can be approximated by the first-order term with respect to $\boldsymbol{F'}$. However, when the presence of the electric field is large enough to observe the higher-order terms, the higher-order terms give rise to various nonlinear optical properties. β_{ijk} and γ_{ijkl} are the tensor components of the first- and the second hyperpolarizabilities, respectively. The magnitude and sign of the hyperpolarizability characterize the nonlinearly of the system under the strong electric fields.

When the coordinate system is reversed, the electric field $\boldsymbol{F}$ comes to be $-\boldsymbol{F}$ in Eq.(1.1.1). However, the even-order terms of the right-hand side of Eq.(1.1.1) are unchangeable. Therefore, the even-order susceptibilities vanish in the centrosymmetric system, while the odd-order susceptibilities usually exist in arbitrary system. This relation also holds in the microscopic polarization. Therefore, in order to exhibit the even-order nonlinear optical effects, both the crystal and its elementary molecules must possess noncentrosymmetric structures.

For most molecular crystals, their nonlinear optical susceptibilities can be expressed as a function of the number density of molecular units (N), local-field factor (L_n), the angle between the molecule-fixed and the laboratory coordinate axes (θ) and the nth-order molecular polarizability ($\alpha^{(\mathrm{n})}$) :

$$\chi^{(n)} = f(N, \mathrm{L}_n, \theta, \alpha^{(n)}) \quad . \tag{1.1.3}$$

For randomly oriented systems such as the gas or liquid phase, $\chi^{(\mathrm{n})}$ can be expressed as

$$\chi^{(n)} = N\mathrm{L}_n \left\langle \alpha^{(n)} \right\rangle \ , \tag{1.1.4}$$

where L_n is a local-field factor determined by the refractive indices of the system. $<\alpha^{(\mathrm{n})}>$ is the orientationally averaged molecular polarizability. For example, the third-order nonlinear susceptibility can be given by

$$\chi^{(3)}_{IJKL} = Ng(\omega)g(\omega_1)g(\omega_2)g(\omega_3)\langle\gamma\rangle_{IJKL} \quad . \tag{1.1.5}$$

Here, $g(\omega)$ is the local-field factors for each of the electric fields. Due to the symmetry of the electric fields along the molecular coordinate axes, γ_{S} for THG can be simplified as [1,60]

$$\gamma_{\mathrm{S}}(-3\omega;\omega,\omega,\omega) = \frac{1}{5}(\gamma_{xxxx} + \gamma_{yyyy} + \gamma_{zzzz} + \gamma_{xxyy} + \gamma_{yyxx} + \gamma_{xxzz} + \gamma_{zzxx} + \gamma_{yyzz} + \gamma_{zzyy}) \ , \tag{1.1.6}$$

in which γ_{ijkl} is the component of γ. Further simplification of Eq.(1.1.6) can be performed for

the static expression of γ_S by Kleinman's symmetry rule. The resultant expression for γ_S is given by

$$\gamma_S = \frac{1}{5}(\gamma_{xxxx} + \gamma_{yyyy} + \gamma_{zzzz} + 2\gamma_{xxyy} + 2\gamma_{yyzz} + 2\gamma_{xxzz}) \ . \tag{1.1.7}$$

In DC-SHG (= EFISH: electronic field induced second harmonic) method, the third-order susceptibility $\chi^{(3)}$ can be expressed as

$$\chi^{(3)}(-2\omega;\omega,\omega,0) = Ng(2\omega)[g(\omega)]^2 g(0)\left(\gamma_S + \frac{\boldsymbol{\mu}_0 \cdot \boldsymbol{\beta}_V}{5kT}\right) \tag{1.1.8}$$

where k is Boltzmann's constant and T is the absolute temperature. $\boldsymbol{\beta}_V$ is the vector given by

$$\boldsymbol{\beta}_V = \begin{pmatrix} \beta_x \\ \beta_y \\ \beta_z \end{pmatrix} = \begin{pmatrix} \beta_{xxx} + \frac{1}{3}(\beta_{xyy} + \beta_{xzz} + \beta_{yyx} + \beta_{zzx}) \\ \beta_{yyy} + \frac{1}{3}(\beta_{yzz} + \beta_{yxx} + \beta_{zzy} + \beta_{xxy}) \\ \beta_{zzz} + \frac{1}{3}(\beta_{zxx} + \beta_{zyy} + \beta_{xxz} + \beta_{yyz}) \end{pmatrix} \tag{1.1.9}$$

For the centrosymmetric systems, γ_S can be obtained from $\chi^{(3)}$ by Eq.(1.1.8) since μ_0 vanishes for the centrosymmetric systems. If γ_S is much smaller than $\mu_0 \cdot \beta_0/5kT$, the projected β_0 on to the direction of μ_0 can be obtained by Eq.(1.1.8). If γ_S is approximately as large as $\mu_0 \cdot \beta_0/5kT$, both β_0 and γ_S can be obtained using Eq.(1.1.8) by the EFISH method with varying the temperature.

1.2. Formulation by time-dependent perturbation theory

The perturbative expressions (without damping) of α, β and γ are given by [34]

$$\alpha_{ij}(-\omega;\omega) = 2\sum_n \mu^i_{0n}\mu^j_{n0}\frac{E_{n0}}{(E^2_{n0} - (\hbar\omega)^2)} \ , \tag{1.2.1}$$

$$\beta_{ijk}\left(-(\omega_1+\omega_2);\omega_1,\omega_2\right)=\frac{1}{4}\sum_{n}\sum_{n'}$$
$$\left[\mu^{j}_{0n},\mu^{i}_{n'n}\cdot\mu^{k}_{n0}\left(\frac{1}{(E_{n'0}+\hbar\omega_1)(E_{n0}-\hbar\omega_2)}\right.\right.$$
$$\left.+\frac{1}{(E_{n'0}+\hbar\omega_1)(E_{n0}-\hbar\omega_2)}\right)$$
$$+\mu^{j}_{0n},\mu^{i}_{n'n}\cdot\mu^{k}_{n0}\left(\frac{1}{(E_{n'0}+\hbar\omega_1)(E_{n0}+\hbar(\omega_1+\omega_2))}\right.$$
$$\left.+\frac{1}{(E_{n'0}-\hbar\omega_1)(E_{n0}-\hbar(\omega_1+\omega_2))}\right)$$
$$+\mu^{j}_{0n},\mu^{i}_{n'n}\cdot\mu^{k}_{n0}\left(\frac{1}{(E_{n'0}+\hbar\omega_2)(E_{n0}+\hbar(\omega_1+\omega_2))}\right.$$
$$\left.\left.+\frac{1}{(E_{n'0}-\hbar\omega_2)(E_{n0}-\hbar(\omega_1+\omega_2))}\right)\right] \quad , \qquad (1.1.3)$$

and

$$\gamma_{ijkl}\left(-(\omega_1+\omega_2+\omega_3);\omega_1,\omega_2,\omega_3\right)=$$
$$\frac{1}{6}\sum_{perm}\left[\sum_{m,n,n'(\neq 0)}\frac{\mu^{i}_{0m}\mu^{j}_{mn}\mu^{k}_{nn'}\mu^{l}_{n'0}}{(E_{m0}-\hbar(\omega_1+\omega_2+\omega_2))(E_{n0}-\hbar\omega_2-\hbar\omega_3)(E_{n'0}-\hbar\omega_3)}\right. \qquad (1.2.3)$$
$$\left.-\sum_{m,n(\neq 0)}\frac{\mu^{i}_{0m}\mu^{j}_{mn}\mu^{k}_{nn'}\mu^{l}_{n'0}}{(E_{m0}-\hbar(\omega_1+\omega_2+\omega_2))(E_{n0}-\hbar\omega_3)(E_{n'0}+\hbar\omega_3)}\right]$$

where μ^{i}_{0n} is the ith component of transition moment between the ground and the nth excited states, μ^{i}_{nm} is the ith component of transition moment between the mth and the nth excited states, μ^{i}_{nn} is the ith component of the difference in dipole moments between the ground and the nth excited states and E_{n0} is the transition energy given by (E_n - E_0). The $\sum_{perm}$ represents the sum of all permutation terms concerning $\omega_1+\omega_2+\omega_3$, ω_1, ω_2 and ω_3 in connection with i, j, k and l.

1.3. Partitioning to virtual excitation processes

As seen from the above formulae, the physical picture, *i.e.*, virtual excitation process, of α is clear, while those of β and γ are difficult to be elucidated. For the β, some reformulation and approximation of the formula have been proposed. For EFISH method, which is usually used

for measuring $\beta_{ijk}(-2\omega;\omega,\omega)$, Eq.(1.2.2) is rewritten as [3,4,16,17,26-28,30,52]

$$\begin{aligned}\beta_{ijk}(-2\omega;\omega,\omega)=\frac{1}{4}\sum_{n}\sum_{n'}&\left[\mu^{j}_{0n'}\mu^{i}_{n'n}\mu^{k}_{n0}\left(\frac{1}{(E_{n'0}+\hbar\omega)(E_{n0}-\hbar\omega)}\right.\right.\\&\left.+\frac{1}{(E_{n'0}-\hbar\omega)(E_{n0}+\hbar\omega)}\right)\\&+\left(\mu^{j}_{0n'}\mu^{k}_{n'n}\mu^{i}_{n0}+\mu^{k}_{0n'}\mu^{j}_{n'n}\mu^{i}_{n0}\right)\\&\times\left(\frac{1}{(E_{n'0}+\hbar\omega)(E_{n0}+2\hbar\omega)}\right.\\&\left.\left.+\frac{1}{(E_{n'0}-\hbar\omega)(E_{n0}+2\hbar\omega)}\right)\right]\end{aligned}\qquad(1.3.1)$$

The virtual excitation process represented by the subscript of transition matrices in Eq.(1.3.1) can be illustrated in Fig.1.2. There are two types of processes, *i.e.*, type (I) involving a kind of excited state and type (II) involving two kinds of excited states. For most strong intramolecular charge-transfer (CT) systems, the transitions from the ground to CT excited states are found to be most contribute to β_{ijk} [61]. Therefore, total β_{ijk} can be well approximated by the contributions of type (I), which represents the interactions between the ground and the CT excited states. This is referred to as the diagonal approximation [62]. Under the diagonal approximation, the expression of β_{ijk} is given as

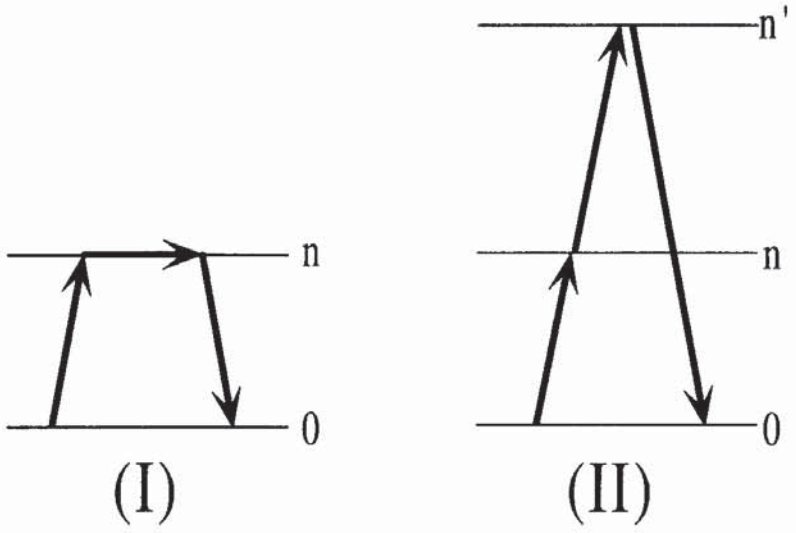

Fig.1.2 Virtual excitation process of β.

$$\beta_{ijk}(-2\omega;\omega,\omega)=$$

$$\frac{1}{2}\sum_{n}\left[\mu^{j}_{0n}\mu^{i}_{nn}\mu^{k}_{n0}\frac{1}{(E^{2}_{n0}-(\hbar\omega)^{2})}\right.$$

$$\left.+\mu^{i}_{0n}(\mu^{k}_{nn}\mu^{j}_{n0}+\mu^{j}_{nn}\mu^{k}_{n0})\frac{E^{2}_{n0}+2(\hbar\omega)^{2}}{(E^{2}_{n0}-(\hbar\omega)^{2})(E^{2}_{n0}-(2\hbar\omega)^{2})}\right] \tag{1.3.2}$$

This expression corresponds to the type (I) shown in Fig. 1.2. The ith component of β_{ijk} is expressed as

$$\beta_{iii}(-2\omega;\omega,\omega)=\frac{3}{2}\sum_{n}\mu^{i}_{0n}\mu^{i}_{nn}\frac{E^{2}_{n0}}{(E^{2}_{n0}-(\hbar\omega)^{2})(E^{2}_{n0}-(2\hbar\omega)^{2})}, \tag{1.3.3}$$

where the index n runs over excited states. When one excited state n and the ground state 0 mainly contribute to total β, the two states approximation [30] can be applied. In this case, Eq.(1.3.3) is approximated as

$$\beta_{iii}(-2\omega;\omega,\omega)=\frac{3}{2}\mu^{i}_{0n}\mu^{i}_{nn}\frac{E^{2}_{n0}}{(E^{2}_{n0}-(\hbar\omega)^{2})(E^{2}_{n0}-(2\hbar\omega)^{2})}, \tag{1.3.4}$$

In the case of the static electric field, Eq.(1.3.4) is represented as follows.

$$\beta_{iii}(0)=\frac{3}{2}\frac{(\mu^{i}_{0n})^{2}\mu^{i}_{nn}}{E^{2}_{n0}}. \tag{1.3.5}$$

It is predicted from this expression that asymmetric systems with strong CT excitation exhibit large β values.

In contrast to the case of β, the formula of γ had not been analyzed readily until Nakano et al. attempted a general analysis of γ [53,63]. To date, several similar analyses have been proposed [57-59]. In this section, the static case is considered for convenience. Based on the exact perturbative expression (Eq. (1.2.3)), the formula of static γ_{iiii} can be partitioned into three types of virtual excitation processes [53,55,64]:

$$\gamma_{iiii}(0)=\sum_{n}\frac{(\mu^{i}_{n0})^{2}(\mu^{i}_{nn})^{2}}{E^{3}_{n0}}-\sum_{n,m}\frac{(\mu^{i}_{n0})^{2}(\mu^{i}_{m0})^{2}}{E_{n0}E^{2}_{m0}}$$

$$+\left(\sum_{n'\neq m}\frac{\mu^{i}_{0n}\mu^{i}_{nn}\mu^{i}_{nm}\mu^{i}_{m0}}{E^{2}_{n0}E_{m0}}+\sum_{n'\neq m\neq n}\frac{\mu^{i}_{0n}\mu^{i}_{nm}\mu^{i}_{mn'}\mu^{i}_{n'0}}{E_{n0}E_{m0}E_{n'0}}\right) \tag{1.3.6}$$

component of difference of dipole moments between states n and 0 (the ground state), and E_{n0} is a transition energy between states n and 0. Similarly to the case of analysis of β, a virtual excitation process in the fourth-order optical process is represented as an expression (0-i-j-k-0). The first, the second and the third terms on the right-hand side of Eq. (1.3.6) correspond to type (I) (0-n-n-n-0), type (II) (0-n-0-m-0) and type (III) contributions, respectively. The type (III) terms can be partitioned into two types of contributions specified by type (III-1) (0-n-n-m-0) and type (III-2) (0-n-m-n'-0). These types are shown schematically in Fig. 1.3. The type (I) (0-n-n-n-0) process, which involves two dipole moment differences between the excited (n) and the ground (0) states (μ_{nn}) on a virtual excitation path, exists only in the case of molecules with noncentrosymmetric charge distributions. The type (II) (0-n-0-m-0) process involves the ground state (0) in the middle of a virtual excitation path. This is negative in sign in the off-resonant region as shown from Eq. (1.3.6). The type (III-1) process (0-n-n-m-0), which involves only one dipole moment difference between the excited (n) and the ground (0) states (μ_{nn}) on a virtual excitation path, exists only in the case of molecules with noncentrosymmetric charge distributions. In contrast, the type (III-2) process (0-n-m-n'-0) (involving the case n=n'), which has no dipole moment difference on a virtual excitation path, can contribute to the γ_{iiii} of arbitrary molecules. The type (III) contributions have the possibility of taking positive or negative value. Thus, the magnitude and sign of total γ are shown to be closely related to each type of virtual excitation process.

1.4. N-state three-type approximation for second hyperpolarizabilities

In order to indicate relations more clearly between virtual excitation paths and γ ($\equiv \gamma_{iiii}$), the Eq. (1.2.3) is approximated by restricting the types (II) and (III) to (II)' (0-n-0-n-0) and (III)' (0-n-m-n-0), respectively. This approximation (three-type approximation) is found to describe the γ for molecular conjugated systems. Under the approximation, the total γ (THG) is expressed by [53]

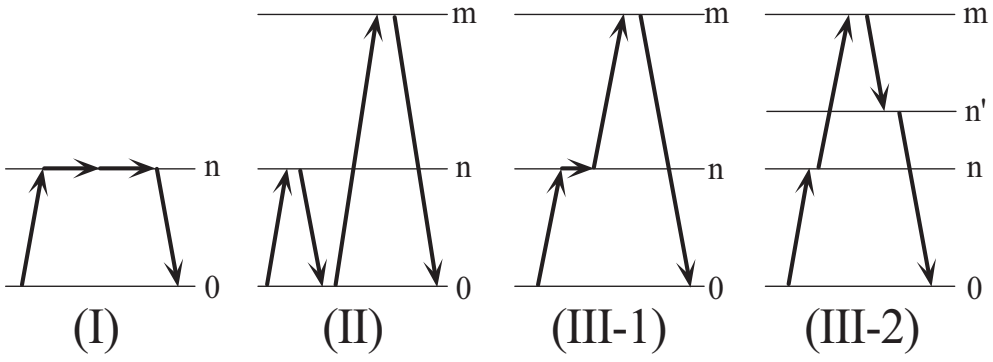

Fig.1.3 Virtual excitation process of γ.

$$\gamma(-3\omega;\omega,\omega,\omega) = \sum_{n=1}(\mu_{n0})^2(\mu_{nn})^2 \frac{E_{n0}(E_{n0}^2+(\hbar\omega)^2)}{(E_{n0}^2-(3\hbar\omega)^2)(E_{n0}^2-(2\hbar\omega)^2)(E_{n0}^2-(\hbar\omega)^2)}$$
$$-\sum_{n=1}(\mu_{n0})^4 \frac{E_{n0}}{(E_{n0}^2-(3\hbar\omega)^2)(E_{n0}^2-(\hbar\omega)^2)} \qquad (1.4.1)$$
$$+\sum_{\substack{m,n=1\\ m\neq n}}(\mu_{n0})^2(\mu_{mn})^2 \frac{E_{n0}^2E_{m0}+4E_{n0}^2(\hbar\omega)^2-3E_{n0}(\hbar\omega)^2}{(E_{n0}^2-(3\hbar\omega)^2)(E_{n0}^2-(\hbar\omega)^2)(E_{m0}^2-(2\hbar\omega)^2)}$$

Here, the first, the second and the third terms on the right-hand side respectively correspond to the type (I), type (II)' and type (III)'. These approximate types are shown schematically in Fig. 1.4. In the static case, this formula is rewritten as follows.

$$\gamma^{(I)+(II)'+(III)'} = \gamma^{(I)} + \gamma^{(II)'} + \gamma^{(III)'} \qquad (1.4.2)$$

where

$$\gamma^{(I)} = \sum_{n=1}\frac{(\mu_{n0})^2(\mu_{nn})^2}{E_{n0}^3} \quad , \qquad (1.4.3)$$

$$\gamma^{(II)'} = -\sum_{n=1}\frac{(\mu_{n0})^4}{E_{n0}^3} \quad , \qquad (1.4.4)$$

and

$$\gamma^{(III)'} = \sum_{\substack{m,n=1\\ (m\neq n)}}\frac{(\mu_{n0})^2(\mu_{mn})^2}{E_{n0}^2E_{m0}}. \qquad (1.4.5)$$

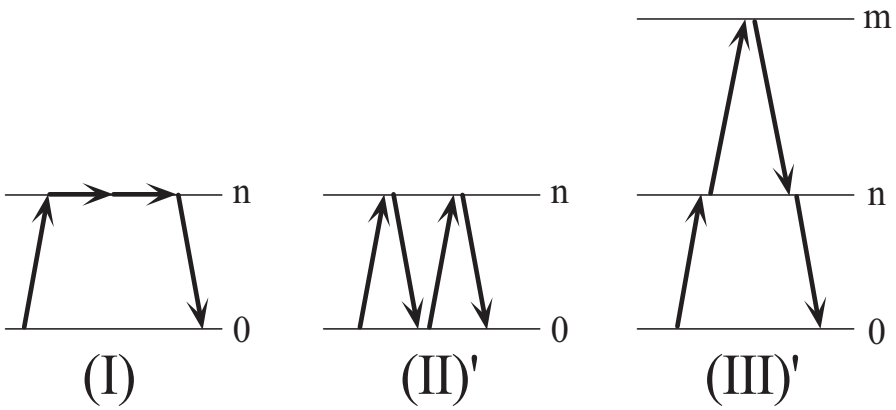

Fig.1.4 Three-type approximation virtual excitation process of γ.

From the Equations. (1.4.2)-(1.4.5), apparently, the contributions of types (I) and (III)' are positive in sign, whereas the contribution of type (II)' is negative. For conventional molecular compounds with large positive γ, there are two characteristic cases: (i) $|\gamma^{(I)}| >> |\gamma^{(II)'}| \approx |\gamma^{(III)'}|$ ($\gamma > 0$) and (ii) $|\gamma^{(I)}| = 0$, $|\gamma^{(II)'}| < |\gamma^{(III)'}|$ ($\gamma > 0$). In the case (i), the compounds have large noncentrosymmetric charge distributions which are responsible for large μ_{nn}, whereas in the case (ii), the compounds are the centrosymmetric systems in which the contributions of type (I) disappear. In section 1.6, the third case, *i.e.*, (iii) $|\gamma^{(I)}| = 0$, $|\gamma^{(II)'}| > |\gamma^{(III)'}|$ ($\gamma < 0$), is particularly considered. Namely, the compounds are centrosymmetric (μ_{nn}) and exhibit strong CT between the ground and the first excited states ($|\mu_{n0}| > |\mu_{mn}|$).

In order to further clarify the characteristics of the classification of compounds with large γ values, we rewrite the three-type approximate formula (Equations.(1.4.2)-(1.4.5)) by the use of the polarizabilities (α_0, α_n) of the ground and excited states. The polarizabilities of the ground and the nth excited states are given by

$$\alpha_0 = 2\sum_{n=1} \frac{(\mu_{n0})^2}{E_{n0}} , \tag{1.4.6}$$

and

$$\alpha_n = 2\left(\sum_{m(\neq n)=1} \frac{(\mu_{mn})^2}{E_{mn}} - \frac{(\mu_{n0})^2}{E_{n0}} \right). \tag{1.4.7}$$

Here, we define factors $\alpha_0(n)$, $\alpha_n(m)$ and $r(m,n)$ as

$$\sum_{n=1} \alpha_0(n) = 2\sum_{n=1} \frac{(\mu_{n0})^2}{E_{n0}} = \alpha_0 , \tag{1.4.8}$$

$$\sum_{m(\neq n)=1}^{N} \alpha_n(m) = \sum_{m(\neq n)=1}^{N} \left(2\frac{(\mu_{mn})^2}{E_{mn}} - \frac{\alpha_0(n)}{N-1} \right) = \alpha_n , \tag{1.4.9}$$

and

$$r(m,n) = \frac{E_{mn}}{E_{m0}} , \tag{1.4.10}$$

where N is the upper limit of the excited states which mainly contribute to γ value, $\alpha_0(n)$ is the contribution of the nth excited states to the ground state polarizability α_0 and $\alpha_n(m)$ is the contribution of the *m*th excited state to the *n*th state polarizability α_n. The factor $r(m,n)$ is either $0 < r(m,n) < 1$ or $r(m,n) < 0$. Using the factors, the three-type approximate formula

(Eqs.(1.4.2)-(1.4.5)) is rewritten as follows.

$$\gamma^{(I)+(II)'+(III)'} = \frac{1}{2}\sum_{n=1}^{N}\left[\frac{\alpha_0(n)}{E_{n0}}\left\{\frac{(\mu_{nn})^2}{E_{n0}}+\frac{1}{2}\sum_{m(\neq n)=1}^{N}\left[\alpha_n(m)r(m,n)-(1-r(m,n))\frac{\alpha_0(n)}{N-1}\right]\right\}\right]. \tag{1.4.11}$$

The formula represents the γ in the three-type approximation including up to the Nth excited states. The first and second terms of Eq.(1.4.11) correspond to the type (I) and type (II+III), respectively. In practice, N can be taken as a finite number since the γ value almost tends to converge by including a finite number of excited states, though N is inherently infinite.

Let us consider the centrosymmetric system (type (I) = 0). As mentioned above, this system has a possibility of exhibiting negative γ. At a first glance of Eq. (1.4.11), the γ becomes negative when $|\alpha_0(n)|$ is larger than $|\alpha_n(m)|$. It is further found that negative contributions ($-(1-r(m,n)\alpha_0(n)/(N-1))$) seems to become larger than positive contributions (corresponding to $\alpha_0(m)r(m,n)$) when the $r(m,n)$ is close to 0. From Eqs. (1.4.6) and (1.4.7), however, the approaching of $r(m,n)$ to 0 is also found to have a tendency of reducing the $\alpha_0(n)$ and enhancing the $\alpha_n(m)$. It is also noted that the effects of the transition moments (numerators of Eqs. (1.4.6) and (1.4.7)) are more significant than those of the transition energies (denominators of Eqs. (1.4.6) and (1.4.7)) because the transition moments contribute quadratically while the transition energies do linearly. It is therefore found that the γ for centrosymmetric systems tend to be large negative in the case of $|\mu_{n0}| > |\mu_{mn}|$ and $E_{mn} > E_{n0}$. Even in the case of large N values, the γ for centrosymmetric systems tends to be large negative when there are many contributing excited states with large $|\alpha_0(n)|$ values. Therefore, it is predicted that centrosymmetric systems with contributions of numerous non-degenerate excited states with small $|\alpha_0(n)|$ tends to exhibit positive γ value, while those with contributions of numerous near-degenerate excited states with large $|\alpha_0(n)|$ have the possibility of exhibiting not only positive but also negative γ values. In the next section, let's consider the characteristics of three-type formula in the three-state approximation, which corresponds to the limiting case of centrosymmetric system with a small N value.

1.5. Three-state three-type approximation for second hyperpolarizabilities

Let's consider the case in which only three states shown in Fig.1.5 contribute to the total γ values. In this case, Eqs. (1.4.3)-(1.4.5) are rewritten as

$$\gamma^{(I)} = \frac{(\mu_{n0})^2(\mu_{nn})^2}{E_{n0}^3}, \tag{1.5.1}$$

$$\gamma^{(\mathrm{II})'} = -\frac{(\mu_{n0})^4}{E_{n0}^3} \quad , \tag{1.5.2}$$

and

$$\gamma^{(\mathrm{III})'} = \frac{(\mu_{n0})^2(\mu_{mn})^2}{E_{n0}^2 E_{m0}} \quad . \tag{1.5.3}$$

Similarly, Eqs. (1.4.6), (1.4.7) and (1.4.10) are rewritten as

$$\alpha_0 = 2\frac{(\mu_{n0})^2}{E_{n0}} \quad , \tag{1.5.4}$$

$$\alpha_n = 2\frac{(\mu_{mn})^2}{E_{mn}} - \alpha_0, \tag{1.5.5}$$

and

$$r = \frac{E_{mn}}{E_{m0}} \quad , \tag{1.5.6}$$

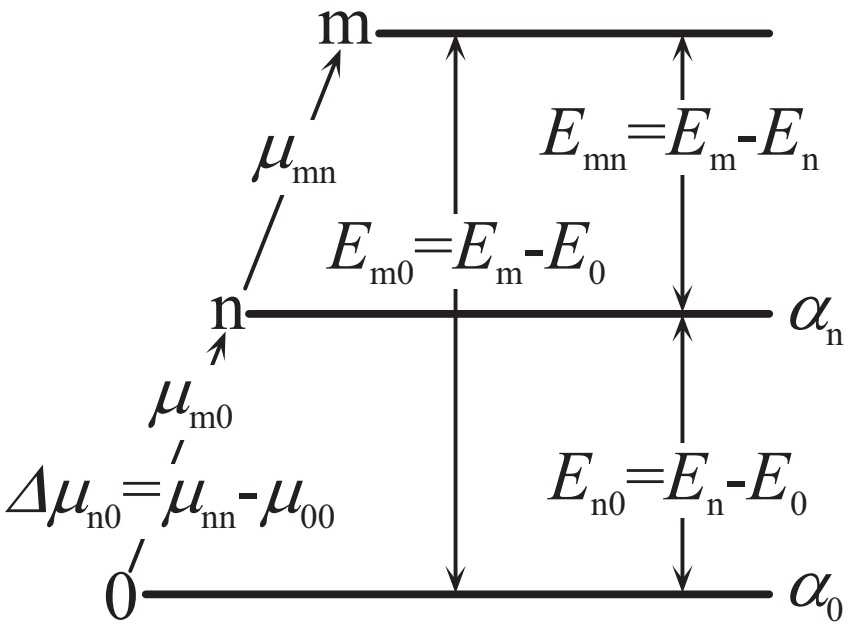

Fig.1.5 Three states involving in the three-type approximation in the three-state approximation

where α_0 and α_n are the polarizabilities of the ground and the nth excited states, respectively, and where the ratio r is $0 < r < 1$. As a result, the three-type approximate formula (Eq.(1.4.11)) in the three-state approximation is

$$\gamma^{(I)+(II)'+(III)'} = \frac{1}{2}\frac{\alpha_0}{E_{n0}}\left\{\frac{(\mu_{nn})^2}{E_{n0}} + \frac{1}{2}(\alpha_n r - \alpha_0(1-r))\right\}. \qquad (1.5.7)$$

Here, the first term corresponds to the type (I) and the second and third terms to the type (II+III)'. From Eqs. (1.5.4.) and (1.5.5), it is evident that α_0 is positive in sign, while α_n can be either positive or negative in sign. It is also noted that Eq. (1.5.7) is exact, not the three-type approximate formula, in the case of centrosymmetric systems only contributed by three states.

1.6. A classification of the systems with large second hyperpolarizabilities

Based on the three-type analysis of γ, a classification rule of γ, which enable to propose a guideline of designing systems with large γ, is able to extract. The classification of the systems with large γ values based on Eq.(1.5.7) is shown in Table 1.1. The criterion of the classification is the symmetry of systems. As the classification shows, for the noncentrosymmetric systems, main contributions to γ values are type (I) processes, so that the total γ values come to be positive and to be enhanced when α_0 and μ_{nn} are large and E_{n0} is small, whereas the centrosymmetric systems (type (I) = 0) are able to exhibit either positive or negative γ values. These criteria are controlled by CT properties among the ground and excited states mainly contributing to the γ.

There is an attracting feature in the γ. It is well-known that almost all the nonlinear optical substances have positive γ in the first off-resonant region. On the contrary, the classification rule supports an existence of systems with negative γ. The sign of a real part of the third-order nonlinear optical susceptibility is important in quantum optics: the positive value causes the self-focusing effect of an incident beam, while the negative one does the self-defocusing effect [60]. Therefore, conditions realizing a system with negative γ value are closely investigated. By understanding these conditions, some novel model systems with negative γ values could be proposed. From Table 1.1, the centrosymmetric systems have a possibility of exhibiting negative γ. However, all the centrosymmetric molecular systems with a small number of contributing excited states reported to date are found to exhibit positive γ values, so that they can be regarded as the case (B-1) in Table 1.1. Table 1.1 further shows that there exist two kinds of new centrosymmetric systems (B-2 and B-3) which possess negative γ values.

Firstly, limiting behaviors of γ values for the centrosymmetric systems (B-1), (B-2) and (B-3) are investigated. The results are obtained as follows.

(B-1) $\alpha_n > 0$, $\gamma > 0$

$$\gamma \approx \frac{1}{4}\frac{\alpha_0\alpha_n}{E_{n0}} r \rightarrow \frac{1}{4}\frac{\alpha_0\alpha_n}{E_{n0}} \quad \text{for} \quad \frac{\alpha_n}{\alpha_0} >> \frac{E_{n0}}{E_{mn}} = \frac{1-r}{r} (r \rightarrow 1) \tag{1.6.1}$$

(B-2) $\alpha_n > 0$, $\gamma < 0$

$$\gamma \approx -\frac{1}{2}\frac{\alpha_0}{E_{n0}^2}\left(\mu_{n0}^2 - \mu_{nm}^2\right) \quad \text{for} \quad r \rightarrow 0 \text{ and } \mu_{n0}^2 > \mu_{nm}^2 \,. \tag{1.6.2}$$

(B-3) $\alpha_n < 0$, $\gamma < 0$

$$\gamma \approx -\frac{1}{4}\frac{\alpha_0^2}{E_{n0}} \quad \text{for} \quad \frac{\mu_{nm}^2}{E_{nm}} << \alpha_0 \,. \tag{1.6.3}$$

It is noted that the case (B-2) is feasible when the excited states are near-degenerate because both the conditions $\alpha_n > 0$ ($\equiv (\mu_{mn}/\mu_{n0})^2 > (E_{mn}/E_{n0})$) and $\gamma < 0$ ($\equiv \mu_{n0}{}^2 > \mu_{mn}{}^2$) come to be satisfied more easily. Therefore, the case ($r \rightarrow 0$ and $\mu_{n0}{}^2 > \mu_{mn}{}^2$) is considered as the limiting case of (B-2). As can be seen from Eqs.(1.5.4)-(1.5.7), the cases (B-2) and (B-3) have a possibility to be realized in the case of large α_0 value. For the limiting case of (B-1), the numerator cannot be so much enlarged since the systems are not allowed to have large α_n and α_0 values at the same time in Eq.(1.5.5). On the other hand, for the limiting cases of (B-2) and (B-3), the γ values are expected to be enhanced with the increase of α_0 values. For the limiting case of (B-3), the α_0 value must be enormously large and must satisfy $\alpha_n \approx -\alpha_0$, so that the case seems to be difficult to realize in usual stable molecular systems.

Table 1.1 Classification of systems with large g values based on the three-type approximation formula in the three-state approximation.

Symmetry of the system	Main process	Criterion	Sign of γ	Type
Noncentrosymmetric	(I), (III)' >> (II)'	large α_0, μ_{mn} small E_{n0}	positive	(A)
Centrosymmetric	(II)', (III)'	$\alpha_n > 0$, $\frac{\alpha_n}{\alpha_0} > \frac{E_{n0}}{E_{mn}}$	positive	(B-1)
		$\alpha_n > 0$, $\frac{\alpha_n}{\alpha_0} < \frac{E_{n0}}{E_{mn}}$	negative	(B-2)
		$\alpha_n < 0$	negative	(B-3)

We next consider a structure-property relation for systems with negative γ [65]. It is elucidated from our classification rule that the symmetric systems with large ground state polarizability tend to exhibit negative γ. Therefore we consider the symmetric structure with large ground state polarizability. As an example, let us consider three charged states (neutral, ion radical and dianion states) of a condensed-ring conjugated system, *i.e.*, pentalene. The longitudinal γ of the ion radical state of pentalene is found to be negative, while the γ of other states are found to be positive. The resonances between polarization structures with mutually opposite directions are shown in Fig. 1.6. For the neutral state, a charge separation occurs in each resonance structure. For the resonance structure, the polarization induces in the mutually opposite direction. This resonance has only a small contribution to the ground-state electronic structure, since these resonance structures are considerably unstable. The small contribution of these resonance structures also corresponds to the fact that the magnitude of transition moment between the ground and the first excited states are small. Similarly, for the dianion state both the resonance structures are considered to have only a small contribution to the ground-state electronic structures, since the resonance structures are unstable. In contrast, for the anion radical state the resonance structures can significantly contribute to the ground-state electronic structure, since the resonance structures are more stable than those of the neutral and dianion states. The polarizations of these resonance structures are induced in the mutually opposite direction. The large contribution of these resonance structures also corresponds to the fact that the magnitude of transition moment between the ground and the first excited states are large. From the comparison among γ values and resonance structures for these systems, a system with resonance structures contributing to the stability of the ground state and inducing the polarization in the mutually opposite direction tends to exhibit negative γ and remarkable electron correlation and structure dependencies of the γ. The large contributions from the stable resonance structures with large dipole moments correspond to an enhancement of the magnitude of the transition moment between the ground and the allowed first excited states. This contribution also leads to a reduction of the transition energy between the ground and the allowed first excited states with large contributions from the resonance structures. Namely, a system whose ground state has a large contribution from this symmetric resonance structure with the inversible (reversible) polarization, which is referred to as SRIP [65] hereafter, satisfies our criteria for the system to have a negative γ.

(a) Neutral state

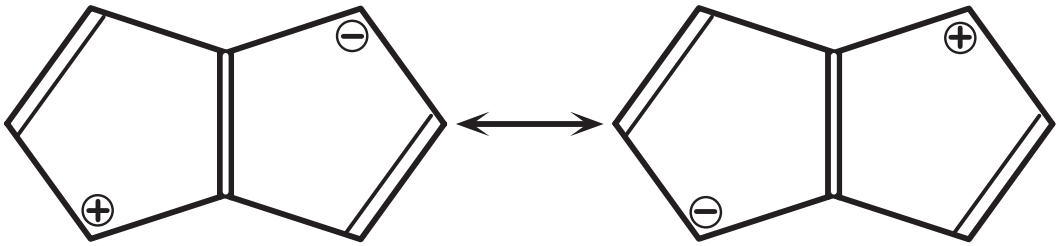

(b) Anion radical state

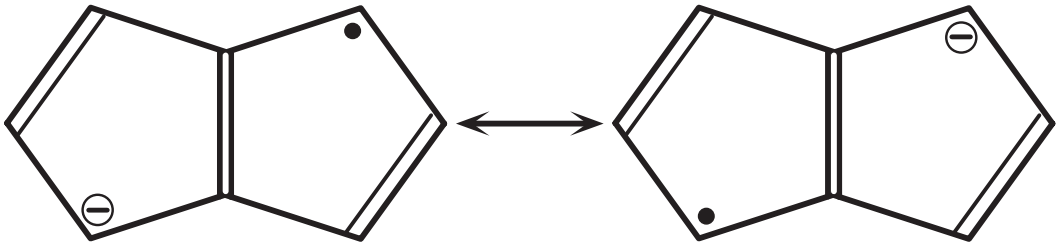

(c) Dianion state

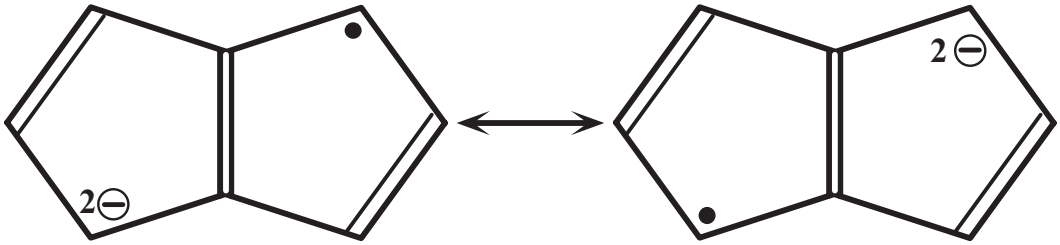

Fig.1.6 Symmetric resonance structures with inversible polarizations (SRIP) of three-charged states (neutral, anion and dianion states) of pentalene.

Chapter 2 *Finite field calculations of polarizability and hyperpolarizabilities by ab initio and semi empirical methods*

In chapter 1, the formulation of polarizability and hyperpolarizabilities based on TDPT is explained. For TDPT approach, calculations of several quantities relating to higher-order excited states are indispensable. In general, however, it is very difficult to estimate the quantities precisely using ab initio MO method. Therefore, in this chapter, variational methods dealing with only the ground state are applied to the calculation of polarizability and hyperpolarizabilities. In section 2.1, the calculation method of polarizability and hyperpolarizabilities based on the coupled-Hartree-Fock (CHF) theory is described. The total energy in the presence of external field can be expanded as the power series of the field. The coefficients of the field represent the dipole-moment, polarizability and hyperpolarizabilities. The total energy in the presence of the field is differentiated with respect to the field. This procedure is referred to as finite-field (FF) method. It is necessary to estimate the total energy of the ground state precisely for reproducing the hyperpolarizabilities accurately using FF method. To calculate the ground state precisely, it is important to estimate the effect of collision of electrons, *i.e.*, dynamical-electron-correlation effect. In section 2.2 several dynamical-electron-correlation methods, *i.e.*, Møller-Plesset perturbation (MP), coupled-cluster (CC) and quadratic-configuration-interaction (QCI) methods are explained. In section 2.3, two method, BLYP and B3LYP, based on density functional theory (DFT) are explained. DFT approach is a novel method including dynamical correlation corrections efficiently. For several molecules, especially for radical molecules, the electronic structure cannot be well described by single-determinant alone, which cannot describe non-dynamical electron-correlation effect. In section 2.4, complete-active-space self-consistent-field (CAS-SCF) method is explained. The CAS-SCF method is one of the typical methods to treat the problem of the non-dynamical electron-correlation by using multi-configuration wavefunction. In section 2.5, one of the semi-empirical MO methods, *i.e.*, intermediate neglect of differential overlap (INDO) method, is explained. This method is applied to the calculation of hyperpolarizabilities for larger size molecules in chapters 7 and 8.

The ab initio MO and DFT calculations are performed by using GAUSSIAN 94 program package [66]. The INDO calculations program performed is programed by M. Nakano.

2.1. Coupled Hartree-Fock (CHF) [67-75] theory and finite field (FF) [76-79] method

The total Hamiltonian in the presence of an electric field $\boldsymbol{F}$ is expressed as

$$H = H_o + \sum_a \boldsymbol{F}\cdot\boldsymbol{r}_a - \sum_A Z_A \boldsymbol{F}\cdot\boldsymbol{R}_A , \tag{2.1.1}$$

where indices a and A signify the ath electrons and the Ath nucleus, respectively. Z_A is the atomic number of the Ath nucleus, and the H_0 is the field-free-Hamiltonian. The total energy ($E(\boldsymbol{F})$) under the external field $\boldsymbol{F}$ and dipole-moment (μ) can be expressed as are expectation value for the wavefunction ψ:

$$E(\boldsymbol{F}) = \langle \psi | H | \psi \rangle \tag{2.1.2}$$

and

$$\mu = \langle \psi | \sum_a \boldsymbol{F}\cdot\boldsymbol{r}_a - \sum_A Z_A \boldsymbol{F}\cdot\boldsymbol{R}_A | \psi \rangle \ . \tag{2.1.3}$$

In the coupled-Hartree-Fock (CHF) method [67], ψ is approximated by a single Slater determinant with orbitals reoptimized for $\boldsymbol{F}$. Differentiation of Eq.(2.1.2) with respect to $\boldsymbol{F}$ gives

$$\frac{\partial E}{\partial F^i} = \left\langle \frac{\partial \psi}{\partial F^i} \middle| H | \psi \right\rangle + \langle \psi | \frac{\partial H}{\partial F^i} | \psi \rangle + \left\langle \psi | H \middle| \frac{\partial \psi}{\partial F^i} \right\rangle \ . \tag{2.1.4}$$

According to the Hellmann-Feynman theorem [79], the first and third terms on the right-hand of Eq.(2.1.4) is equal to zero, if the ψ is recognized as the true wavefunction. The CHF method satisfies the theorem. If the Hellmann-Feynman theorem is satisfied, μ defined by Eq.(2.1.3) can be expressed as

$$\mu^i = -\frac{\partial E}{\partial F^i} \quad (i = x, y \text{ and } z). \tag{2.1.5}$$

Therefore, from Equations (2.1.1)-(2.1.5), $E(\boldsymbol{F})$ and μ can be expressed as follows,

$$E(\boldsymbol{F}) = E_o - \sum_i \mu_i F^i - \frac{1}{2}\sum_{ij} \alpha_{ij} F^i F^j - \frac{1}{3}\sum_{ijk} \beta_{ijk} F^i F^j F^k - \frac{1}{4}\sum_{ijkl} \gamma_{ijkl} F^i F^j F^k F^l + \ldots . \tag{2.1.6}$$

$$\mu^i = \mu_0{}^i + \sum_j \alpha_{ij} F^j + \sum_{jk} \beta_{ijk} F^j F^k + \sum_{jkl} \gamma_{ijkl} F^j F^k F^l + \cdots \quad . \tag{2.1.7}$$

Here, μ_0 is the permanent dipole-moment and E_0 is the electric-field-free total energy.

From this formula, the component of μ, polarizability (α) and hyperpolarizabilities (β, γ, etc.) can be evaluated by numerical differentiation of the SCF energy with respect to the external field, namely,

$$\alpha_{ij} = -\left. \frac{\partial^2 E}{\partial F^i \partial F^j} \right|_{F^i, F^j \to 0} \quad , \tag{2.1.8}$$

$$\beta_{ijk} = -\frac{1}{2!} \left. \frac{\partial^3 E}{\partial F^i \partial F^j \partial F^k} \right|_{F^i, F^j, F^k \to 0} \quad , \tag{2.1.9}$$

and

$$\gamma_{ijkl} = -\frac{1}{3!} \left. \frac{\partial^4 E}{\partial F^i \partial F^j \partial F^k \partial F^l} \right|_{F^i, F^j, F^k, F^l \to 0} \quad . \tag{2.1.10}$$

This procedure is referred to as the finite-field (FF) method (See Appendix 1). One advantage of the FF method is that it can be applied to any quantum chemical theories.

2.2. Several dynamical-electron-correlation methods

Hartree-Fock theory neglects the instantaneous interaction between the electrons, so-called electron-correlation. Electron-correlation is determined by the "deviation" of the instantaneous Coulomb potential between two electrons from the average, *i.e.*, Hartree-Fock, potential they exert on one another. If two electrons are tightly packed into one orbital, two electrons will "collide" and consequently "deviate" from average potential. This is a physical significance of dynamical electron-correlation effect [80-82]. In order to calculate nonlinear optical properties precisely, the electron-correlation effect is important. The electron excitation effects in configuration-interaction (CI) correspond to the dynamical electron-correlation effect. Truncated CI methods, however, does not satisfy size-consistency. Beside full-CI calculation, which satisfies size-consistency, cannot be carried out for large molecules since the number of dimension increases excessively as the number of basis-set increases. Therefore, several dynamical-electron-correlation methods satisfying the size-consistency are proposed. Following methods are the dynamical-electron-correlation methods applied to the calculation of second hyperpolarizabilities in this study are explained as follows.

A Møller-Plesset perturbation theory [83]

When the zeroth-order Hamiltonian is chosen as the Fock operator in the Rayreigh-Schrödinger perturbation theory (RSPT), the electron-correlation can be included in the perturbation calculation. The Møller-Plesset (MP) perturbation theory suitable for the evaluation of the electron-correlation effect if the system can be well described by a single determinant.

Let's consider exact Hamiltonian as H, and the Hartree-Fock Hamiltonian as H_0. The time independent Schrödinger equation is expressed as

$$H|\Psi_{exact}\rangle = (H_0 + V)|\Psi_{exact}\rangle = \left(\sum_p F_p + V\right)|\Psi_{exact}\rangle \tag{2.2.1}$$

Here, F_p means Fock operator for p orbital. V means the interaction energy for a pair of electrons and is regarded as perturbation operator in MP theory.

The second-order MP (MP2) formula for the correlation energy in terms of spin orbitals is expressed as

$$E^{(2)} = \sum_u^D \frac{V_{0u}V_{u0}}{E_0 - E_u}. \tag{2.2.2}$$

Here, μ means double (D) excited configuration, *i.e.*, occupied a and b spin orbitals in reference Slater determinant (0, *e.g.*, HF) are replaced with virtual r and s spin orbitals. E0 means a summation of orbital energy (ε_a). Therefore, the difference between E_0 and E_μ is expressed using orbital energy as

$$E_0 - E_\mu = \varepsilon_a + \varepsilon_b - \varepsilon_r - \varepsilon_s \tag{2.2.3}$$

The $V_{0\mu}$ in Eq.(2.2.2) denote an antisymmetrized two electron integral as follows:

$$V_{u0} \equiv \langle u|0\rangle = \langle rs\|ab\rangle = \langle ab|rs\rangle - \langle ab|sr\rangle. \tag{2.2.3}$$

The third-order MP (MP3) formula for the correlation energy is expressed as same manner;

$$E^{(3)} = \sum_{uv}^D \frac{V_{0u}V_{uv}V_{v0}}{(E_0 - E_u)(E - E_v)}. \tag{2.2.4}$$

The forth-order MP (MP4) correlation formula is expressed as

$$E^{(4)} = \sum_{uv}^{D} \frac{V_{0u}V_{u0}V_{0v}V_{v0}}{(E_0 - E_u)(E - E_v)^2} + \sum_{uv}^{D}\sum_{t}^{SDTQ} \frac{V_{0u}\tilde{V}_{uv}\tilde{V}_{vt}V_{t0}}{(E_0 - E_u)(E_0 - E_v)(E_0 - E_t)} , \qquad (2.2.5)$$

where,

$$\tilde{V}_{uv} = V_{uv} - V_{00}\delta_{uv} . \qquad (2.2.6)$$

By restricting t in the second term of Eq.(2.2.5), MP4 correlation can be divided into five parts as follows:

$$E^{(4)} = E_R^{(4)} + E_S^{(4)} + E_D^{(4)} + E_T^{(4)} + E_Q^{(4)} . \qquad (2.2.7)$$

Namely, the effects of each types of electron excitations are examined.

In order to evaluate the hyperpolarizability, the CHF orbitals are used. In this case, the effect of the external field can be included variationally by the CHF calculation.

B Coupled-cluster (CC) theory [84-89]

In coupled-cluster theory, the accurate wave function Ψ_{CC} is obtained starting from single determinant Φ_0 as

$$|\Psi_{CC}\rangle = e^T|\Phi_0\rangle . \qquad (2.2.8)$$

Here, cluster operator T is usually separated into n-electrons excitation operators (T_n; n = 1, 2, 3, etc.) as follows:

$$T = T_1 + T_2 + T_3 + \ldots \qquad (2.2.9)$$

When the single excitation operator (T_1) alone is chosen as cluster operator, the CC wavefunction $|\psi_{CC}\rangle$ accord with HF wavefunction $|\psi_{HF}\rangle$. The dynamical electron-correlation effects can be include by choosing n-electron (n > 1) excitation operator as cluster operator. One of the advantage of the CC method is that the size-consistency is satisfied on a truncated of T at any order.

Coupled-cluster correlation energy is determined by the condition that the CC wave function (Eq.(2.2.9)) satisfy the Schrödiger equation:

$$He^T|\Phi_0\rangle = Ee^T|\Phi_0\rangle . \qquad (2.2.11)$$

Multiplying Eq.(2.2.11) by e^{-T} on the left, we have,

$$e^{-T}He^{T}\left|\Phi_0\right\rangle = E\left|\Phi_0\right\rangle \quad . \tag{2.2.12}$$

Namely, the Schrödiger equation is solved by improvement of the Hamiltonian using e^{T}. The coupled-cluster energy is calculated as follows;

$$E = \left\langle \Phi_0 \left| e^{-T}He^{T} \right| \Phi_0 \right\rangle \quad . \tag{2.2.13}$$

As a matter of fact, Eq.(2.2.13) is solved by reiteration calculation.

C Quadratic configuration-interaction theory [90]

The normal equations of (linear) configuration interaction theory are modified by introducing new terms which are quadratic in the configuration coefficients and which ensure size consistency in the resulting total energy. If the space is restricted to double (D) substitution, the method is so-called QCID method. QCID method coincide with CCD exactly. The QCISD method, in which the space is restricted to single and double substitution, can reproduce the energy at the CCSD level [91].

2.3. Density functional theory (DFT) approach

Since the seminal work of Hohenberg, Kohn and Sham [92], the density functional theory (DFT) of electronic structure has seen significant theoretical and formal advances. In DFT, the exact exchange (HF) for a single determinant is replaced by a more general expression, the exchange-correlation functional, which can include terms accounting for both exchange energy and the dynamical-electron-correlation.

In this work we used two types of DFT approaches, *i.e.,* the BLYP and B3LYP methods. The BLYP method uses the Becke's functional (B) as the exchange functional [93], which includes the Slater exchange along with correlations involving the gradient of the density, and also uses the functional developed by Lee, Yang and Parr (LYP) as the correlation functional [94], which includes both local and non-local terms. The B3LYP method is the Becke's three parameter hybrid method [95-97] using the LYP correlation functional. Becke determined the parameters in the following exchange-correlation approximation form,

$$E_{XC} = a \cdot E_{XC}{}^{HF} + (1-a) \cdot E_{XC}{}^{LSDA} + b \cdot \Delta E_{XC}{}^{B88} + c \cdot \Delta E_{C}{}^{PW91} . \tag{2.3.1}$$

Here, $E_{XC}{}^{LSDA}$ means the exchange in the local-spin-density exchange-correlation approximation, $E_{XC}{}^{exact}$ is the HF exchange for a single determinant, $\Delta E_{XC}{}^{B88}$ is the Becke's 1988 gradient correction for exchange, and $\Delta E_{C}{}^{PW91}$ is the 1991 gradient correction for correlation of

Perdew and Wang [98]. Becke claimed that this functional performs significantly better than previous functionals with gradient corrections only. In the case of nonlinear optical properties also, Matsuzawa and Dickson used the several DFT approaches and claimed the effectiveness of this method [99]. Therefore, we applied the B3LYP and BLYP methods to the calculation of the response property of nitronyl nitroxide radical.

2.4. Complete-active-space self-consistent-field (CAS-SCF) method [100]

There is a difficulty originating in the non-dynamical correlation effects on the description of a state of system, which cannot be well described by using the single determinant alone. The problems related to the breakdown of the single-configuration approximation can be efficiently treated by using multi-configuration (MC) wavefunctions. However, there is no general rule to build a set of important configurations. The complete-active-space-SCF (CAS-SCF) method proposed by Roos [100] uses configurations generated in the active orbital space and can efficiently describe the electronic structures of the systems with large non-dynamical correlations. In CAS-SCF calculation, the MCSCF calculations are performed using a special type of MC wavefunction. The MC wavefunction considered is constructed from two sets of occupied orbitals: the inactive and active orbitals. The inactive orbitals are doubly occupied in all configurations in the MC wavefunctions. Conversely, the active orbitals define a subset of the total orbital space, in which the configuration expansion is chosen to be complete. The wavefunction constructed in this way is called the complete active space (CAS) wavefunction. This type of MC expansion has several conceptual advantages as well as computational one. First, orbital rotations within the inactive and active subspaces leave the energy unchanged, and then do not need to be considered. Second, with the use of a complete CI wavefunction in the active subspace, the sometimes difficult choice of the "dominant" configurations is completely avoided and the only remaining "chemical" problem is the choice of active orbitals. This method was also applied to the calculation of the response properties of several small molecules [101].

2.5. Intermediate neglect of differential overlap (INDO) method [102]

When the power of computer system was not sufficient for carrying out ab initio MO calculations in order to reproduce several properties of molecules precisely, several approximation approaches were suggested. These approximation methods were called semi-empirical method. Some semi-empirical methods are useful for studying larger size molecules even now. One of the semi-empirical methods is the intermediate neglect of differential overlap (INDO) approximation proposed by Pople. Under the INDO approximation, the Fock matrix is expressed as follows:

$$F_{rr} = U_{rr} + \frac{1}{2} P_{rr}\gamma_{AA} + \sum_{s\neq r}^{\text{on a}} P_{ss}\left[(rr|ss) - \frac{1}{2}(rs|rs)\right] + \sum_{A\neq B}(P_{BB} - Z_B)\gamma_{AB}, \qquad (2.5.1)$$

$$F_{rs} = P_{rs}\left[\frac{3}{2}(rs|rs) - \frac{1}{2}(rr|ss)\right] \text{ (} r \neq s\text{; r and s belong to atom A)}$$

$$\frac{1}{2}S_{rs}(\beta_A + \beta_B) - \frac{1}{2}P_{rs}\gamma_{AB} \text{ (r and s belong to atom A and B, respectively) .(2.5.2)}$$

Here, r and s incident atomic orbitals (2s, $2p_x$,$2p_y$ and $2p_z$). The parameter β_A is inherent in atom a and determined by the obtained using ab initio calculation for small molecules. The core integral U_{rr} is expressed as follows:

$$\begin{aligned} U_{ss} &= -\frac{1}{2}(I_A + A_A)_s - \left(Z_A - \frac{1}{2}\right)F^0 + \frac{1}{6}\left(Z_A - \frac{3}{2}\right)G^1 \\ U_{pp} &= -\frac{1}{2}(I_A + A_A)_p - \left(Z_A - \frac{1}{2}\right)F^0 + \frac{1}{3}G^1 + \frac{2}{25}\left(Z_A - \frac{5}{2}\right)F^2 \end{aligned} \qquad (2.5.3)$$

Here, I_A and A_A signify the ionization potential and electron affinity, respectively. The I_A and A_A are estimated by experimental data's. Bond order matrix element P_{rs} in Eq.(2.5.2) is expressed as

$$P_{rs} = 2\sum_i C_r^i C_s^i \ . \qquad (2.5.4)$$

Here C_r^1 is the linear coefficient of the atomic orbital r in molecular orbital i. The one-center electron repulsion integral γ_{ab} is estimated by Slater-Condon's parameters as follows:

$$\begin{aligned} (ss|ss) &= (ss|xx) = F^0 = \gamma_{AA} \\ (xx|xx) &= F^0 + \frac{4}{25}F^2 \\ (xx|yy) &= F^0 - \frac{2}{25}F^2 \\ (sx|sx) &= \frac{1}{3}G^1 \\ (xy|xy) &= \frac{3}{25}F^2 \end{aligned} \qquad (2.5.5)$$

Here, F^0 is calculated by using Slater type orbital of atom A. Other parameters are determined using atomic spectral data.

Appendix

Finite-Field method

The polarizability (α) can be evaluated by second-order derivatives of the total energy with respect to the field as follows:

$$\alpha_{ii} = -\frac{2\{E(3F^i)+E(-3F^i)\}-27\{E(2F^i)+E(-2F^i)\}+270\{E(F^i)+E(-F^i)\}-490E_0}{180(F^i)^2} \tag{A.1}$$

and

$$\begin{aligned}\alpha_{ij} = -\frac{1}{48F^iF^j}\Big[&\{E(2F^i,2F^j)-E(2F^i,-2F^j)-E(-2F^i,2F^j)+E(-2F^i,-2F^j)\}\\ &+16\{E(F^i,F^j)-E(F^i,-F^j)-E(-F^i,F^j)+E(-F^i,-F^j)\}\Big]\end{aligned} \tag{A.2}$$

The first hyperpolarizability (β) can be evaluated by third-order derivatives of the total energy with respect to the field as follows:

$$\beta_{iii} = -\frac{-\{E(3F^i)-E(-3F^i)\}+8\{E(2F^i)-E(-2F^i)\}-13\{E(F^i)-E(-F^i)\}}{16(F^i)^3}, \tag{A.3}$$

$$\begin{aligned}\beta_{iij} = -\frac{1}{48(F^i)^2F^j}\Big[&-\{E(2F^i,F^j)-E(2F^i,-F^j)+E(-2F^i,F^j)-E(-2F^i,-F^j)\}\\ &-2\{E(F^i,2F^j)-E(F^i,-2F^j)+E(-F^i,2F^j)-E(-F^i,-2F^j)\}\\ &+20\{E(F^i,F^j)-E(F^i,-F^j)+E(-F^i,F^j)-E(-F^i,-F^j)\}\\ &+4\{E(2F^j)-E(-2F^j)\}-38\{E(F^j)-E(-F^j)\}\Big]\end{aligned} \tag{A.4}$$

and

$$\begin{aligned}\beta_{ijk} = -\frac{1}{16F^iF^jF^k}\Big[&\{E(F^i,F^j,F^k)-E(F^i,F^j,-F^k)\}-\{E(F^i,-F^j,F^k)-E(F^i,-F^j,-F^k)\}\\ &-\{E(-F^i,F^j,F^k)-E(-F^i,F^j,-F^k)\}+\{E(-F^i,-F^j,F^k)-E(-F^i,-F^j,-F^k)\}\Big]\end{aligned} \tag{A.5}$$

The second hyperpolarizability (γ) can be evaluated by fourth-order derivatives of the total energy with respect to the field as follows:

$$\gamma_{iiii} = -\frac{-\{E(3F^i)+E(-3F^i)\}+12\{E(2F^i)+E(-2F^i)\}-39\{E(F^i)+E(-F^i)\}+56E_0}{36(F^i)^4},$$

(A.6)

$$\begin{aligned}\gamma_{iijj} = -\frac{1}{72(F^i)^2(F^j)^2}\Big[&-\{E(2F^i,F^j)+E(2F^i,-F^j)+E(-2F^i,F^j)+E(-2F^i,-F^j)\}\\&-\{E(F^i,2F^j)+E(F^i,-2F^j)+E(-F^i,2F^j)+E(-F^i,-2F^j)\}\\&+20\{E(F^i,F^j)+E(F^i,-F^j)+E(-F^i,F^j)+E(-F^i,-F^j)\}\\&+2\{E(2F^i)+E(-2F^i)+E(2F^j)+E(-2F^j)\}\\&-38\{E(F^i)+E(-F^i)+E(F^j)+E(-F^j)\}+72E_0\Big]\end{aligned}$$

(A.7)

$$\begin{aligned}\gamma_{iiij} = -\frac{1}{24(F^i)^3F^j}\Big[&\{E(2F^i,F^j)-E(2F^i,-F^j)-E(-2F^i,F^j)+E(-2F^i,-F^j)\}\\&-2\{E(F^i,F^j)-E(F^i,-F^j)-E(-F^i,F^j)+E(-F^i,-F^j)\}\Big]\end{aligned}$$

(A.8)

and

$$\begin{aligned}\gamma_{iijk} = -\frac{1}{24(F^i)^2F^jF^k}\Big[&\{E(F^i,F^j,F^k)-E(F^i,F^j,-F^k)-E(F^i,-F^j,F^k)+E(F^i,-F^j,-F^k)\}\\&+\{E(-F^i,F^j,F^k)-E(-F^i,F^j,-F^k)-E(-F^i,-F^j,F^k)+E(-F^i,-F^j,-F^k)\}\\&-2\{E(F^j,F^k)-E(F^j,-F^k)-E(-F^j,F^k)+E(-F^j,-F^k)\}\Big]\end{aligned}$$

(A.9)

Indeed, the polarizability and hyperpolarizabilities obtained by using FF method are liable to involve some numerical errors. In order to avoid numerical errors, it is necessary to use several minimum fields strengths. After numerical differentiations using these fields, we adopt a numerically stable value of hyperpolarizabilites.

Chapter 3 Hyperpolarizability density analysis

In sections 1, we introduced perturbative approaches to the response properties, and provided a method for analysis which includes partitioning of quantum processes (virtual excitation processes). This analysis method is a powerful tool for exploring the characteristics of the contributions from each virtual excitation path. However, this approach cannot elucidate the spatial contributions to the high-order polarizabilities and also cannot be applied to the FF method, which only needs the ground state of the system. In section 3.1, as an analysis method of response property, we define a new concept "polarizability and hyperpolarizability densities" by improving the idea proposed by Chopra et al. [72]. This analysis method has advantages in the points that plots of hyperpolarizability and polarizability densities visualize the spatial characteristics of the contribution to the total polarizability and hyperpolarizability.

3.1. *A definition and an analysis method by the one-electron reduced hyperpolarizability density plot*

Chopra et al. [71] proposed an analysis method by using a plot of the *n*th derivatives of charge densities with respect to the applied field strength, weighted by the distance from the internuclear axis for linear conjugated systems. The magnitudes of the plotted quantities depend on the position of the origin of the used coordinated axis, though their method is useful for revealing spatial characteristics of hyperpolarizability. In this section, therefore, an alternative analysis method of polarizability and hyperpolarizability based on charge-density derivatives is presented. Namely, a concept "(hyper)polarizability density [65,103,104]" is introduced and an analysis method using a direct plot of the (hyper)polarizability densities, which can provide pictorial and intuitive understanding of (hyper)polarizability is presented. The (hyper)polarizability densities can be defined for arbitrary systems irrespective of the origin of the used coordinate axis.

The charge density function $\rho(\boldsymbol{r},\boldsymbol{F})$ can be expanded in powers of the field F in the same as the expansions of energy and dipole moment. The charge density function $\rho(\boldsymbol{r},\boldsymbol{F})$ are expressed as [65]

$$\rho(\mathbf{r},\mathbf{F}) = \rho^{(0)}(\mathbf{r}) + \sum_j \rho^{(1)}(\mathbf{r})F^j + \frac{1}{2!}\sum_{jk}\rho^{(2)}(\mathbf{r})F^jF^k + \frac{1}{3!}\sum_{jkl}\rho^{(3)}(\mathbf{r})F^jF^kF^l + \ldots . \qquad (3.1.1)$$

The dipole moment expansion can be represented as follows.

$$\begin{aligned}\mu^i(\mathbf{F}) &\equiv -\int r^i\rho(\mathbf{r},\mathbf{F})d^3\mathbf{r} \\ &= \mu_0^i + \sum_j \alpha_{ij}F^j + \sum_{jk}\beta_{ijk}F^jF^k + \sum_{jkl}\gamma_{ijkl}F^jF^kF^l + \ldots \\ &= -\int r^i\rho^{(0)}(\mathbf{r})d^3\mathbf{r} - \sum_j\int r^i\rho_j^{(1)}(\mathbf{r})d^3\mathbf{r}F^j - \frac{1}{2!}\sum_{jk}\int r^i\rho_{jk}^{(2)}(\mathbf{r})d^3\mathbf{r}F^jF^k \\ &\quad -\frac{1}{3!}\sum_{jkl}\int r^i\rho_{jkl}^{(3)}(\mathbf{r})d^3\mathbf{r}F^jF^kF^l - \ldots\end{aligned} \qquad (3.1.2)$$

Here, the r^i is the i component of the electron coordinate. From Eqs. (3.1.1) and (3.1.2), polarizability and the first and the second hyperpolarizabilities can be expressed by [65]

$$\alpha_{ij} = -\int r^i\rho_j^{(1)}(\mathbf{r})d^3\mathbf{r}\ , \qquad (3.1.3)$$

$$\beta_{ijk} = -\frac{1}{2!}\int r^i\rho_{jk}^{(2)}(\mathbf{r})d^3\mathbf{r}\ , \qquad (3.1.4)$$

and

$$\gamma_{ijkl} = -\frac{1}{3!}\int r^i \rho^{(3)}_{jkl}(\mathbf{r}) d^3\mathbf{r} \ . \tag{3.1.5}$$

Here,

$$\rho^{(1)}_j(\mathbf{r}) = \left.\frac{\partial \rho}{\partial F^j}\right|_{\mathbf{F}=0} , \tag{3.1.6}$$

$$\rho^{(2)}_{jk}(\mathbf{r}) = \left.\frac{\partial^2 \rho}{\partial F^j \partial F^k}\right|_{\mathbf{F}=0} , \tag{3.1.7}$$

and

$$\rho^{(3)}_{jkl}(\mathbf{r}) = \left.\frac{\partial^3 \rho}{\partial F^j \partial F^k \partial F^l}\right|_{\mathbf{F}=0} . \tag{3.1.8}$$

These derivatives of electron densities with respect to external electric fields are referred to as polarizability and hyperpolarizability densities. The $\rho^{(1)}{}_j(\boldsymbol{r})$, $\rho^{(2)}{}_{jk}(\boldsymbol{r})$ and $\rho^{(3)}{}_{jkl}(\boldsymbol{r})$ correspond to α_{ij}, β_{ijk} and γ_{ijkl} densities, respectively. These quantities can be calculated in a good precision by discretizing the space and by using the efficient numerical differentiation method. For example, the $\rho^{(1)}{}_i(\boldsymbol{r})$, $\rho^{(2)}{}_{ii}(\boldsymbol{r})$ and $\rho^{(3)}{}_{iii}(\boldsymbol{r})$ are calculated by using the following numerical differentiation formulae [65]:

$$\rho^{(1)}_i(\mathbf{r}) = \frac{\rho(\mathbf{r}, F^i) - \rho(\mathbf{r}, -F^i)}{2F^i} , \tag{3.1.9}$$

$$\rho^{(2)}_{ii}(\mathbf{r}) = \frac{\rho(\mathbf{r}, F^i) + \rho(\mathbf{r}, -F^i) - 2\rho(\mathbf{r}, 0)}{(F^i)^2} , \tag{3.1.10}$$

and

$$\rho^{(3)}_{iii}(\mathbf{r}) = \frac{\{\rho(\mathbf{r}, 2F^i) - \rho(\mathbf{r}, -2F^i)\} - 2\{\rho(\mathbf{r}, F^i) - \rho(\mathbf{r}, -F^i)\}}{2(F^i)^3} , \tag{3.1.11}$$

where $\rho(\boldsymbol{r},F^i)$ represents a reduced one-electron density at a spatial point $\boldsymbol{r}$ in the presence of the field. The numerically precise values of these densities are useful for investigating the effects of basis sets and electron correlations on the hyperpolarizabilities of three dimensional systems in the ab initio method.

Let's next consider the hyperpolarizability density analysis using the Mulliken population calculated by semi-empirical MO method. The charge density $(\mathbf{PS})_{ss}$ partitioned into each atomic orbital s is considered according to the Mulliken population analysis.

$$\rho(\boldsymbol{r}) = \sum_{s,t} (\mathbf{P})_{st} \phi_s(\boldsymbol{r}) \phi_t(\boldsymbol{r}) \ , \tag{3.1.12}$$

where $\phi_s(\boldsymbol{r})$ denotes the atomic orbital s. From Eq.(3.1.12),

$$\int \rho(\boldsymbol{r}) d^3\boldsymbol{r} = \sum_s (\mathbf{PS})_{ss} = \sum_s \rho_s(\boldsymbol{r}) d^3\boldsymbol{r} \ . \tag{3.1.13}$$

Here, the $(\mathbf{S})_s$ is the overlap matrix element and the $(\mathbf{P})_{st}$ is the bond-order matrix element. Equation (3.1.2) can be rewritten as follows by the use of the charge density function $\rho_s(\boldsymbol{r})$ divided into each atomic orbital s. [103]

$$\mu^i(\mathbf{F}) = -\sum_s \left(\int r^i \rho_s^{(0)}(\boldsymbol{r}) d^3\boldsymbol{r} + \sum_j \int r^i \rho_{s,j}^{(1)}(\boldsymbol{r}) d^3\mathbf{r} F^j + \frac{1}{2!} \sum_{jk} \int r^i \rho_{s,jk}^{(1)}(\boldsymbol{r}) d^3\boldsymbol{r} F^j F^k \right.$$
$$\left. + \frac{1}{3!} \sum_{jkl} \int r^i \rho_{s,jkl}^{(1)}(\boldsymbol{r}) d^3\boldsymbol{r} F^j F^k F^l + \ \ldots \right) \tag{3.1.14}$$

The following approximation is attempted to the charge density function $\rho_s(\boldsymbol{r})$.

$$\rho_s(\boldsymbol{r}) = (\mathbf{PS})_{ss} \delta(\boldsymbol{r} - \boldsymbol{r}_s) \ . \tag{3.1.15}$$

This approximation implies that the $\rho_s(\boldsymbol{r})$ is concentrated to the center $\boldsymbol{r}_s$ of the atomic orbital s. Substituting Eq.(3.1.15) into Eq.(3.1.14), the following relation is obtained.[103]

$$\mu^i(\mathbf{F}) \approx -\sum_s \left(r_s^i (\mathbf{PS})_{ss}^{(0)} + \sum_j r_s^i (\mathbf{PS})_{ss,j}^{(1)} F^j + \frac{1}{2!} \sum_{jk} r_s^i (\mathbf{PS})_{ss,jk}^{(2)} F^j F^k \right.$$
$$\left. + \frac{1}{3!} \sum_{jkl} r_s^i (\mathbf{PS})_{ss,jkl}^{(3)} F^j F^k F^l + \ \ldots \right) \tag{3.1.16}$$

From this equation, we obtain approximate polarizability and hyperpolarizability as

$$\alpha_{ij} \approx -\sum_s r_s^i (\mathbf{PS})_{ss,j}^{(1)} \ , \tag{3.1.17}$$

$$\beta_{ijk} \approx -\frac{1}{2!} \sum_s r_s^i (\mathbf{PS})_{ss,jk}^{(2)} \ , \tag{3.1.18}$$

and

$$\gamma_{ijkl} \approx -\frac{1}{3!}\sum_{s} r_s^i (\mathbf{PS})^{(3)}_{ss,jkl} \ , \tag{3.1.19}$$

where

$$(\mathbf{PS})^{(1)}_{ss,j} = \left.\frac{\partial(\mathbf{PS})_{ss}}{\partial F^j}\right|_{F=0} , \tag{3.1.20}$$

$$(\mathbf{PS})^{(2)}_{ss,jk} = \left.\frac{\partial(\mathbf{PS})_{ss}}{\partial F^j \partial F^k}\right|_{F=0} , \tag{3.1.21}$$

and

$$(\mathbf{PS})^{(3)}_{ss,jkl} = \left.\frac{\partial(\mathbf{PS})_{ss}}{\partial F^j \partial F^k \partial F^l}\right|_{F=0} . \tag{3.1.22}$$

These quantities represent polarizability and hyperpolarizability densities by using the Mulliken population. Here, the r_s^i represents the i component of the coordinate of the atom located at the center of the atomic orbital s.

The quantity $(\mathbf{PS})^{(3)}_{ss,iii}$, namely the γ_{iiii} density of atomic orbital s, is calculated by the four-point numerical derivative method as follows. [103,104]

$$(\mathbf{PS})^{(3)}_{ss,iii} = \frac{\left\{(\mathbf{PS})_{ss}(2F^i) - (\mathbf{PS})_{ss}(-2F^i)\right\} - 2\left\{(\mathbf{PS})_{ss}(F^i) - (\mathbf{PS})_{ss}(-F^i)\right\}}{2(F^i)^3} . \tag{3.1.23}$$

Here, the $(\mathbf{PS})_{ss}(F^i)$ is the Mulliken charge density of the atomic orbital s in the presence of the field F^i. The other important approximate polarizability and hyperpolarizability (α_{ij}, β_{ijj} and γ_{iijj}) densities in the SHG and the THG can be calculated as follows. [103]

$$(\mathbf{PS})^{(1)}_{ss,j} = \frac{(\mathbf{PS})_{ss}(F^j) - (\mathbf{PS})_{ss}(-F^j)}{2F^j} , \tag{3.1.24}$$

$$(\mathbf{PS})^{(2)}_{ss,jj} = \frac{(\mathbf{PS})_{ss}(F^j) + (\mathbf{PS})_{ss}(-F^j) - 2(\mathbf{PS})_{ss}(0)}{(F^j)^2} , \tag{3.1.25}$$

and

$$(\mathbf{PS})^{(3)}_{ss,ijj} = \frac{1}{2F^i\left(F^j\right)^2}\Big[\big\{(\mathbf{PS})_{ss}(F^i,F^j)+(\mathbf{PS})_{ss}(F^i,-F^j)-2(\mathbf{PS})_{ss}(F^i)\big\} - \big\{(\mathbf{PS})_{ss}(-F^i,F^j)+(\mathbf{PS})_{ss}(-F^i,-F^j)-2(\mathbf{PS})_{ss}(-F^i)\big\}\Big] \quad (3.1.26)$$

In order to explain a method for analysis employing the plots of reduced one-electron (hyper)polarizability densities, we consider a pair of localized $\rho^{(3)}_{iii}$ shown in Fig.3.1. The positive sign of the $\rho^{(3)}_{iii}(x)$ implies that the second derivative of the charge density increases with the increase in the field. As can be seen from Eq. (3.1.5), the arrow from positive to negative $\rho^{(3)}_{iii}(x)$ shows the sign of the contribution to γ_{iiii} determined by the relative spatial configuration between the two $\rho^{(3)}_{iii}(x)$'s. Namely, the sign of the contribution to γ_{iiii} becomes positive when the direction of the thick arrow coincides with the positive direction of the coordinate system. The contribution to γ_{iiii} determined by the $\rho^{(3)}_{iii}(x)$'s of the two points is more significant, when their distance is larger.

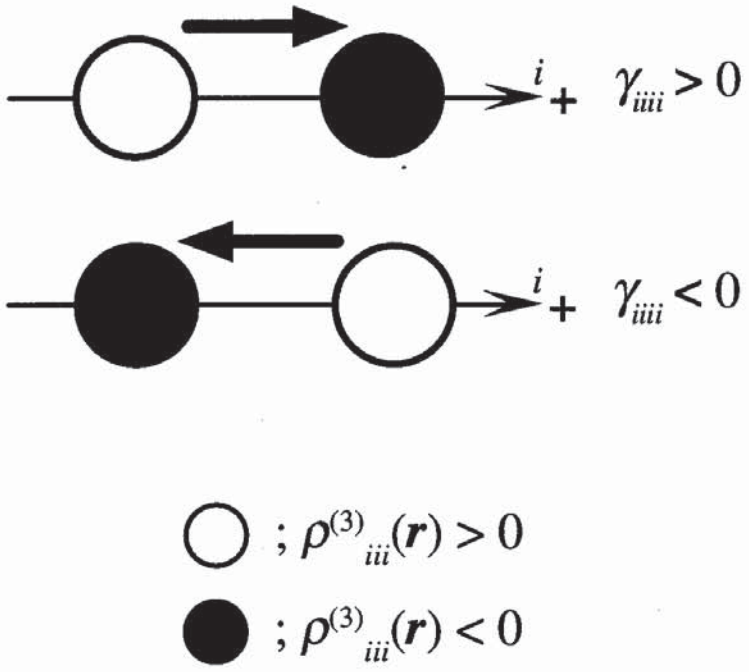

Fig.3.1. Schematic diagram of the second hyperpolarizability (γ_{iiii}) densities $\rho^{(3)}_{iii}(\boldsymbol{r})$. The size of circle represents the magnitude of $\rho^{(3)}_{iii}(\boldsymbol{r})$ and the arrow shows the sign of γ_{iiii} determined by the relative spatial configuration between these two $\rho^{(3)}_{iii}(\boldsymbol{r})$.

3.2. Example: The second hyperpolarizability density analysis for ethylene molecule

In this section, basis set and electron-correlation dependencies for ethylene molecule is examined by using hyperpolarizability density analysis as an example of usefulness of this method.

It is well known that using an extended basis set is indispensable for reproducing semi-quantitative γ value. To elucidate the basis set dependency of γ for ethylene, two basis sets, *i.e.*, 6-311G and 6-311G+*f*/*d*, are applied to the calculations of the γ_{xxxx}. The 6-311G basis set is one of the triple split valence basis set. The 6-311G+*f*/*d* basis set is an extended basis set, which involves diffuse and polarization *f* function on C atom (ζ = 0.04384) and *d* function on H atom (ζ = 0.03240) in addition to 6-311G basis set. The exponents of diffuse and polarization *f*/*d* function is determined from outermost two exponents of 6-311G by using the even-tempered method.

Figure 3.2 shows the geometry and coordinate system of ethylene molecule. The geometry of ethylene is optimized by using B3LYP method with 6-311++G(3*d*,3*p*) basis set.

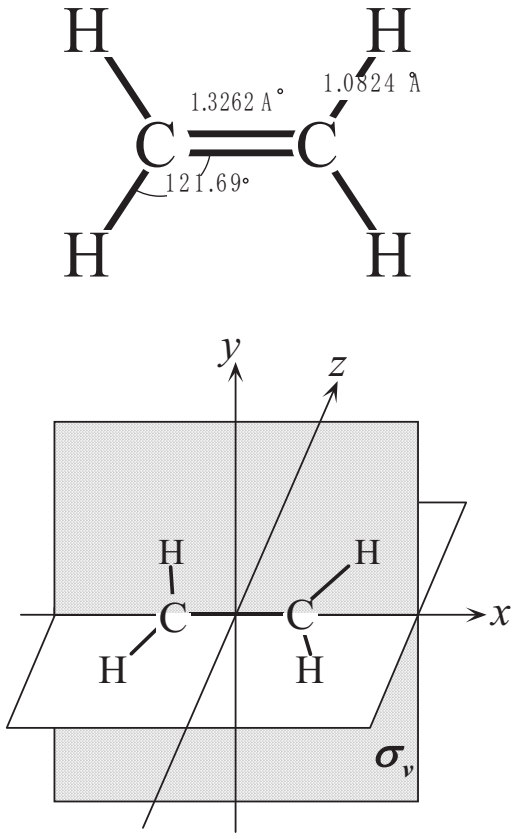

Fig.3.2 Molecular geometries of C_2H_4 optimized by using B3LYP method with 6-311++G(3*d*,3*p*) basis set. The σ_v plane represents the reflection plane of C_2H_4.

Figure 3.3 shows the γ_{xxxx} values and $\rho^{(3)}_{xxx}(\boldsymbol{r})$ distributions of ethylene. The plane at which the $\rho^{(3)}_{xxx}(\boldsymbol{r})$ distributions are drawn is σ_v plane of ethylene molecule. As shown in Fig.3.3(a), the sign of middle right of $\rho^{(3)}_{xxx}(\boldsymbol{r})$ for ethylene obtained using HF method with 6-311G basis set is shown to be negative, while the middle left of $\rho^{(3)}_{xxx}(\boldsymbol{r})$ is shown to be positive. The right and left side of the plane in Fig.3.3 corresponds to positive and negative *x* direction, respectively. Therefore, the sign of contribution of middle regions of $\rho^{(3)}_{xxx}(\boldsymbol{r})$, which are considered to reflect the σ electron of ethylene, to the total γ_{xxxx} of ethylene obtained by using HF method with 6-311G basis set is found to be positive. On the other hand, the sign of above and below right regions of $\rho^{(3)}_{xxx}(\boldsymbol{r})$ for ethylene obtained by using HF method with 6-311G basis set is shown to be positive, while the above and below left regions of $\rho^{(3)}_{xxx}(\boldsymbol{r})$ are shown to be negative (See Fig.3.3(a)). Therefore, the sign of contribution of above and below regions of $\rho^{(3)}_{xxx}(\boldsymbol{r})$, which are considered to reflect the π electron of ethylene, to the total γ_{xxxx} obtained using HF method with 6-311G basis set is found to be negative. The areas of above and below $\rho^{(3)}_{xxx}(\boldsymbol{r})$ regions obtained HF method with 6-311G basis set are shown to be much larger than the area of middle regions of $\rho^{(3)}_{xxx}(\boldsymbol{r})$. Therefore, it is found that the negative contribution originating in π electron at the HF/6-311G level exceeds the positive contribution originating in σ electron. The feature of $\rho^{(3)}_{xxx}(\boldsymbol{r})$ distribution is considered to support the γ_{xxxx} value obtained by using HF method with 6-311G basis set.

Figure 3.3(b) shows the γ_{xxxx} value and $\rho^{(3)}_{xxx}(\boldsymbol{r})$ distribution obtained using HF method with 6-311G+p/d extended basis set. The basis set dependency of γ_{xxxx} for ethylene can be clarified by comparing the $\rho^{(3)}_{xxx}(\boldsymbol{r})$ distribution at the HF/6-311G+*f*/*d* with the $\rho^{(3)}_{xxx}(\boldsymbol{r})$ distribution at the HF/ 6-311G. As shown in Fig.3.3(b), two new distribution of $\rho^{(3)}_{xxx}(\boldsymbol{r})$ are shown to appear at far right and left regions. The sign of far right regions of $\rho^{(3)}_{xxx}(\boldsymbol{r})$ at the HF/6-311G+*f*/*d* is shown to be negative, while the far left region of $\rho^{(3)}_{xxx}(\boldsymbol{r})$ is shown to be positive. Therefore, the contribution to the total γ_{xxxx} of ethylene at the HF/6-311G+*f*/*d* by the far right and left regions of $\rho^{(3)}_{xxx}(\boldsymbol{r})$ is positive. This contribution is considered to reflect the effect of augmented diffuse and polarization *f*/*d* functions. Since the distance between far right and left regions of $\rho^{(3)}_{xxx}(\boldsymbol{r})$ is relatively large, the contribution of these regions is expected to be large. Judging from the positive γ_{xxxx} value at the HF/6-311G+*f*/*d*, the positive contribution of far right and left regions of $\rho^{(3)}_{xxx}(\boldsymbol{r})$ is considered to exceed the negative contribution of the above and below regions of $\rho^{(3)}_{xxx}(\boldsymbol{r})$.

Figure 3.3(c) shows the γ_{xxxx} value and $\rho^{(3)}_{xxx}(\boldsymbol{r})$ distribution obtained by using QCISD method with 6-311G+*f*/*d* basis set. In comparison of Fig.3.3(c) with Fig.3.3(b), the $\rho^{(3)}_{xxx}(\boldsymbol{r})$ distribution at the QCISD level is shown to be changed dramatically. Namely, the signs of middle regions of $\rho^{(3)}_{xxx}(\boldsymbol{r})$, which are considered to originate in σ electrons of ethylene, is shown to be reversed. The signs of the above and below regions of $\rho^{(3)}_{xxx}(\boldsymbol{r})$, which are considered to originate in π electrons, are also shown to be reversed, beside the area of the above and below regions of $\rho^{(3)}_{xxx}(\boldsymbol{r})$ are shown to be reduced. On the other hand, the far right and left regions of $\rho^{(3)}_{xxx}(\boldsymbol{r})$ are shown to expand. The γ density analysis is found to elucidate the electron-correlation effect

on γ for ethylene more remarkably than the analysis based only on the difference between the HF and the QCISD γ values.

(a) HF/6-311G γ_{xxxx} = -189 a.u.

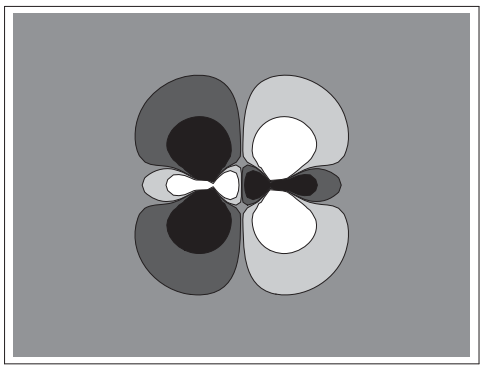

(b) HF/6-311G+*f*/*d* γ_{xxxx} = 899 a.u.

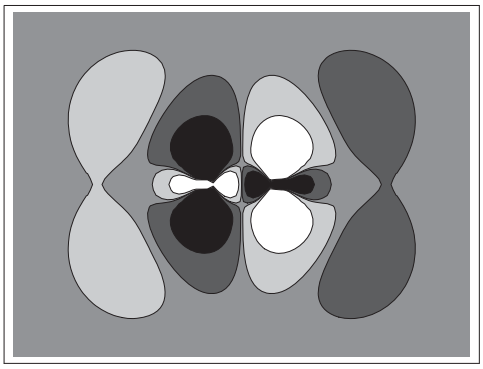

(c) QCISD/6-311G+*f*/*d* γ_{xxxx} = 899 a.u.

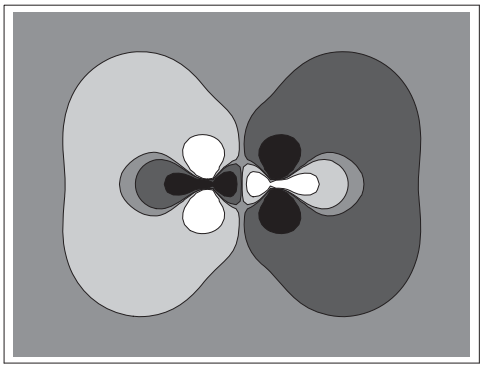

Fig.3.3 γ_{xxxx} values and contour plots of $\rho^{(3)}_{xxx}(\boldsymbol{r})$ distribution on the σ_v plane of ethylenes by using the HF and QCISD methods. Contours are drawn from -10.0 to 10.0 a.u. Lighter areas represent the spatial regions with larger $\rho^{(3)}_{xxx}(\boldsymbol{r})$ values. The white regions correspond to those with $\rho^{(3)}_{xxx}(\boldsymbol{r})$ larger than 10.0 a.u., while the black regions correspond to those with $\rho^{(3)}_{xxx}(\boldsymbol{r})$ smaller than -10.0 a.u.

Chapter 4 Static second hyperpolarizabilities of nitroxide radical and formaldehyde

In this study [105], we investigate the basis set and electron-correlation dependencies of γ for H_2NO and formaldehyde (H_2CO), which is considered as the reference closed-shell system. In general, the γ exhibit large electron-correlation and basis-set dependencies. Moreover, the electronic states of radical species itself have large electronic-correlation dependency. These unique feature of radical species, electron-correlation effects for γ and a necessity of using extended basis sets are shown by using hyperpolarizability density analysis.

4.1. Calculation methods and molecular geometries

Figure 4.1 shows molecular geometries of H_2NO and H_2CO optimized by the ab initio Møller-Plesset second order perturbation (MP2) method using 6-31G basis set, the coordinate axis and the reflection plane σ_v.

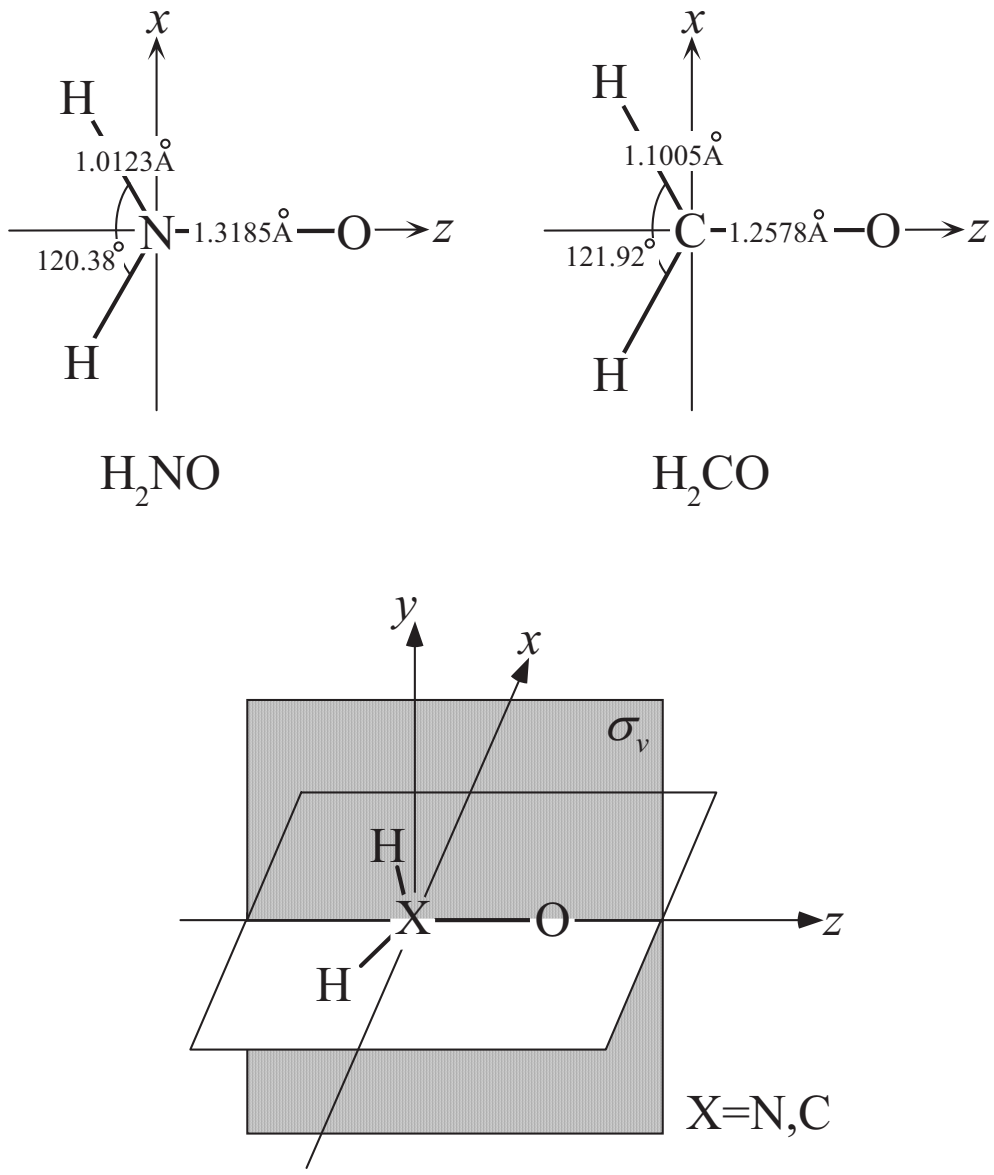

Fig.4.1. Molecular geometries of H_2NO and H_2CO optimized by the ab initio Møller-Plesset second-order (MP2) method using 6-31G basis set. The σ_v plane represents the reflection plane of H2XO (X=N or C).

Firstly, some standard (minimal (STO-3G) and split-valence (6-31G)) and extended basis sets augmented by diffuse and polarization functions (*p* and *d*), which are known to be essential for reproducing semi-quantitative γ, in order to investigate the basis set dependence of γ. The extended basis sets used in this study are given in Table 4.1. The first three extended basis sets, *i.e.*, 6-31G+*p*, 6-31G+*d* and 6-31G+*pd*, are attempted to clarify the effects of the augmentations on C, N and O atoms, while the last two basis sets, *i.e.*, 6-31G+*pd*/*s* and 6-31G+*pd*/*sp*, are done for the augmentations on H atoms. These exponents are all determined by the even tempered method.

Secondly, the effects of electron correlations on γ are examined by performing the following various electron correlation methods, *i.e.*, MP2, MP3, MP4DQ, MP4SDQ, MP4SDTQ, QCID (=CCD), QCISD, CCSD and CCSD(T). Here, the symbols S, D, T and Q imply the inclusion of the correlation effects caused by the single, double, triple and quadruple excitations, respectively. The CC method can include these correlation effects till infinite order. The QCI method is known to be able to well reproduce the total energy calculated by the CC method.

Main components of γ (γ_{zzzz}) of H_2NO and H_2CO are calculated by the Eq.(A.6). The minimum field strength employed here is 0.01 a.u., which seems to be most appropriate to assess the calculated results.

Table 1 Exponential Gaussian orbital parameters for polarization and diffuse functions.

	C		N		O		H	
	p	d	*p*	*d*	*p*	d	*s*	p
6-31G+*p*	0.0523		0.0582		0.0719			
6-31G+*d*		0.0523		0.0582		0.0719		
6-31G+*pd*	0.0523	0.0523	0.0582	0.0582	0.0719	0.0719		
6-31G+*pd*/*s*	0.0523	0.0523	0.0582	0.0582	0.0719	0.0719	0.0406	
6-31G+*pd*/*sp*	0.0523	0.0523	0.0582	0.0582	0.0719	0.0719	0.0406	0.0406

4.2. Results and discussion

4.2.1. Basis set dependence of γ_{zzzz}

Figure 4.2 shows variations in γ_{zzzz} of H_2NO and H_2CO for various types of basis sets and electron correlation effects. The figures for H_2NO and H_2CO indicates that the basis sets in the absence of diffuse *p* and *d* functions (STO-3G and 6-31G) cannot provide the sufficient magnitude of γ_{zzzz} and an adequate description of relative electron correlation dependence of γ_{zzzz}. It is shown that the extended basis sets including either diffuse *p* or *d* function (6-31G+*p* and 6-31G+*d*) also provide insufficient magnitudes of γ_{zzzz} for these systems, though the γ_{zzzz} values become relatively larger than those by the standard basis sets. The extended basis sets including both diffuse *p* and *d* functions (6-31G+*pd*, 6-31G+*pd*/*s* and 6-31G+*pd*/*sp*) are found to be able to provide sufficiently large $|\gamma_{zzzz}|$ and reliable variations of γ_{zzzz} with respect to electron correlation effects. As also seen from the results in γ_{zzzz} by using 6-31G+*pd*, 6-31G+*pd*/*s* and 6-31G+*pd*/*sp* basis sets, the augmentation of diffuse *s* and/or *p* functions on H atoms tends to negligibly effect the γ_{zzzz} in this case. Therefore, the γ_{zzzz} calculated by using the 6-31G+*pd* basis set are used in the following discussion concerning electron correlation dependence of γ_{zzzz}.

4.2.2. Electron correlation dependence of γ_{zzzz}

Firstly, we shall confine our attention to the correlation effects on γ_{zzzz} by various kinds of ab initio MO based methods. Apparently, the γ_{zzzz} of H_2NO and H_2CO calculated by the MP2 method are shown to be relatively equal to the γ_{zzzz} calculated by the CCSD method. On the other hand, we can see some remarkable differences in the electron correlation dependence of γ_{zzzz} between these compounds. In particular, it is revealed that the correlation effects by MP2 decrease the $|\gamma_{zzzz}|$ of H_2NO, while the $|\gamma_{zzzz}|$ of H_2CO is increased by including the correlation effects by MP2. The correlation effects by MP3 are found to decrease the MP2 $|\gamma_{zzzz}|$ values for H_2NO and H_2CO. From the γ_{zzzz} by some MP4 level calculations, it is shown that the effects of S and T excitations increase the $|\gamma_{zzzz}|$ of H_2CO, whereas, for H_2NO, the effects of S excitations decrease the $|\gamma_{zzzz}|$ contrary to the effects of T excitations. From the comparison between the CCD and MP4DQ γ_{zzzz} for H_2NO and H_2CO, it is presumed that the correlation effects originating higher-order D excitations beyond the fourth order are negligible. The $|\gamma_{zzzz}|$ of H_2NO calculated by the CCSD method is shown to be slightly smaller than that by the CCD method. In contrast, the $|\gamma_{zzzz}|$ of H_2CO calculated by the CCSD method is shown to be considerably larger than that by the CCD method. From these results, we can recognize that the correlation corrections originating from higher-order S excitations are needed to evaluate the $|\gamma_{zzzz}|$ quantitatively. In addition, as shown from the fact that the γ_{zzzz} of H_2NO and H_2CO by the CCSD method are close to those by the MP4SDQ method, it is clear that the higher-order

correlation effects caused by S and D excitations beyond the fourth order little contribute to the γ_{zzzz} for these compounds. Although the γ_{zzzz} of H_2NO by the QCISD method are shown to be relatively larger than those by the CCSD method, the QCISD method is considered to be able to provide qualitatively correct description of the γ_{zzzz} judging from its approximation level, which is similar to that of the CCSD method. Further, the $|\gamma_{zzzz}|$ of H_2NO and H_2CO by the CCSD(T) method are shown to be nearly equal to those by the CCSD method, respectively. It is concluded that the γ_{zzzz} by the CCSD(T) and CCSD methods are sufficiently converged values for H_2NO and H_2CO judging from the magnitudes and signs of γ_{zzzz}, and they can be qualitatively well reproduced by the MP2 method.

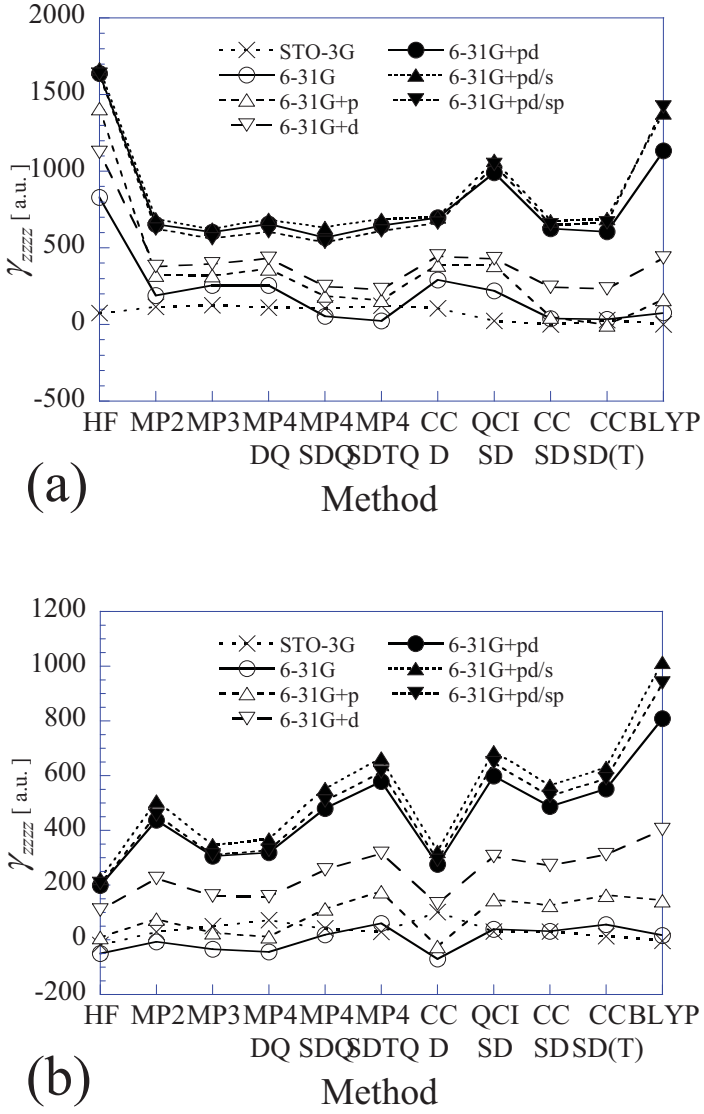

Fig.4.2. Variations of the γ_{zzzz} values of (a) H_2NO and (b) H_2CO for various kinds of basis sets (STO-3G, 6-31G, 6-31G+*p*, 6-31G+*d*, 6-31G+*pd*, 6-31G+*pd*/*s* and 6-31G+*pd*/*sp*) and electron correlation methods (HF, MP2, MP3, MP4DQ, MP4SDQ, MP4SDTQ, CCD, QCISD, CCSD, QCISD(T) and BLYP).

Next, we consider the γ_{zzzz} calculated by the BLYP method. Although there are various types of DFT approaches, the BLYP method is found to reproduce the α, β and γ comparable to those at the ab initio MP2 level for closed-shell organic compounds [106]. As can be seen from Fig.4.2, the γ_{zzzz} of H_2NO and H_2CO by the BLYP method are shown to be relatively larger than those by the CCSD(T) method. In the next section, we investigate the spatial contributions to these γ_{zzzz} by using the plots of $\rho^{(3)}_{zzz}(\boldsymbol{r})$ in order to reveal the characteristics of electron correlation effects.

4.2.3. Elucidation of spatial contributions to γ_{zzzz} by the hyperpolarizability density analysis

In this section, we explore the effects of basis sets and electron correlations on γ_{zzzz} from the view point of the spatial contributions of γ_{zzzz} density derivative ($\rho^{(3)}_{zzz}(\boldsymbol{r})$). Figures 4.3 and 4.4 give contour plots of $\rho^{(3)}_{zzz}(\boldsymbol{r})$ on the σ_v planes of H_2NO and H_2CO shown in Fig.4.1 for several kinds of electron correlation methods. Lighter regions represent the spatial regions with larger $\rho^{(3)}_{zzz}(\boldsymbol{r})$ values. The white regions correspond to the regions with $\rho^{(3)}_{zzz}(\boldsymbol{r})$ that is larger than 0.625 a.u., while the black regions correspond to the regions with $\rho^{(3)}_{zzz}(\boldsymbol{r})$ that is smaller than -0.625 a.u.

From the plot of $\rho^{(3)}_{zzz}(\boldsymbol{r})$ by the HF method using 6-31G basis set (HF/6-31G) for H_2NO (Figures 4.3(a) and (b)), diffuse *p* and *d* functions are shown to enlarge the regions of π electron contributions to γ_{zzzz}. On the other hand, for H_2CO (Figures 4.4(a) and (b)), the augmentations of diffuse *p* and *d* functions are found to create the outer regions which possess large π electron contributions (positive) with the opposite sign to the internal small π electron contributions (negative). It is also found that the π electrons provide the main contributions which are opposite in sign to those of σ electrons (in the direction of N-O and C-O bond axis). Further, it is shown that the $\rho^{(3)}_{zzz}(\boldsymbol{r})$ distribution of π electrons for H_2CO at the HF/6-31G (Fig.4.4(a)) provide negative contributions to the total $\rho^{(3)}_{zzz}(\boldsymbol{r})$ contrary to the case of H_2NO at the HF/6-31G (Fig.4.3(a)).

As seen from the comparison among the plots of $\rho^{(3)}_{zzz}(\boldsymbol{r})$ distribution for H_2CO at the HF/6-31G+*pd*, MP2/6-31G+*pd*, CCD/6-31G+*pd* and QCISD/6-31G+*pd* (Figures 4.4(b), (c), (d) and (e)), the outer spatial contributions are enlarged by the electron correlation effects. This leads to the increase of the $\rho^{(3)}_{zzz}(\boldsymbol{r})$ distribution of H_2CO at the HF/6-31G+*pd*. The plots of $\rho^{(3)}_{zzz}(\boldsymbol{r})$ distribution for H_2CO at the CCD/6-31G+*pd* and QCISD/6-31G+*pd* (Figures 4.4(d) and (e)) tell us that the inclusion of the infinite-order single excitations slightly reduce the size of internal regions and enlarge the outer regions. It is also found that the distribution of $\rho^{(3)}_{zzz}(\boldsymbol{r})$ of H_2CO at the QCISD/6-31G+*pd* (Fig.4.4(e)) is very similar to that at the BLYP/6-31G+*pd* (Fig.4.4(f)). It follows that the BLYP/6-31G+*pd* method can provide the semi-quantitative γ_{zzzz} values including sufficient electron correlation effects for this closed-shell system.

(a) HF/6-31G γ_{zzzz} = 830 a.u.

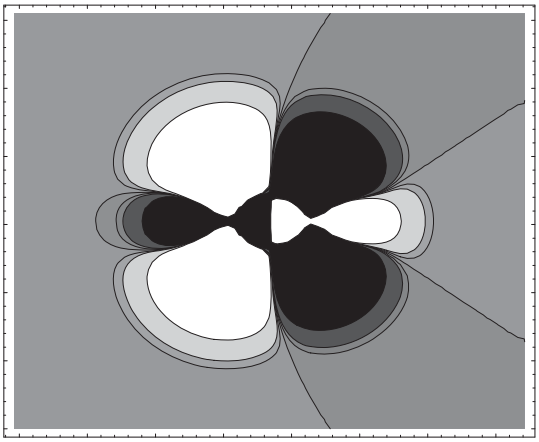

(b) HF/6-31G+pd γ_{zzzz} = 1670 a.u.

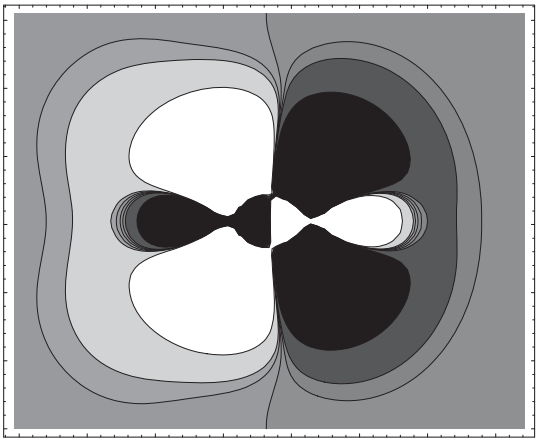

(c) MP2/6-31G+pd γ_{zzzz} = 786 a.u.

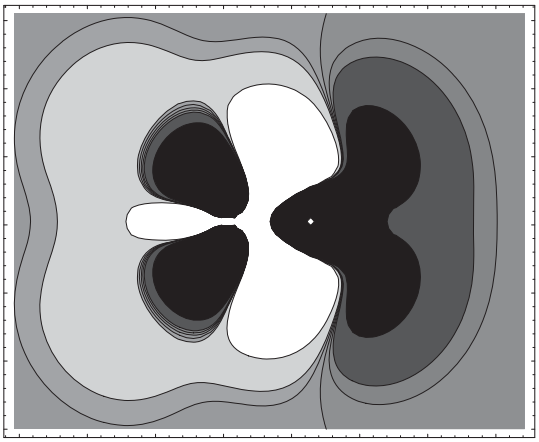

(d) CCD/6-31G+pd γ_{zzzz} = 777 a.u.

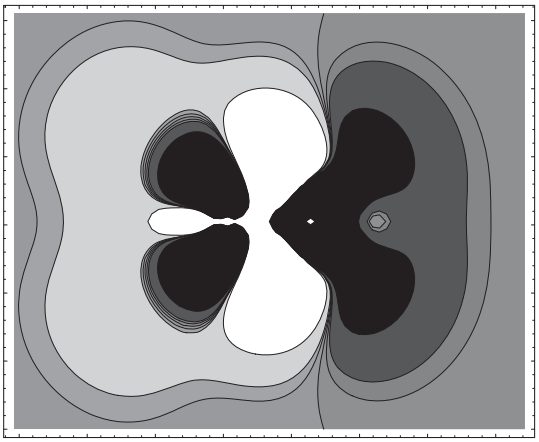

(e) QCISD/6-31G+pd γ_{zzzz} = 995 a.u.

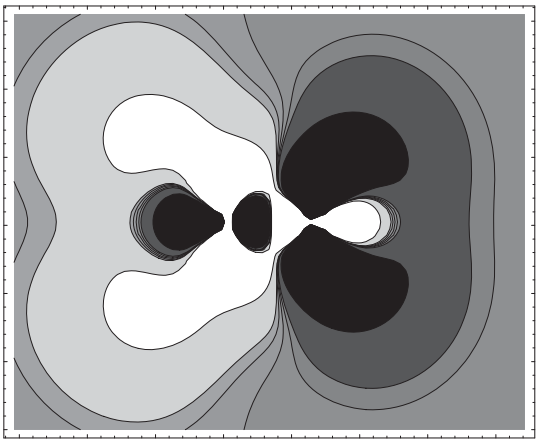

(f) BLYP/6-31G+pd γ_{zzzz} = 1130 a.u.

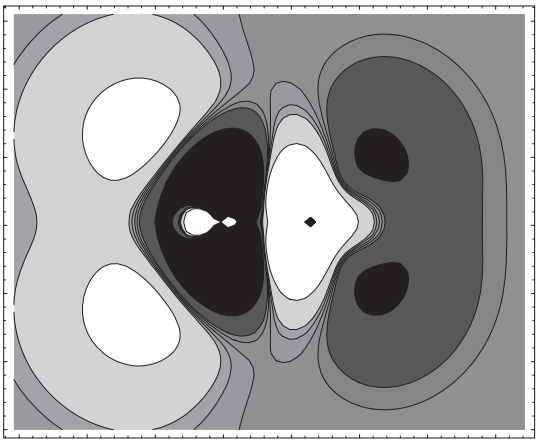

Fig.4.3. Contour plots of γ_{zzzz} densities on the σ_v'+1.0 plane of H_2NO (fig. 1) and γ_{zzzz} values for various calculation methods (HF, MP2, CCD, QCISD and BLYP). Contours are drawn at 0.625, 0.125, 0.0625, 0.0, -0.0625, -0.125 and -0.625 a.u..

(a) HF/6-31G γ_{zzzz} = -49.1 a.u.

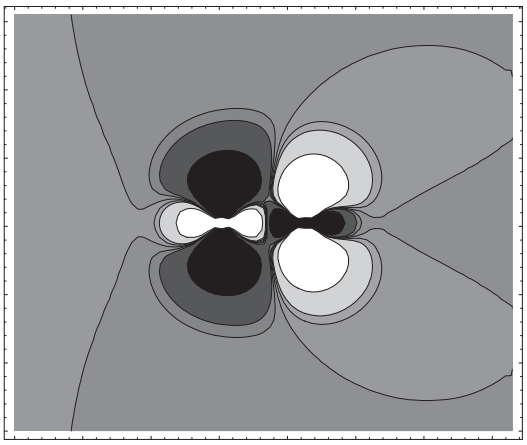

(b) HF/6-31G+pd γ_{zzzz} = 199 a.u.

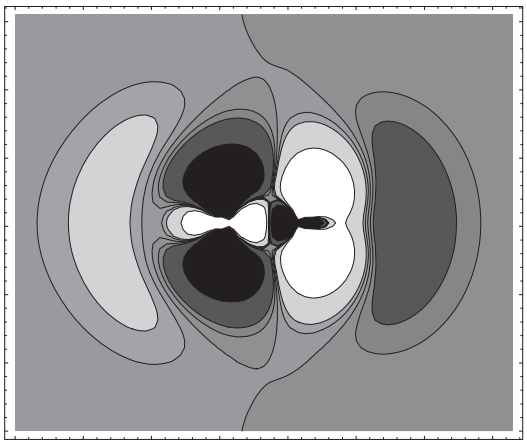

(c) MP2/6-31G+pd γ_{zzzz} = 437 a.u.

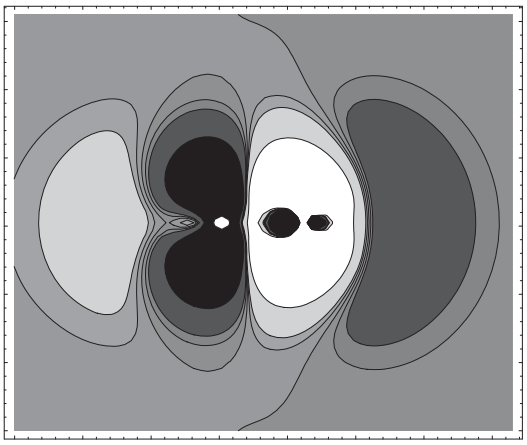

(d) CCD/6-31G+pd γ_{zzzz} = 277 a.u.

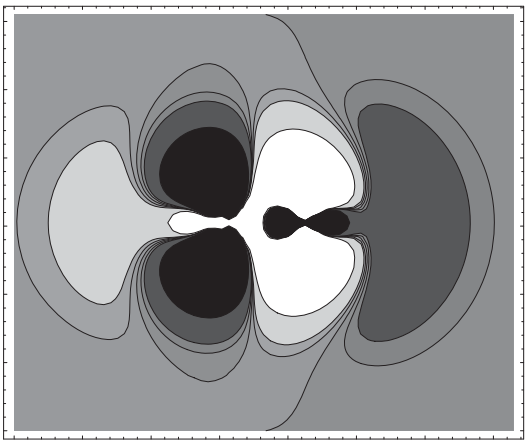

(e) QCISD/6-31G+pd γ_{zzzz} = 599 a.u.

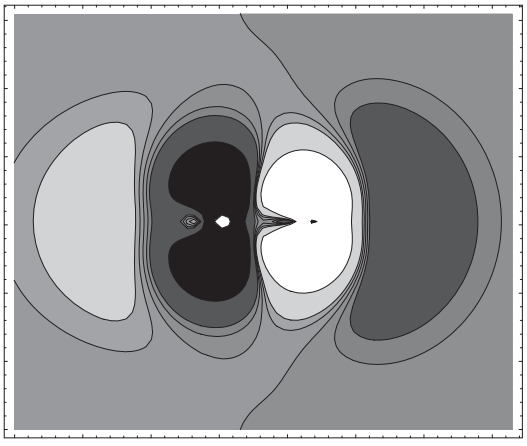

(f) BLYP/6-31G+pd γ_{zzzz} = 809 a.u.

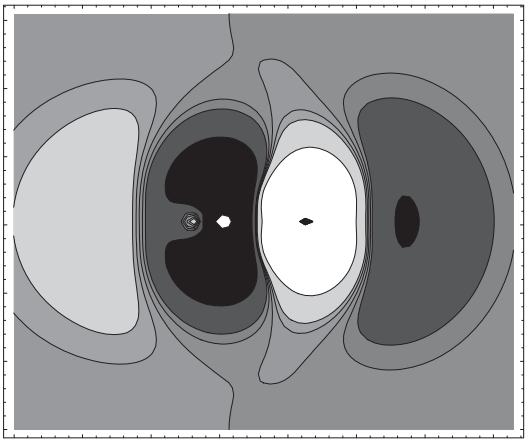

Fig.4.4. Contour plots of $\rho^{(3)}_{zzz}(\boldsymbol{r})$ distribution on the σ_v plane of H_2CO (fig. 1) and γ_{zzzz} for various calculation methods (HF, MP2, CCD, QCISD and BLYP). Contours are drawn at 0.625, 0.125, 0.0625, 0.0, -0.0625, -0.125 and -0.625 a.u.

In contrast, there are remarkable qualitative differences among the distributions of $\rho^{(3)}_{zzz}(\boldsymbol{r})$ distribution for H_2NO at the HF/6-31G+*pd*, CCD/6-31G+*pd* and QCISD/6-31G+*pd* (Figs. 4.3(b), (d) and (e)). The distribution of $\rho^{(3)}_{zzz}(\boldsymbol{r})$ distribution for H_2NO at the MP2/6-31G+*pd* (Fig.4.3(c)) is shown to be nearly equal to that at the CCD/6-31G+*pd* (Fig.4.3(d)). From Figures.4.3(c) and (d), the infinite-order D excitations are found to vanish the regions contributed by σ electrons and newly create the regions with negative sign inside π electron regions with positive contributions. Further, the inclusion of the infinite-order S excitations extremely change the distributions at the CCD/6-31G+*pd* as shown in Fig.4.3(e). The characteristics of variation in a distribution of $\rho^{(3)}_{zzz}(\boldsymbol{r})$ caused by S excitation effects involved in the QCISD method are presumed to be somewhat similar to those of the CCSD method judging from the similarity of the approximation level between the QCISD and CCSD methods. The distribution of *p* electron $\rho^{(3)}_{zzz}(\boldsymbol{r})$ that is larger than 0.625 a.u. at the QCISD/6-31G+*pd* (Fig.4.3(e)) is shown to be squeezed and be stretched to more outside regions compared with that at the HF/6-31G+*pd* (Fig.4.3(b)). It is also shown that the distribution of $\rho^{(3)}_{zzz}(\boldsymbol{r})$ at the BLYP/6-31G+*pd* is different from that at the QCISD/6-31G+*pd* in the internal bond region, though the calculated γ_{zzzz} values are very similar with each other. The good agreement between these two γ_{zzzz} seems to be achieved by the primary contributions from the outer regions which exhibit very similar distributions of $\rho^{(3)}_{zzz}(\boldsymbol{r})$ between two methods.

From the above results, we can recognize that the spatial distribution of $\rho^{(3)}_{zzz}(\boldsymbol{r})$ for H_2NO hard to be reproduced correctly without higher-order electron correlation effects in comparison with H_2CO, even if the calculated total γ_{zzzz} for H_2NO calculated by including low-order correlation effects comes to be unexpectedly in good agreement with the γ_{zzzz} with sufficient correlation effects.

4.3. Concluding remarks

In this study, it is found that the MP2 calculation using split-valence plus diffuse *p* and *d* basis set (6-31G+*pd*) can reproduce the γ_{zzzz}, which are in semi-quantitatively good agreement with those including sufficient electron correlation. However, it is also found that the correct distributions of γ_{zzzz} for H_2NO cannot be reproduced at the MP2 level in contrast to the case of H_2CO. In such a case, the CCSD and QCISD calculations are expected to be essential for obtaining qualitatively correct description of the distribution of $\rho^{(3)}_{zzz}(\boldsymbol{r})$.

From the plots of $\rho^{(3)}_{zzz}(\boldsymbol{r})$ distribution for H_2CO, the BLYP method with sufficiently augmented basis sets is shown to be able to reproduce the γ_{zzzz} and distributions of $\rho^{(3)}_{zzz}(\boldsymbol{r})$ at the QCISD level. In contrast, for H_2NO, the BLYP method is found to provide rather different distribution of $\rho^{(3)}_{zzz}(\boldsymbol{r})$ in the internal bond region compared to that by the QCISD method, though the calculated total γ_{zzzz} becomes very similar to that by the QCISD method. The good agreement between these total γ_{zzzz} values is considered to be caused by the primary contributions from the outer regions which provide similar distributions of $\rho^{(3)}_{zzz}(\boldsymbol{r})$ between the QCISD and

BLYP method. More profound investigations of the hyperpolarizabilities and the distributions of hyperpolarizability density derivatives for various kinds of open-shell systems are necessary for elucidating the applicability of the DFT approach to the calculation of hyperpolarizabilities of open-shell systems.

The extremely large electron correlation effects detected in open-shell nitroxide system (H_2NO) are presumed to be caused by the remarkable fluctuation of charges on N-O group, the effects of which are found to be evaluated qualitatively by the infinite-order single excitation correlations involved in the CCSD and QCISD methods. The remarkable fluctuation of charges on H_2NO is expected to be a peculiarity of open-shell system. As mention in chapter 1, a symmetric system with fluctuation of charges have enormous possibility for realizing of the organic system with negative γ.

Chapter 5 Second hyperpolarizabilities of symmetric small-size radicals

In chapter 4, it is found that an open-shell system, H_2NO, have unique electron-correlation dependency of γ. This large electron-correlation dependency of γ for H_2NO is considered to be caused by the remarkable fluctuation of charges on N-O group. It is expected that the fluctuation of charges is shown in some open-shell systems. As mentioned in chapter 2, the structure-property correlation rule based on time-dependent perturbation theory indicates that a system with large symmetric resonance structure with inversible polarization (SRIP) contribution to the ground state, plays an important role. Namely, a system whose ground state has a large contribution of SRIP tends to exhibit negative γ and indicates remarkable electron-correlation dependence of γ. The existence of charge fluctuation is expected to lead to increase in SRIP contribution for symmetric radical systems. In this chapter, the values of γ are investigated in order to inspect the effect of SRIP for two types of iso-electric small symmetric radicals, *i.e.*, one-center radicals [107] and three-center radicals [108,109].

5.1. Second hyperpolarizabilities of one-center radicals

In this study, we investigate γ for small charged and neutral radicals, *i.e.*, BH_3^-, CH_3 and NH_3^+. They are referred to as one-center radicals. All these radicals have 9 electrons. Therefore, differences in the feature of γ are expected to reflect each charged state.

5.1.1. Geometries of one-center radicals and calculation method

Figure 5.1 shows the SRIP of the one-center radicals. The one-center radicals are assumed to be planar structures. Their geometries are optimized by using the B3LYP method with 6-311G(3*d*2*f*,3*p*2*d*) basis set.

It is well-known that using extended basis sets, which are augmented by diffuse and polarization functions, is indispensable for reproducing semi-quantitative γ, especially for small systems. Firstly, we investigate the basis set dependencies of γ for one-center radicals. We employed some standard and extended basis sets. All the exponents are determined by the even-temper method.

As mentioned before, an effect of electron correlation on γ is important, especially for the system with large SRIP contribution. The electron-correlation effects on γ for one-center radicals are examined by the MP*n* and CC methods.

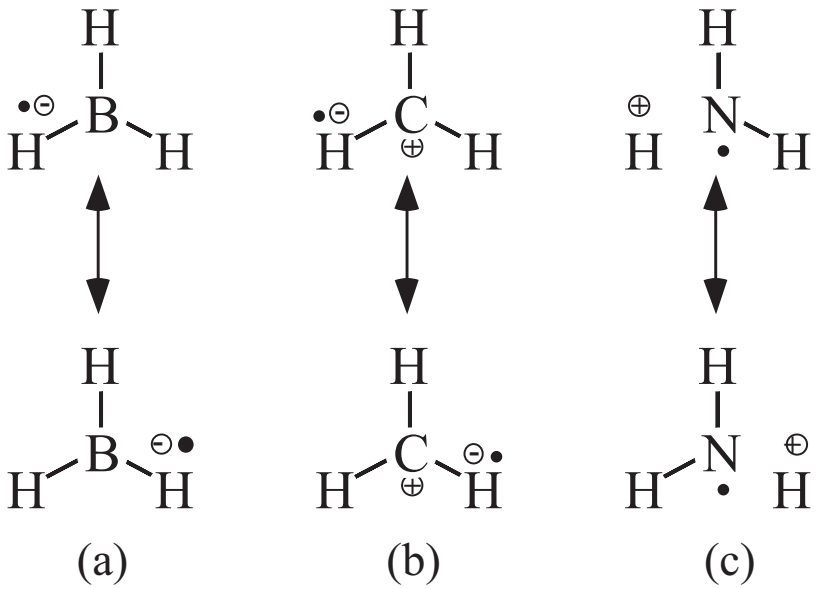

Fig.5.1. Symmetric resonance structures with inversible polarization (SRIP) for (a) BH_3^- (B-H=1.2118Å), (b) CH_3 (C-H=1.0776Å) and (c) NH_3^+ (C-H=1.0237Å). The structures of all radicals are optimized using B3LYP/6-311(3*d*2*f*,3*p*2*d*).

We confine our attention to the main components of γ for one-center radical, *i.e.*, γ_{xxxx}. The γ_{xxxx} values are calculated by the FF method. To elucidate the spatial contribution to the γ_{xxxx}, the hyperpolarizability density analysis is applied.

5.1.2. Results and discussion

5.1.2.1. Basis set dependency

Figure 5.2 shows electron-correlation and basis-set dependencies of γ_{xxxx} for the one-center radicals. It is found that one-center radicals, especially BH_3^-, have large basis set dependencies. For BH_3^- (See Figs. 5.2(a) and 5.2(b)), the effects of polarization functions are considered to enhance the each electron-correlation effects on γ of BH_3^-. As shown in Fig.5.2(a), the difference in the types of adding diffuse and polarization functions is considered to represent a degree of enhancement of the electron-correlation effect on γ of BH_3^-. Namely, the diffuse d/f functions are shown to slightly enhance the electron-correlation effect on γ for BH_3^-, while the diffuse *f/d* functions are shown to enormously enhance the effects. The augmentation of inner polarization *d/p* functions is also shown to enhance the electron-correlation effect on γ for BH_3^- (See Fig.5.2(b)). However, little difference is shown between the electron-correlation effects on γ of BH_3^- by using 6-311G(2*d*,2*p*)+*f/d* basis set and those by 6-311G(3*d*,3*p*)+*f/d* basis set. Namely, the effect of adding polarization functions for BH_3^- is considered to be sufficiently converged at 6-311G(3*d*,3*p*)+*f/d* basis set.

For CH_3 (See Figs. 5.2(c) and 5.2(d)), the electron-correlation dependencies of γ by using the basis sets are shown to be similar to each other. The augmentations of diffuse and polarization functions are shown to enhance electron-correlation effect on γ of CH_3 (See Fig.5.2(c)). On the other hand, the augmentations of inner polarization *d/p* functions to the extended 6-311G+*f/d* basis set are shown to reduce the electron-correlation effect on γ of CH_3 (See Fig.5.2(d)). Such reduction of electron-correlation effect on γ for CH_3 is considered to be innegligible. Namely, the use of both diffuse *f/d* function and inner polarization *d/p* functions are found to be indispensable for reproducing reliable γ.

As shown in Figs. 5.2(e) and 5.2(f), the magnitudes of γ for NH_3^+ by using extended basis sets are shown to be larger than those by using standard 6-311G basis set at all electron-correlation levels. However, as shown in Fig.5.2(e), the variation in γ of NH_3^+ for the electron-correlation methods is considered to depend on the types of extended basis sets used. For example, the γ of NH_3^+ obtained using 6-311G+*d/p* basis set at the MP*n* and the CC levels are smaller than those at the HF level, while the γ using 6-311G+*f/d* basis set at the CC levels are larger than those at the HF level. However, the variations in γ of NH_3^+ by using 6-311G+*f/d*, 6-311G+*pf/sd* and 6-311G+*df/pd* are similar to each other. Namely, the electron-correlation dependencies of γ for NH_3^+ using the extended basis sets augmented by diffuse and polarization *p/s* or *d/p* functions to the extended 6-311G+*f/d* basis set are considered to be almost same as the electron-correlation dependency using 6-311G+*f/d* basis set. On the contrary, as shown in

Fig.5.2(f), the electron correlation-dependencies of γ for NH_3^+ using the extended basis sets augmented inner polarization *d/f* functions to the 6-311G+*f/d* basis set are shown to be quite different from each other. Namely, the use of the extended basis sets, *e.g.*, 6-311G(3*d*,3*p*)+*f/d* is considered to be essential for describing the electronic states of NH_3^+, so that the basis set dependency of γ for NH_3^+ is shown to be enormously large. However, electron-correlation dependency of γ for NH_3^+ is shown to be small by using the 6-311G(3*d*,3*p*)+*f/d* basis set. Namely, this basis set is presumed to compensate deficiency in electron-correlation correction at the lower-order levels.

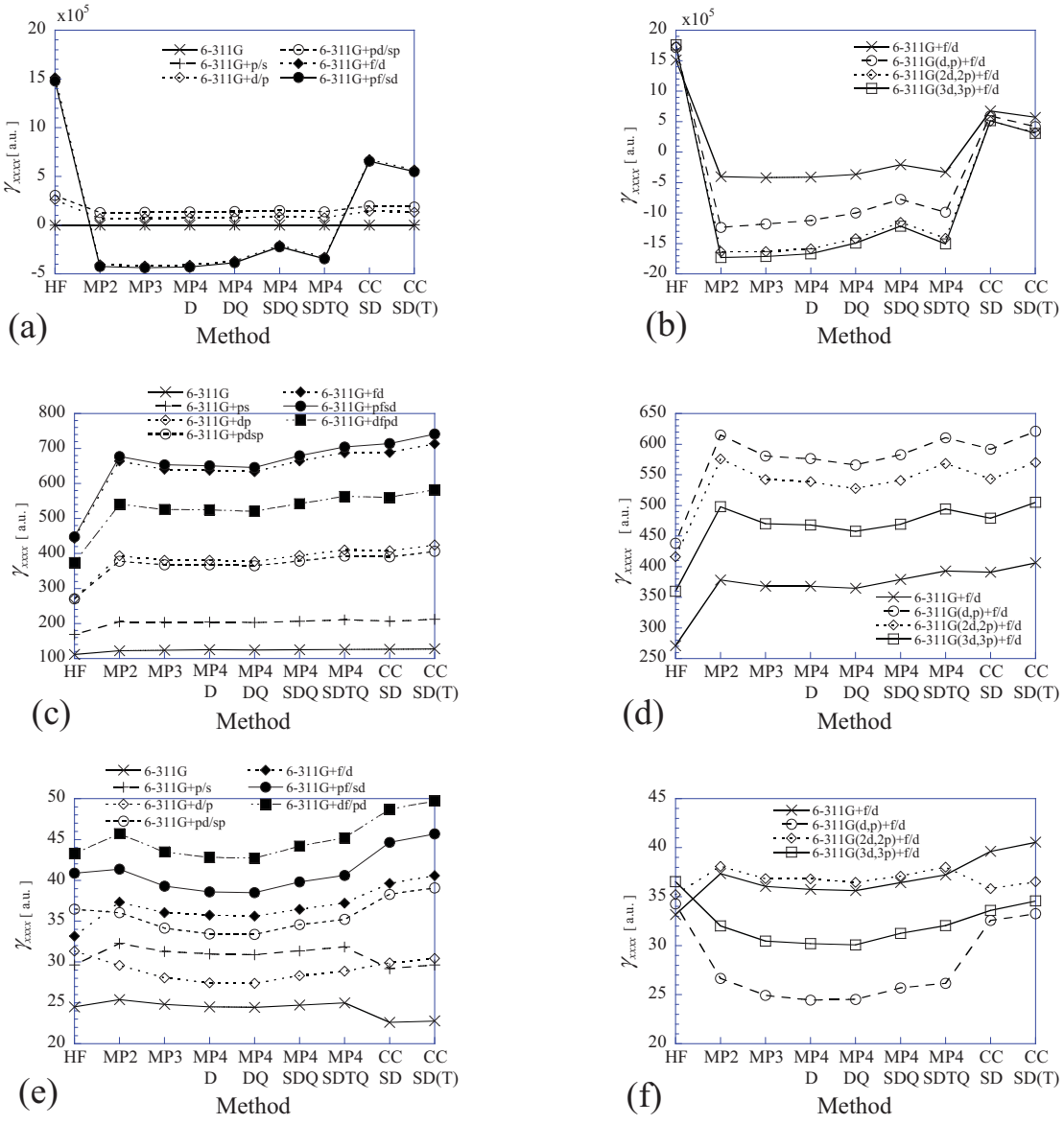

Fig.5.2. Variations in the γ_{xxxx} of three-center radicals ((a) and (b) BH_3^-; (c) and (d) CH_3; (e) and (f) NH_3^+) for various basis sets and electron correlation methods.

Jading from the basis-set dependencies of the γ_{xxxx} for radicals, the 6-311G(3d,3p)+*f/d* basis set is expected to provide precisely γ_{xxxx} for each radicals at all electron-correlation levels, so that the 6-311G(3d,3p)+*f/d* is used in the following discussion on the electron-correlation dependencies of the γ_{xxxx} for each radicals.

5.1.2.2. Electron-correlation dependency

As shown in Fig.5.2, there are remarkable differences in the magnitude and electron-correlation dependence of γ_{xxxx} for the radicals. The $|\gamma_{xxxx}|$ of BH_3^- is found to be the largest and $|\gamma_{xxxx}|$ of NH_3^+ is also found to be the smallest. As shown in Fig.5.2 (a), a remarkable electron-correlation dependency is observed for BH_3^-. All the MP*n* methods provide large negative γ_{xxxx} for BH_3^-, while CC methods provide positive γ_{xxxx}. Namely, higher-order electron correlation methods, *i.e.*, CCSD method at least, are found to be indispensable for obtaining a reliable γ_{xxxx} of BH_3^-. As shown in Fig.5.2(b), electron-correlation effect on the γ_{xxxx} of CH_3 is not small. However, electron-correlation effect beyond the MP2 level is considered to be relatively small. The electron-correlation dependence of NH_3^+ is obviously small as shown in Fig.5.2 (c). It is found from these results that electron-correlation dependence of γ_{xxxx} is mainly determined by charged states for these radicals.

The remarkable electron-correlation dependence of γ_{xxxx} for BH_3^- is considered to originate in the SRIP (see Fig.5.1(a)) contribution to the ground state of BH_3^-. However, the sign of γ_{xxxx} for BH_3^- at the CCSD(T) level is shown to be positive. If the SRIP of BH_3^- contributed significantly to the ground state, BH_3^- would have negative γ_{xxxx}. Therefore, SRIP contribution for BH_3^- is considered not to be so large. This implies that the resonant structures are not so stable. As can be seen from Fig.5.1, it is presumed that the resonant structures of SRIP for CH_3 and NH_3^+ are unstable and then the SRIP contributions become smaller compared with the case of BH_3^-.

5.1.2.3. γ density analysis

Figures 5.3 - 5.5 show the result of γ_{xxxx} density analysis for the radicals by using HF, MP2, QCISD and B3LYP methods. All the γ density distributions are obtained using extended 6-311G(3*d*,3*p*)+*f/d* (Figs. 5.3(b), 5.4(b) and 5.5(b)) basis set. A plane at which the γ_{xxxx} densities are drawn is located at 1.0 a.u. above the molecular plane.

As shown in Fig.5.3, all the γ_{xxxx} density distribution patterns of BH_3^- are similar to each other, except for the case at the MP2 level (See Fig.5.3(b)). Namely, inner regions of γ_{xxxx} density exhibit negative contribution, while outer regions exhibit dominant positive contributions. The γ_{xxxx} density distribution pattern of BH_3^- obtained by MP2 method is shown to be reversed. This γ_{xxxx} density distribution obtained using MP2 method is considered to reflect the lower-order electron-correlation effect on the γ_{xxxx} of BH_3^-. Namely, electron-correlation effect at the MP*n* level is considered to enhance negative contribution for the γ_{xxxx} of BH_3^-. In comparison with the γ density distribution of BH_3^- at the HF level, the outer γ density regions at the QCISD level

are shown to reduce (See Fig.5.3(c)). Namely, the electron-correlation effect at the QCISD levels is shown to decrease the positive contribution of BH_3^-, so that the magnitude of γ for BH_3^- is shown to decrease. As shown in Fig.5.3(d), the γ density distribution of BH_3^- obtained using B3LYP method is shown to more similar to those using QCISD method than HF method. Therefore, the B3LYP method is considered to be close to the QCISD method in electron-correlation effect on γ for BH_3^-.

Figure 5.4 shows the γ density distribution of CH_3. In comparison with the γ density distribution of CH_3 at the HF level (See Fig.5.4(a)), the electron-correlation effect at the MP2 level on the γ density distribution is shown to enhance the outer γ density region, which provides positive contribution to total γ, so that the magnitude of γ is shown to increase. Judging from the γ density distribution of CH_3 at the QCISD level (See Fig.5.4(c)), there is no great difference in the electron correlation effects on γ density of CH_3 at the MP2 and QCISD levels. This result is considered to be much agreement with the electron-correlation dependency of CH_3 (See Fig.5.3(b)). As shown in Fig.5.4(d), the γ density distribution of CH_3 obtained using B3LYP method is similar to those using QCISD method. Namely, the electron-correlation effect on γ of CH_3 at the B3LYP level is considered to be much similar to that at the QCISD level.

Figure 5.5 shows the γ density distribution of NH_3^+. All the distributions are much similar to each other. Namely, the electron-correlation effects hardly change the γ density distribution of NH_3^+. This result is considered to be in good agreement with that for NH_3^+ (See Fig.5.3(c)).

As can be seen from the γ density distributions of the radicals at the QCISD level (See Figures 5.3(c), 5.4(c) and 5.5(c)), there is no great difference in the distribution patterns. Although the γ_{xxxx} density distribution patterns are similar to each other, an essential difference in the γ_{xxxx} density distributions is observed in their magnitudes. Namely, the dominant γ_{xxxx} density region of BH_3^-, which has the largest $|\gamma_{xxxx}|$, is considered to be much larger than that of NH_3^+, which has the smallest $|\gamma_{xxxx}|$. Apparently, this feature reflects the fact that the anion radical has an extended charge distribution, while the cation radical has a small charge distribution. It can be concluded from the present study that the difference in γ_{xxxx} density distributions sensitively reflects the difference in the charge distributions and the degree of SRIP contributions.

It is found that magnitude, signs and electron-correlation dependencies of γ for one-center radicals sensitively reflect the difference in the charge distributions and the degree of SRIP contribution. Namely, the anion radical (BH_3^-) is found to have a positive γ at high-order electron-correlation level, though it is considered to somewhat have SRIP contribution. This suggests that SRIP contribution in BH_3^- is significantly reduced due to strong Coulomb repulsion in the resonance structures, and that an excess electron in BH_3^- enhances the positive contribution originating in the virtual excitation processes involving high-lying excited states.

(a) HF/6-311G(3d,3p)+*f*/*d* γ_{xxxx} = 1760000 a.u. (b) MP2/6-311G(3d,3p)+*f*/*d* γ_{xxxx} = -1730000 a.u.

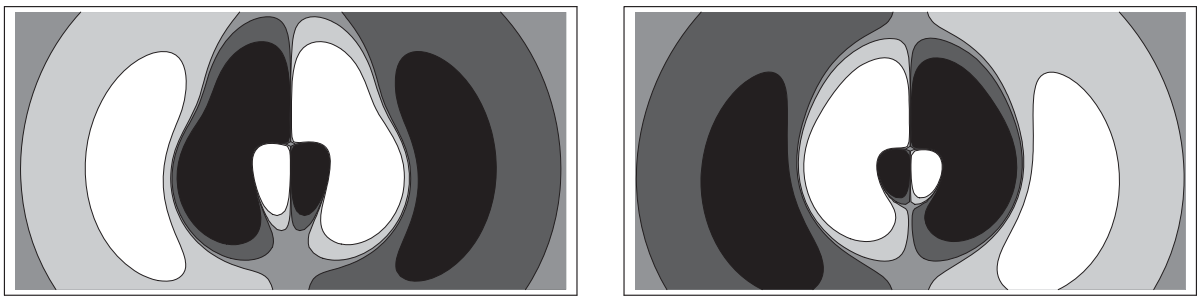

(c) QCISD/6-311G(3d,3p)+*f*/*d* γ_{xxxx} = 791000 a.u. (d) B3LYP/6-311G(3d,3p)+*f*/*d* γ_{xxxx} = 1000000 a.u.

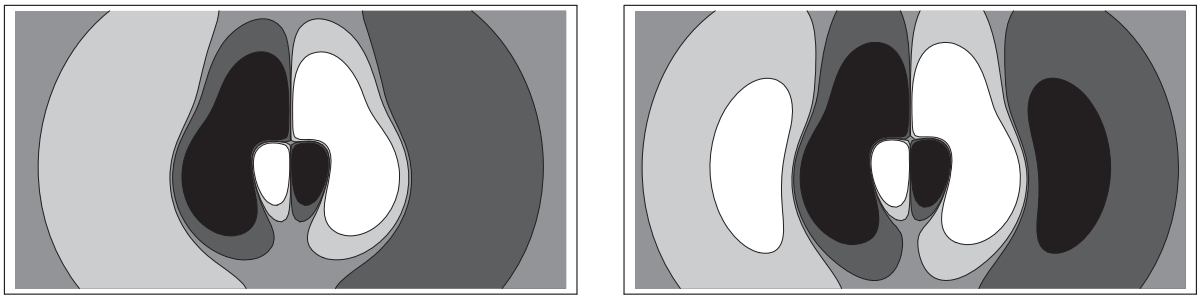

Fig.5.3. Contour plots of $\rho^{(3)}_{xxx}(\boldsymbol{r})$ distribution on the σ_v + 1.0 a.u. plane for BH_3^-. Contours are drawn from -100.0 to 100.0 a.u.. Lighter areas represent the spatial regions with larger $\rho^{(3)}_{xxx}(\boldsymbol{r})$ values. The white regions correspond to those with $\rho^{(3)}_{xxx}(\boldsymbol{r})$ larger than 100.0 a.u., while the black regions correspond to those with $\rho^{(3)}_{xxx}(\boldsymbol{r})$ smaller than -100.0 a.u.

(a) HF/6-311G(3d,3p)+*f*/*d* γ_{xxxx} = 361 a.u. (b) MP2/6-311G(3d,3p)+*f*/*d* γ_{xxxx} = 498 a.u.

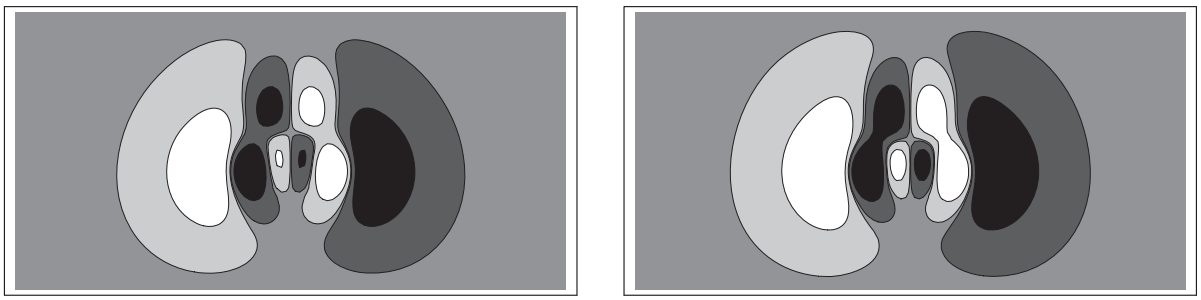

(c) QCISD/6-311G(3d,3p)+*f*/*d* γ_{xxxx} = 480 a.u. (d) B3LYP/6-311G(3d,3p)+*f*/*d* γ_{xxxx} = 791 a.u.

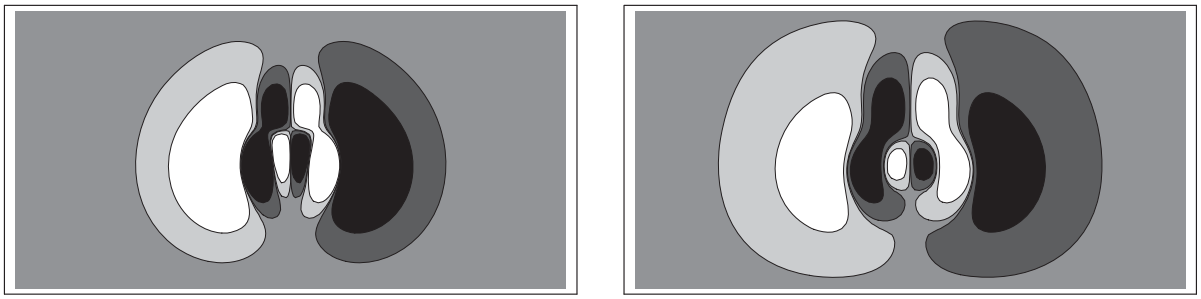

Fig.5.4. Contour plots of $\rho^{(3)}_{xxx}(\boldsymbol{r})$ distribution on the σ_v + 1.0 a.u. plane for CH_3. Contours are drawn from -1.0 to 1.0 a.u.. Lighter areas represent the spatial regions with larger $\rho^{(3)}_{xxx}(\boldsymbol{r})$ values. The white regions correspond to those with $\rho^{(3)}_{xxx}(\boldsymbol{r})$ larger than 1.0 a.u., while the black regions correspond to those with $\rho^{(3)}_{xxx}(\boldsymbol{r})$ smaller than -1.0 a.u.

(a) HF/6-311G(3d,3p)+*f*/*d* γ_{xxxx} = 37.5 a.u. (b) MP2/6-311G(3d,3p)+*f*/*d* γ_{xxxx} = 36.4 a.u.

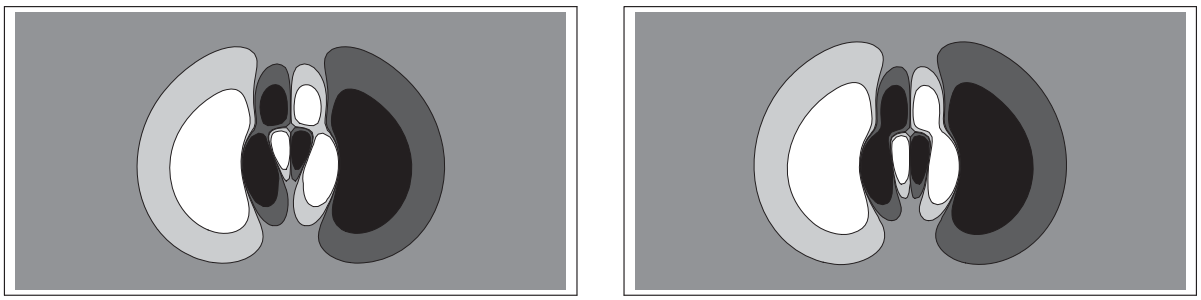

(c) QCISD/6-311G(3d,3p)+*f*/*d* γ_{xxxx} = 40.4 a.u. (d) B3LYP/6-311G(3d,3p)+*f*/*d* γ_{xxxx} = 49.4 a.u.

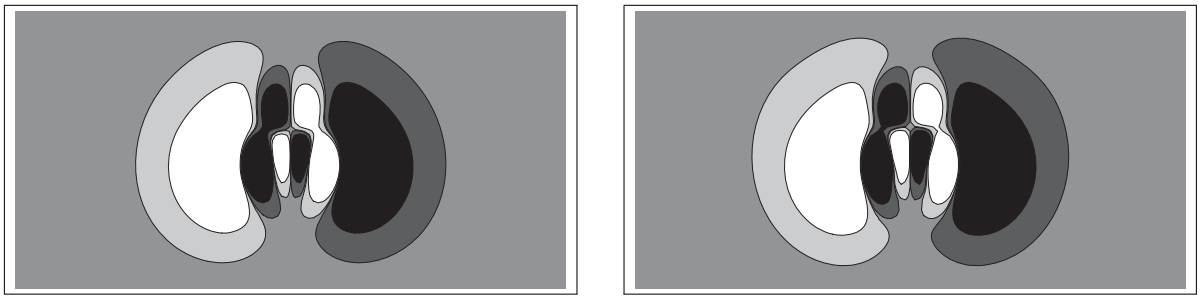

Fig.5.5. Contour plots of $\rho^{(3)}_{xxx}(\boldsymbol{r})$ distribution on the σ_v + 1.0 a.u. plane for NH_3^+. Contours are drawn from -0.10 to 0.10 a.u.. Lighter areas represent the spatial regions with larger $\rho^{(3)}_{xxx}(\boldsymbol{r})$ values. The white regions correspond to those with $\rho^{(3)}_{xxx}(\boldsymbol{r})$ larger than 0.10 a.u., while the black regions correspond to those with $\rho^{(3)}_{xxx}(\boldsymbol{r})$ smaller than -0.10 a.u.

5.2. Second hyperpolarizabilities of three-center radicals

In the previous section, it is found that magnitude, signs and electron-correlation dependencies of γ for one-center radicals sensitively reflect the difference in the charge distributions and the degree of SRIP contribution. In this section, to further develop nature of γ for open-shell systems and SRIP contribution, we investigate the γ for novel iso-electronic small radicals, *i.e.*, $BH(CH_2)_2^-$, $CH(CH_2)_2$ and $NH(CH_2)_2^+$. They are referred to as three-center radicals.

Fig.5.6 shows the SRIP of three-center radicals. As shown in Fig.5.6, $CH(CH_2)_2$ is not expected to have large SRIP contribution by the destabilization of the resonance structures due to the charge separation, while $BH(CH_2)_2^-$ and $NH(CH_2)_2^+$ are expected to have large SRIP contributions. However, judging from the case of one-center anion radical, the SRIP contribution in $BH(CH_2)_2^-$ is predicted to be considerably reduced and an excess electron in $BH(CH_2)_2^-$ tends to enhance the positive contribution (given by $\gamma^{(1)}$). Thus, the γ_{xxxx} of $BH(CH_2)_2^-$ is predicted to be positive. As a result, only $NH(CH_2)_2^+$ is expected to have a negative γ_{xxxx}.

5.2.1. Calculation methods and molecular geometries

The three-center radicals are assumed to be planar structures in order to clarify the contribution of π electron to the γ. Figure 5.7 shows the geometry of three-center radicals. The geometries of three-center radicals are optimized by using the B3LYP method with 6-311G(2*d*,2*p*) basis set.

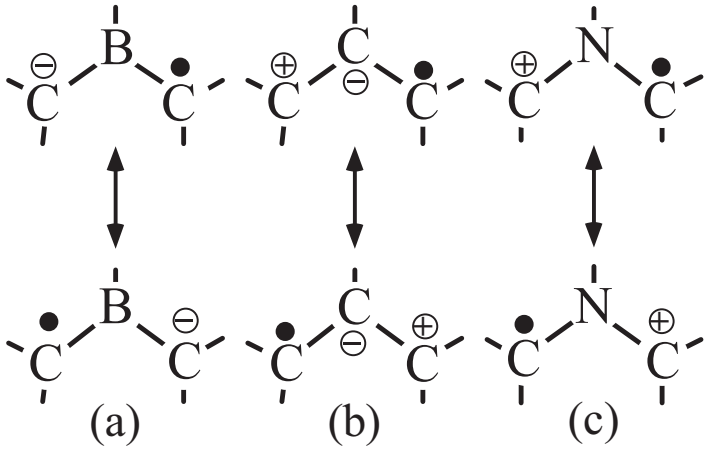

Fig.5.6. Symmetric resonance structures with inversible polarization (SRIP) for (a) $BH(CH_2)_2^-$, (b) $CH(CH_2)_2$ and (c) $NH(CH_2)_2^+$.

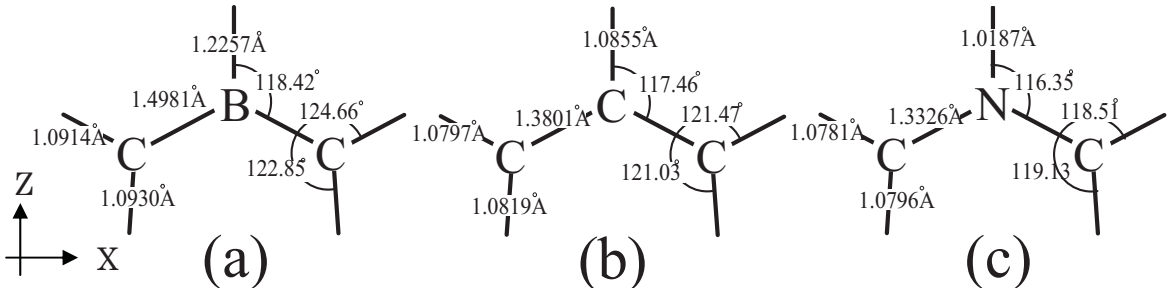

Fig.5.7. Molecular geometries of three-center radicals ((a) $BH(CH_2)_2^-$, (b) $CH(CH_2)_2$ and (c) $NH(CH_2)_2^+$) optimized using B3LYP method with 6-311G(2d,2p).

It is well known that an augmentation of diffuse and polarization functions to standard basis sets is necessary for obtaining qualitatively reliable γ value, especially for small systems. Therefore, we investigate basis set dependence of γ for three-center radicals. We use the standard 6-311G and 6-311G(*d*,*p*) basis sets and extended basis sets (See Table 1).

The effects of electron correlation on the γ are examined by the MPn, coupled-cluster CC and QCI methods. We confine our attention to longitudinal components of γ, *i.e.*, γ_{xxxx}, of three-center radicals since relations among γ_{xxxx} and the resonance structures with polarization in the longitudinal direction are primarily considered. The γ_{xxxx} is calculated by Eq.(A.6). In order to avoid numerical errors, we use several minimum field strengths. After numerical differentiations using these fields, we adopt a numerically stable γ_{xxxx}, which is found to be obtained by using fields 0.002 a.u. for these systems.

5.2.2. Results and discussion

5.2.2.1 Basis set dependency

Figure 5.8 shows basis sets and electron-correlation dependencies of γ_{xxxx} for the three-center radicals. As shown in Fig.5.8(a), the augmentation of diffuse and polarization functions is found to remarkably enhance the electron-correlation effect on γ_{xxxx} of $BH(CH_2)_2^-$, as especially shown at the higher-order electron-correlation levels, *i.e.*, CC and QCISD levels. Namely, the signs of γ_{xxxx} for $BH(CH_2)_2^-$ obtained using extended basis set are found to be positive as well as those using standard basis set at all MP*n* levels, while at the CC and QCI levels the γ_{xxxx} values using extended and standard basis sets are found to be positive and negative, respectively.

As shown in Fig.5.8 (b), the value of γ_{xxxx} for $CH(CH_2)_2$ obtained using extended basis set is much larger than that using standard basis set at all electron-correlation levels, though both the calculation methods using extended and standard basis sets provide positive γ_{xxxx}. Namely, the effect of the augmentation of diffuse and polarization function to the γ_{xxxx} for the neutral radical, *i.e.*, $CH(CH_2)_2$, is shown to be innegligible. In contrast, for the γ_{xxxx} of $NH(CH_2)_2^+$, the calculation

methods using standard and extended basis sets provide almost the same values at all electron-correlation levels (See Fig.5.8(c)).

The difference in basis set dependencies of γ_{xxxx} for $BH(CH_2)_2^-$ and $NH(CH_2)_2^+$ is considered to reflect the difference in charged states of the radicals. Since a charge distribution region of the anion radical ($BH(CH_2)_2^-$) is considered to be larger than that of the cation radical ($NH(CH_2)_2^+$), the augmentation of diffuse and polarization functions is considered to be more important for the γ_{xxxx} of $BH(CH_2)_2^-$ than for $NH(CH_2)_2^+$.

Based on the above results, the results calculated using 6-311G+*f/d* basis set are employed in the following discussion on electron-correlation dependencies of γ_{xxxx} for the three-center radicals.

5.2.2.2. Electron-correlation dependency

As shown in Fig.5.8(a), a remarkable electron-correlation dependence is observed for $BH(CH_2)_2^-$. All the MPn methods provide negative γ_{xxxx} for $BH(CH_2)_2^-$, while CC and QCISD methods provide large positive γ_{xxxx}. Although such remarkable electron-correlation dependencies of γ_{xxxx} for $BH(CH_2)_2^-$ seem to suggest the existence of SRIP contributions, the higher-order electron-correlation methods are found to provide large positive γ_{xxxx} for $BH(CH_2)_2^-$. This indicates that the positive contribution of γ_{xxxx} ($\gamma^{(III)}$) for $BH(CH_2)_2^-$ exceeds the negative contribution of the γ_{xxxx} ($\gamma^{(II)}$) at the higher-order electron-correlation levels. This situation is considered to be achieved by the decrease in the $|\gamma^{(II)}|$ and increase in the $|\gamma^{(III)}|$. The decrease in $|\gamma^{(II)}|$ is considered to be caused by the reduction of SRIP contribution owing to strong Coulomb repulsion in the resonance structures as in the case of BH_3^-. The large $\gamma^{(III)}$ contribution of γ_{xxxx} for $BH(CH_2)_2^-$ is presumed to reflect the large charge distribution, which enhances the contribution of higher-order virtual excitation process. This presumption is also considered to be supported by the basis set dependency of γ_{xxxx} for $BH(CH_2)_2^-$ (See Fig.5.8(a)). Namely, the signs of γ_{xxxx} obtained using extended basis set, which is necessary for sufficiently describing the extent of charge distribution for the anion radical, is shown to be positive, though the γ_{xxxx} obtained using standard basis set is shown to be negative at the higher-order electron-correlation levels.

As shown in Fig.5.8(b), the sign of γ_{xxxx} for $CH(CH_2)_2$ is positive and the electron-correlation effect on the γ_{xxxx} beyond the MP2 level is relatively small. Both the positive sign and small electron-correlation dependency of γ_{xxxx} for $CH(CH_2)_2$ coincide with our prediction. Namely, the charge separation of SRIP for $CH(CH_2)_2$ is considered to have small contribution to the ground state.

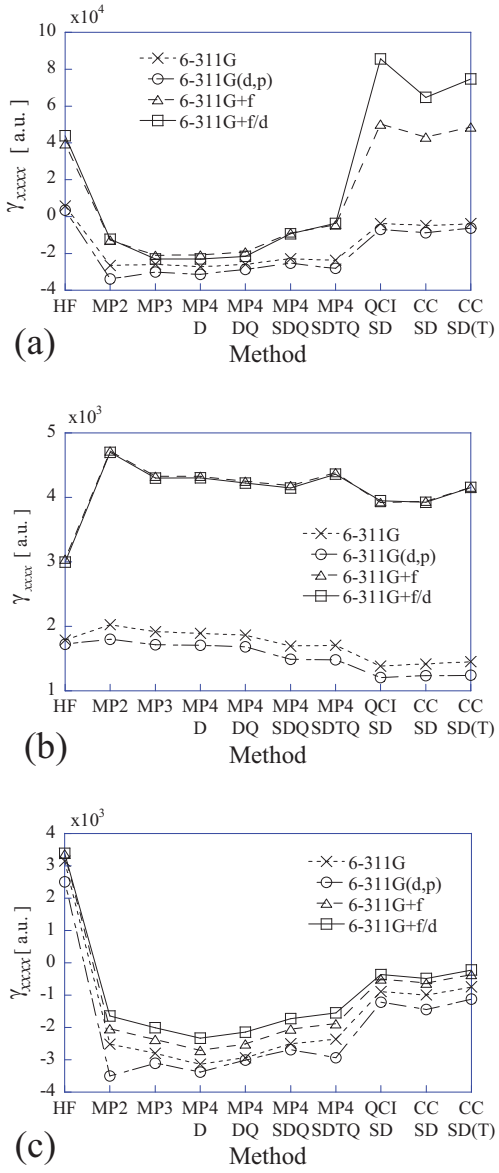

Fig.5.8. Variations in the γ_{xxxx} of three-center radicals ((a) $BH(CH_2)_2^-$, (b) $CH(CH_2)_2$ and (c) $NH(CH_2)_2^+$) for various basis sets and electron correlation methods.

The signs of γ_{xxxx} for $NH(CH_2)_2^+$ at the MP*n* levels are negative similarly to the case of $BH(CH_2)_2^-$ (See Fig.5.8(c)). On the other hand, the γ_{xxxx} of $NH(CH_2)_2^+$ remains negative at the higher-order electron-correlation levels. This indicates that the $\gamma^{(II)}$ contribution in $NH(CH_2)_2^+$ exceeds the $\gamma^{(III)}$ contribution at the higher-order electron-correlation levels. This features also coincides with our prediction based on the large SRIP contribution for $NH(CH_2)_2^+$.

5.2.2.3. Second hyperpolarizability density analysis

Figures 5.9 - 5.11 show the results of $\rho^{(3)}_{xxx}(\boldsymbol{r})$ analysis for the three-center radicals obtained

by using HF, QCISD and B3LYP methods. As shown in Fig.5.9(a) and (b), the $\rho^{(3)}_{xxx}(\boldsymbol{r})$ distributions of $BH(CH_2)_2^-$ at the HF level have same distribution pattern. Namely, the inner $\rho^{(3)}_{xxx}(\boldsymbol{r})$ regions are shown to have negative contribution to the total γ_{xxxx} of $BH(CH_2)_2^-$ and the outer $\rho^{(3)}_{xxx}(\boldsymbol{r})$ regions are shown to have positively dominant contribution. In comparison with the standard basis set, the $\rho^{(3)}_{xxx}(\boldsymbol{r})$ regions using extended basis set are shown to be enlarged. Namely, the magnitude of $\rho^{(3)}_{xxx}(\boldsymbol{r})$ using extended basis set is considered to be enhanced by augmentation of diffuse and polarization *f/d* functions. This difference in magnitude of γ_{xxxx} densities for $BH(CH_2)_2^-$ is considered to be in good agreement with the large basis set dependency of γ_{xxxx} for $BH(CH_2)_2^-$. As shown in Fig.5.9(c), the $\rho^{(3)}_{xxx}(\boldsymbol{r})$ distribution pattern at the QCISD level is shown to be similar to those at the HF level. However, the outer $\rho^{(3)}_{xxx}(\boldsymbol{r})$ region obtained using QCISD method is shown to expand, while the inner $\rho^{(3)}_{xxx}(\boldsymbol{r})$ regions are also shown to expand. The difference in $\rho^{(3)}_{xxx}(\boldsymbol{r})$ distribution of $BH(CH_2)_2^-$ at the HF and QCISD levels is considered to correspond to the difference in the γ_{xxxx} magnitudes. The $\rho^{(3)}_{xxx}(\boldsymbol{r})$ distribution of $BH(CH_2)_2^-$ using B3LYP method is shown to be dissimilar to those obtained using QCISD and HF methods. Namely, the electronic states described using B3LYP method is considered to be incorrect.

Figure 5.10 shows the $\rho^{(3)}_{xxx}(\boldsymbol{r})$ distribution of $CH(CH_2)_2$. As shown in Figs. 5.10(a) and (b), there is no noticeable difference in the $\rho^{(3)}_{xxx}(\boldsymbol{r})$ distributions of $CH(CH_2)_2$ between using standard and extended basis sets at the HF level. Namely, the $\rho^{(3)}_{xxx}(\boldsymbol{r})$ of $CH(CH_2)_2$ are shown to provide positive contribution to the total γ_{xxxx}. Similarly to the case of $BH(CH_2)_2^-$, using the extended basis set is shown to only change the size of $\rho^{(3)}_{xxx}(\boldsymbol{r})$ for $CH(CH_2)_2$. The size of $\rho^{(3)}_{xxx}(\boldsymbol{r})$ region. It is also find that there is no great difference in the $\rho^{(3)}_{xxx}(\boldsymbol{r})$ distribution pattern of $CH(CH_2)_2$ between at the HF level and at the QCISD level (See Figs. 5.10(b) and (c)). Namely, the electron-correlation effect on $\rho^{(3)}_{xxx}(\boldsymbol{r})$ distribution of $CH(CH_2)_2$ is considered to be small. This result is considered to be in good agreement with the prediction using SRIP contribution for ground state of $CH(CH_2)_2$. As shown in Fig.5.10(d), the $\rho^{(3)}_{xxx}(\boldsymbol{r})$ distribution of $CH(CH_2)_2$ using B3LYP method resembles those using QCISD method. Unlike the case of $BH(CH_2)_2^-$, therefore, B3LYP method can reproduce the reliable $\rho^{(3)}_{xxx}(\boldsymbol{r})$ distribution of $CH(CH_2)_2$.

(a) HF/6-311G γ_{xxxx} = 5790 a.u.

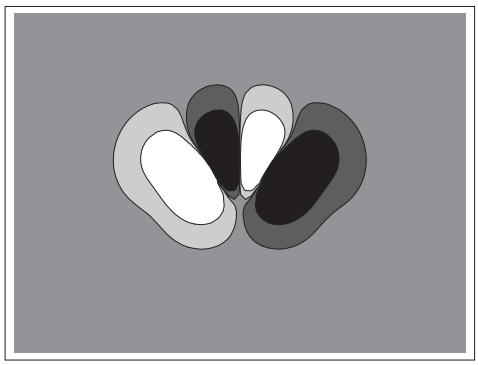

(b) HF/6-311G+*f*/*d* γ_{xxxx} = 43800 a.u.

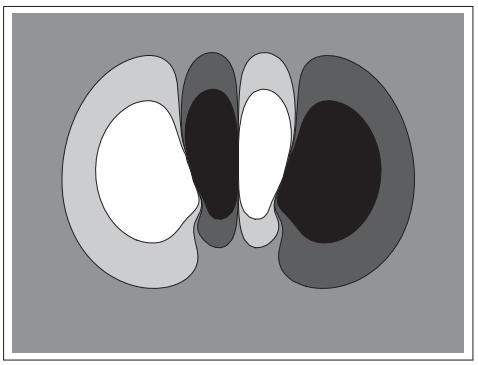

(c) QCISD/6-311G+*f*/*d* γ_{xxxx} = 50200 a.u.

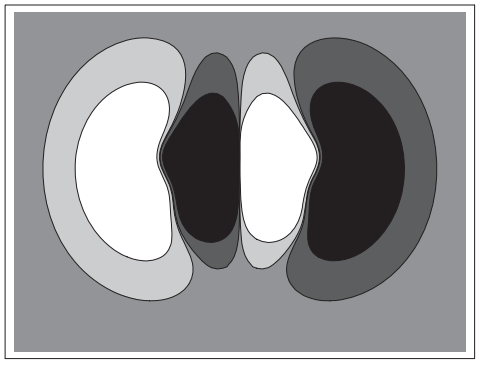

(d) B3LYP/6-311G+*f*/*d* γ_{xxxx} = 60000 a.u.

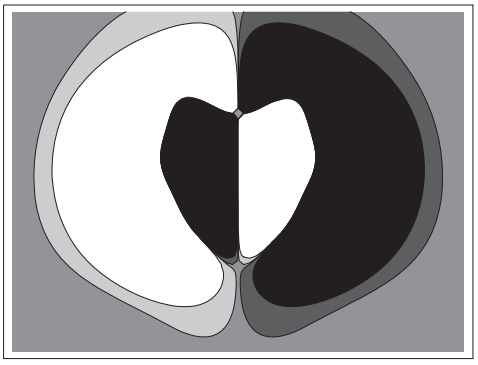

Fig.5.9. Contour plots of $\rho^{(3)}_{xxx}(\boldsymbol{r})$ distribution on the σ_v + 1.0 a.u. plane for $BH(CH_2)_2^-$. Contours are drawn from -10.0 to 10.0 a.u.. Lighter areas represent the spatial regions with larger $\rho^{(3)}_{xxx}(\boldsymbol{r})$ values. The white regions correspond to those with $\rho^{(3)}_{xxx}(\boldsymbol{r})$ larger than 10.0 a.u., while the black regions correspond to those with $\rho^{(3)}_{xxx}(\boldsymbol{r})$ smaller than -10.0 a.u.

(a) HF/6-311G γ_{xxxx} = 1790 a.u.

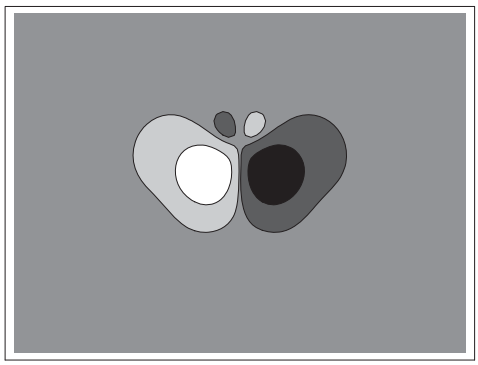

(b) HF/6-311G+*f*/*d* γ_{xxxx} = 3000 a.u.

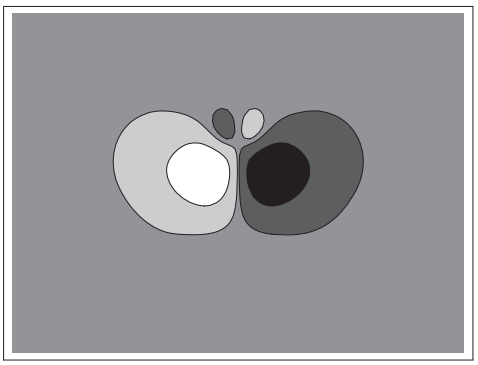

(c) QCISD/6-311G+*f*/*d* γ_{xxxx} = 3950 a.u.

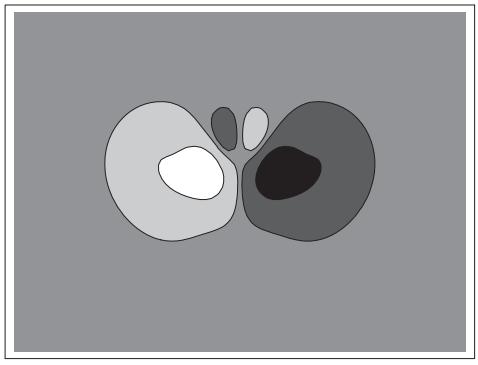

(d) B3LYP/6-311G+*f*/*d* γ_{xxxx} = 3760 a.u.

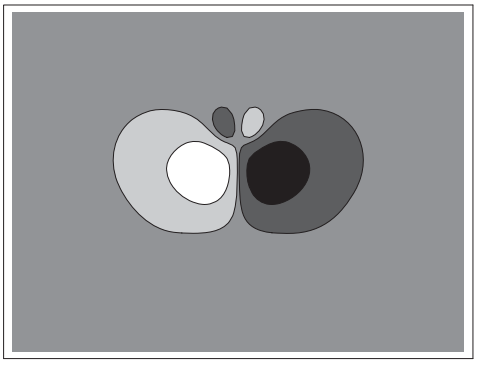

Fig.5.10. Contour plots of $\rho^{(3)}_{xxx}(\boldsymbol{r})$ distribution on the σ_v + 1.0 a.u. plane for $CH(CH_2)_2$. Contours are drawn from -10.0 to 10.0 a.u.. Lighter areas represent the spatial regions with larger $\rho^{(3)}_{xxx}(\boldsymbol{r})$ values. The white regions correspond to those with $\rho^{(3)}_{xxx}(\boldsymbol{r})$ larger than 10.0 a.u., while the black regions correspond to those with $\rho^{(3)}_{xxx}(\boldsymbol{r})$ smaller than -10.0 a.u.

(a) HF/6-311G γ_{xxxx} = 3140 a.u.

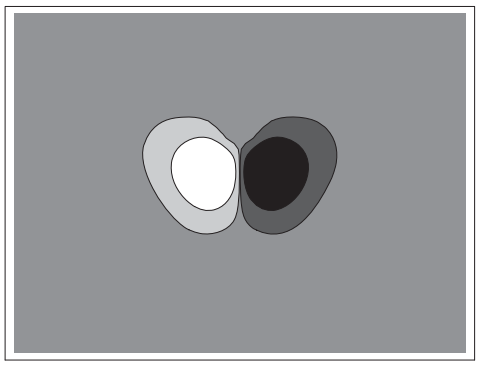

(b) HF/6-311G+*f*/*d* γ_{xxxx} = 3390 a.u.

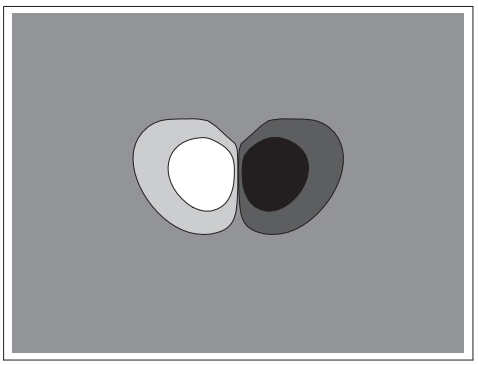

(c) QCISD/6-311G+*f*/*d* γ_{xxxx} = -361 a.u.

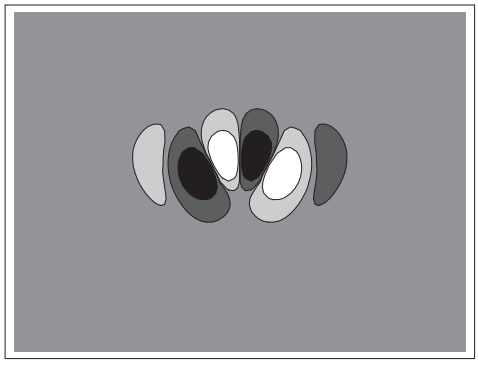

(d) B3LYP/6-311G+*f*/*d* γ_{xxxx} = -419 a.u.

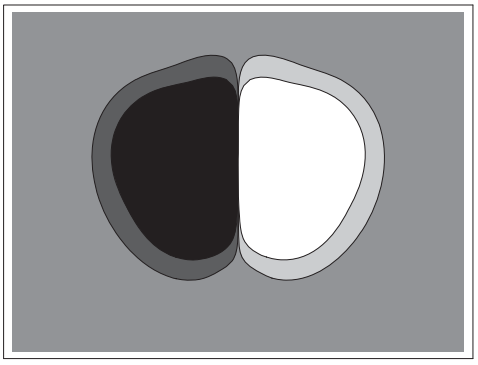

Fig.5.11.Contour plots of $\rho^{(3)}_{xxx}(\boldsymbol{r})$ distribution on the σ_v + 1.0 a.u. plane for $NH(CH_2)_2^+$. Contours are drawn from -10.0 to 10.0 a.u.. Lighter areas represent the spatial regions with larger $\rho^{(3)}_{xxx}(\boldsymbol{r})$ values. The white regions correspond to those with $\rho^{(3)}_{xxx}(\boldsymbol{r})$ larger than 10.0 a.u., while the black regions correspond to those with $\rho^{(3)}_{xxx}(\boldsymbol{r})$ smaller than -10.0 a.u.

We hardly find difference in the $\rho^{(3)}_{xxx}(\boldsymbol{r})$ distributions of $NH(CH_2)_2^+$ between using standard and extended basis sets at the HF level (See Fig.5.11(a) and (b)). This result is considered to accord with the small basis-set dependency of γ_{xxxx} value for $NH(CH_2)_2^+$. In contrast, the electron-correlation effect on the $\rho^{(3)}_{xxx}(\boldsymbol{r})$ distribution of $NH(CH_2)_2^+$ is shown to be enormously large. Although there are only two $\rho^{(3)}_{xxx}(\boldsymbol{r})$ regions, which provide positive contribution to the γ_{xxxx} of $NH(CH_2)_2^+$, at the HF level (See Fig.5.11(b)), the negative contribution regions appear at the QCISD level (Fig.5.11(c)). The negative contribution regions are considered to provide dominant contribution to the total γ_{xxxx} of $NH(CH_2)_2^+$, though the outer and inner $\rho^{(3)}_{xxx}(\boldsymbol{r})$ regions provide relatively small positive contribution to the total γ_{xxxx}. Obviously, this negative contribution is considered to originate in the large SRIP contribution, which enhances the $\gamma^{(II)}$ contribution. The $\rho^{(3)}_{xxx}(\boldsymbol{r})$ distribution pattern of $NH(CH_2)_2^+$ using B3LYP method (See Fig.5.11(d)) is shown to be quite dissimilar to those obtained using QCISD method (See Fig.5.11(c)), while the γ_{xxxx} values using QCISD and B3LYP methods seem to coincide to each other in their signs and magnitudes. Therefore, B3LYP method is considered to be able to reproduce reliable electronic states of $NH(CH_2)_2^+$, in contrast to the case of $BH(CH_2)_2$.

5.3. Concluding remarks

It is found from the present study that an augmentation of diffuse and polarization function is essential for reproducing the reliable γ of one- and three-center radicals, especially for the anion radical. It is also found that the γ of charged radicals, except for NH_3^+, exhibit remarkable electron-correlation dependencies, which can be predicted based on the SRIP contributions for the radicals. As expected from our structure-property correlation rule using SRIP contribution, the values of γ_{xxxx} for the anion and cation radicals are found to be large positive and small negative in sign, respectively. It is also found from the hyperpolarizability density analysis that the difference in the signs and magnitudes of the γ_{xxxx} for one- and three-center radicals reflect the difference in their charge distributions.

It is concluded that the γ values of iso-electronic one- and three-canter radicals sensitively reflect the features of the charge distributions and the degree of SRIP contributions as follows: First, the large charge distribution in anion radicals is considered to enhance the contribution of $\gamma^{(III)}$. Therefore, the $\gamma^{(III)}$ is shown to far exceed the $\gamma^{(II)}$ contribution, although the anion radical have somewhat SRIP contribution to the ground state. This is considered to be caused by the fact that the strong Coulomb repulsion by the excess electron in the SRIP for the anion radical systems leads to reduce the SRIP contribution, while the excess electron in the extended region contribute to the enhancement of $\gamma^{(III)}$. Second, the charge polarization structure of SRIP in neutral radicals is considered to have slight contributions to the ground states of the neutral radicals. Therefore, the $\gamma^{(III)}$ contributions of the neutral radicals are shown to exceed the $\gamma^{(II)}$ contributions. Third, the defect of charge in three-center cation radical is considered to enhance the SRIP contribution. Therefore the $\gamma^{(II)}$ contribution is shown to exceed the $\gamma^{(III)}$ contribution, so

that the three-center cation radical ($NH(CH_2)_2^+$) exhibits negative γ. However, the magnitude of the γ for $NH(CH_2)_2^+$ is small, since the distribution of charge is restricted to small region.

Judging from the results in this study, the magnitude of γ for cation radicals is presumed to be small even if the sign of γ is negative. On the other hand, anion radicals are also presumed to tend to have positive γ. However, if charge polarization structure of a neutral radical sufficiently contribute to the ground state, it is expected that the neutral radical have large negative γ. In the next chapter, γ of a neutral radical, which expected to have large SRIP contribution, is examined.

Chapter 6 The second hyperpolarizability of a neutral five-center radical

In chapter 5, it is found that γ values of the small radicals sensitively reflect the degree of SRIP contributions and are influenced by features of each charged state. In the one-center radicals only the anion radical (BH_3^-) is predicted to have SRIP contribution. However, the excess electron of BH_3^- is considered to decrease the SRIP contribution and increase the $\gamma^{(III)}$ contribution, so that BH_3^- is found to have negative γ. In the three-center radicals, the SRIP's of anion radical ($BH(CH_2)_2^-$) and the cation radical ($NH(CH_2)_2^+$) seem to stabilize the ground states of the radicals. However, the γ of $BH(CH_2)_2^-$ is found to be positive similarly to BH_3^-, since the existence of excess electron is considered to cause a reduction of $\gamma^{(II)}$ and an enhancement of $\gamma^{(III)}$ of $BH(CH_2)_2^-$. Although the γ of $NH(CH_2)_2^+$ is found to be negative, the magnitude of γ is relatively small since the charge distribution is restricted to small spatial region. In both three- and one- center radicals, the neutral radicals (CH_3 and $CH(CH_2)_2$) are predicted to have small SRIP contribution because of the instability of their charge polarization structures. However, if such SRIP including charge separation is realized by stabilizing these structures, the neutral radical will have large negative γ. In chapter 4, it is found that the charge polarization of nitroxide group in H_2NO play an important role in the γ of H_2NO. In this chapter, therefore, the γ of a neutral five-center radical, *i.e.*, nitronyl nitroxide radical (N^2-oxidoformamidin-N^1-yloxyl radical; NN) [110,111], which involve two nitroxide group symmetrically, is investigated.

First, the basis-set and dynamical electron-correlation dependencies of the γ for NN are investigated by using the ab initio MO methods, *i.e.*, HF, MPn, QCI and CC methods [110]. The hyperpolarizability density analysis is also employed. Next, non-dynamical electron-correlation dependency of γ for NN is examined by using CAS-SCF method [111]. Finally, an availability of the DFT approaches for calculation of γ for NN is examined using the second hyperpolarizability density analysis [111].

6.1. Calculation methods and molecular geometry

Figure 6.1 shows the molecular geometry and a coordinate system of NN radical optimized by the MP2 method using the 6-311G** basis set. The experimental geometry data are not available for this molecule. The purpose of our study is to obtain a qualitative electron-correlation and basis-set dependence and the sign of γ for NN, which satisfies our structure-property correlation rule. Although the geometry optimized by the MP2 method may not be in good agreement with the unobserved experimental geometry, the obtained geometry satisfies the structure-property correlation rule and is considered to be sufficient for our purpose.

Figure 6.2 shows the corresponding resonance structures for the NN radical. As shown in Fig.6.2, this molecule involves two nitroxide groups (N-O·) arranged symmetrically. In the resonance structures, this characteristic structure leads to a transfer of the radical spin and charge from one side to the other side of the NO group. Such resonance structure (SRIP) implies an important contribution to the stability of the ground state of this system. Namely, the sign of γ_{xxxx}, the component of the γ in the direction of the O-N-C-N-O unit, is expected to be negative.

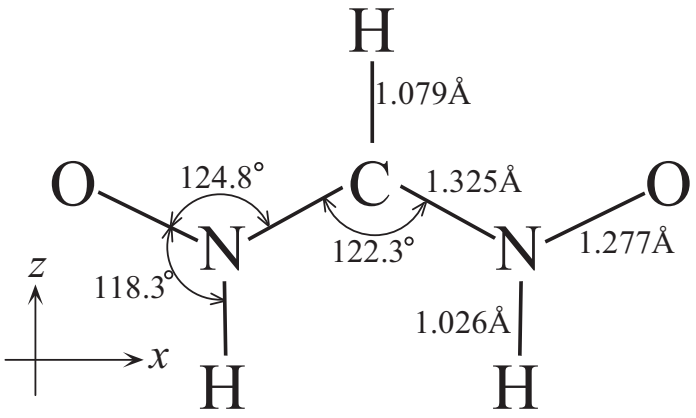

Fig.6.1. Molecular geometry and the coordinate system of nitronyl nitroxide radical optimized by UMP2 method using 6-311G** basis set.

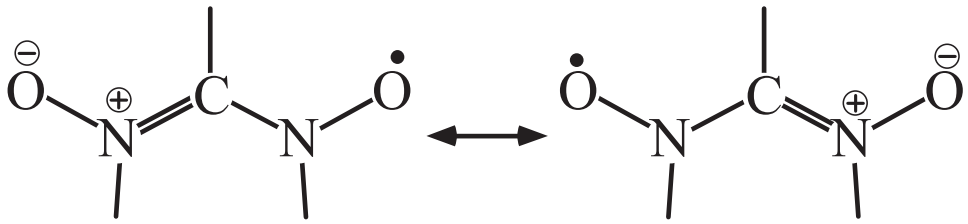

Fig.6.2. Symmetric resonance structures with inversible polarization (SRIP) for nitronyl nitroxide radical.

Firstly, the basis-set dependence of the γ_{xxxx} is investigated by applying the standard (minimal (STO-3G), split-valence (6-31G)) and extended basis sets augmented by diffuse and polarization functions (*p* and *d*), which are known to be essential for reproducing semi-quantitative γ for organic π-conjugated systems. It is noted that diffuse s-type functions are involved, since we use diffuse six-memberd *d* type functions. The extended basis sets are given in Table 4.1. These exponents were all determined from the outermost two exponents of 6-31G by an even-tempered method. Secondly, the effects of electron correlations on the γ were examined by the MP2, MP3, MP4DQ, MP4SDQ, MP4SDTQ, CCD (=QCID), QCISD, CCSD and CCSD(T) methods.

The γ_{xxxx} of NN calculated by Eq.(A.6) From the γ_{xxxx} values calculated using several minimum field strengths (F^x) from 0.0005 to 0.005 a.u, the numerically stable γ_{xxxx} is adopted. Numerically stable γ_{xxxx} values were found to be obtained by using fields of around 0.0015 au.

The systems with SRIP have two symmetric resonating structures with large contributions to the ground state of the systems. Therefore the electronic structures of the systems with SRIP cannot be well described by using a single determinant alone. The problems related to the breakdown of a single-configuration approximation can be efficiently treated by using multi-configuration wavefunctions. The CAS-SCF method uses configurations generated in the active orbital space. In this study, the CAS-SCF calculations using 7 π-electrons in the 5 π_y type molecular orbitals obtained by the restricted open-shell HF (ROHF) calculation (See Fig.6.3), which is referred to as the CAS-SCF(7,5), is examined to provide the γ of NN. Since the split-valence basis set and extended basis sets augmented by diffuse and polarization functions are used, there are other 5 π_y type valence orbitals arising from the outer *p* functions. Therefore, the CAS-SCF calculation by using 7 π-electrons in the 5 inner and 5 outer π_y type ROHF molecular orbitals. This CAS-SCF calculation is referred to as the CAS-SCF(7,10), is also performed.

As mention in chapter 4, however, the BLYP method does not well describe the second hyperpolarizabilities for the nitroxide radical, though they can well reproduce them at the QCISD level for formaldehyde. In chapter 5, however, the B3LYP method can reproduce the reliable γ density distributions for neutral radicals. In this chapter, therefore, we use the BLYP and B3LYP methods for the calculation of γ.

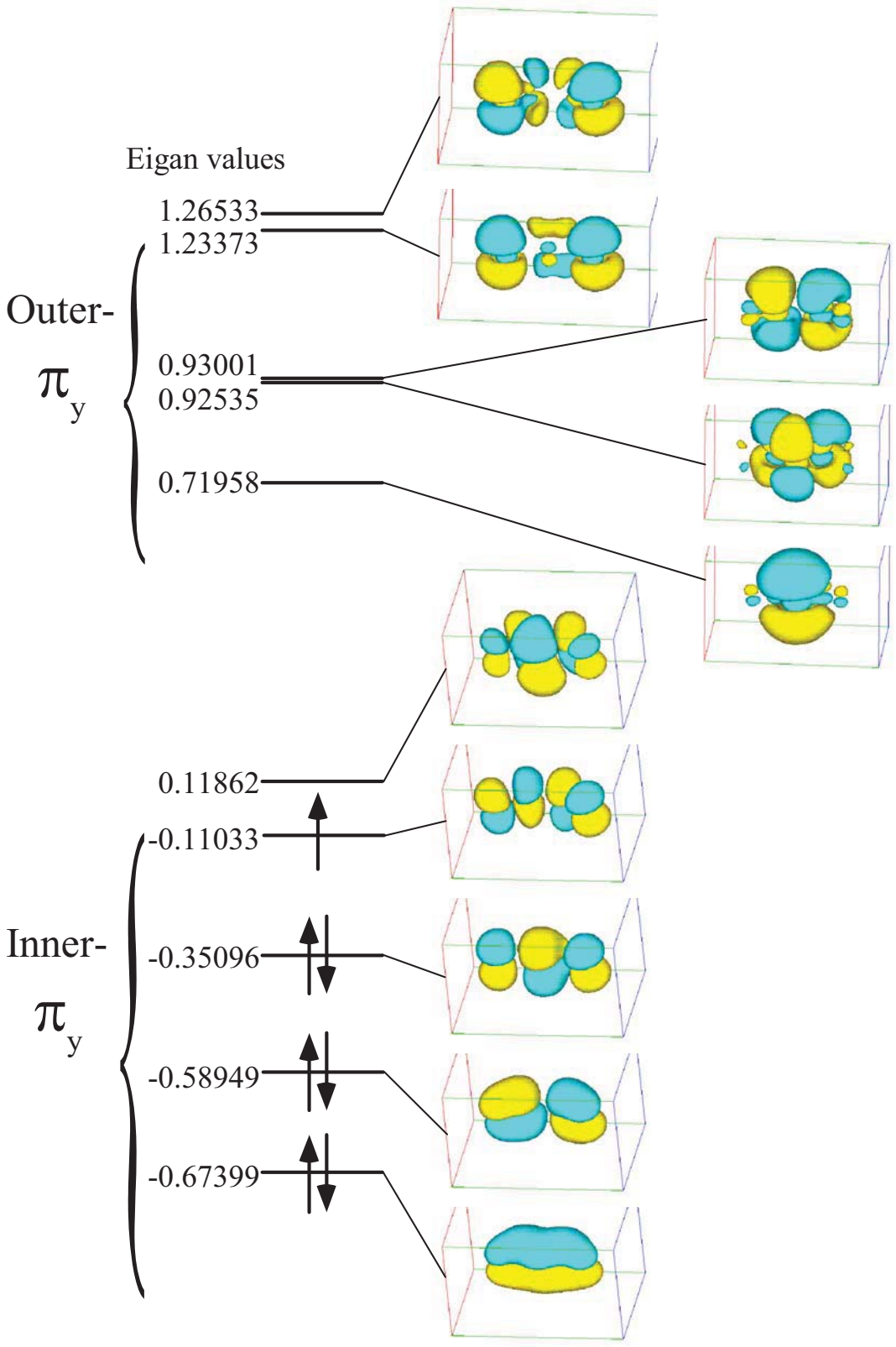

Fig.6.3. ROHF molecular orbitals for the active spaces used in the CAS-SCF (7,5) calculations.

6.2. *Results and discussion*

6.2.1. Basis Set Dependence of γ_{xxxx}.

Fig.6.4 shows variations in γ_{xxxx} of the NN radical for different basis sets and electron-correlation methods. This figure indicates that the minimal (STO-3G) and standard split-valence (6-31G) basis sets cannot provide a sufficient magnitude of γ_{xxxx}. In contrast, extended basis sets (6-31G+*p* and 6-31G+*d*) are shown to significantly increase the magnitudes of γ_{xxxx}. The 6-31G+*pd* basis set is found to provide similar electron correlation dependences to those at the 6-31G+*p* and 6-31G+*d* basis sets, though the magnitudes of γ_{xxxx} at the 6-31G+*pd* are slightly enhanced. Therefore, we consider that the 6-31G+*pd* basis set can provide a qualitative description of the dependence of γ_{xxxx} on the various electron correlation effects. This feature is similar to those of other closed-shell conjugated organic systems. This basis-set dependence was investigated using the hyperpolarizability densities for the results by using 6-31G and 6-31G+*pd* at the HF level. In the following discussion concerning the electron-correlation dependence of γ_{xxxx}, the γ_{xxxx} calculated using the most extended basis set, 6-31G+*pd*, are used.

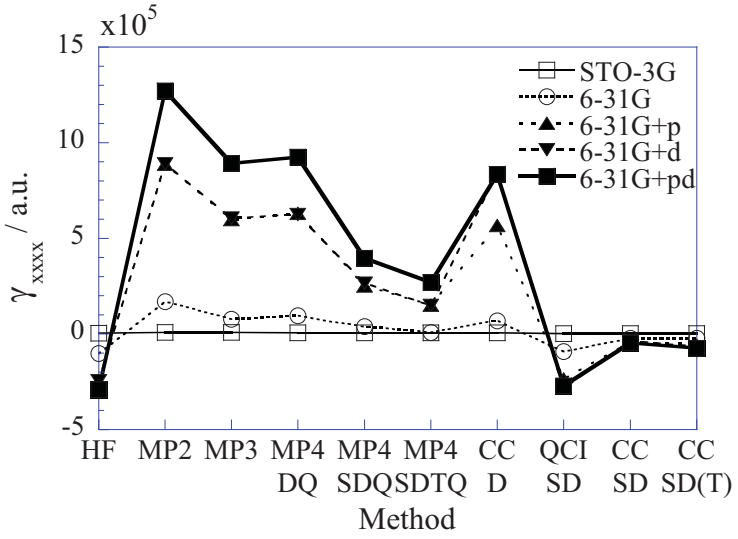

Fig.6.4. Variations in the γ_{xxxx} of nitronyl nitroxide radical for various basis sets and electron correlation methods.

6.2.2 Dynamical-electron-correlation dependence of γ_{xxxx}.

As shown in Fig.6.4, a remarkable electron correlation dependence of the γ_{xxxx} is observed. The HF method provides a large negative γ_{xxxx}, while the D effects by the MP2 method change the sign and enhance the magnitude of γ_{xxxx} by the HF method. The D effects by the MP3 method decrease γ_{xxxx} by the MP2 method. The D and Q effects involved in the MP4 method are found to provide only a slight positive contribution to the γ_{xxxx}. A comparison between the CCD and MP4DQ γ_{xxxx} indicates that the correlation effects originating from the higher-order D beyond the fourth-order are not important. The S and T effects involved in the MP4 method decrease γ_{xxxx}. Particularly, the S effects involved in the CCSD method remarkably decrease CCD γ_{xxxx} and then reverse its sign. This feature implies that the contribution from the higher-order S effects beyond the fourth-order is indispensable for a reliable description of the γ_{xxxx} for this system. The QCISD method cannot satisfactorily reproduce γ_{xxxx} by the CCSD method, though its approximation level is generally considered to be similar to that of the latter method. However, the sign of γ_{xxxx} by the QCISD method coincides with that by the CCSD method, and is thus considered to be a good approximation of that by the CCSD method. The γ_{xxxx} by the CCSD(T) method is shown to be nearly equal to that by the CCSD method. Therefore, γ_{xxxx} by the CCSD method seems to be sufficiently converged.

6.2.3 Non-dynamical electron correlation effects on γ

As shown in Table 6.1, we obtained γ_{xxxx} values by the CAS-SCF calculations using two kinds of active spaces, *i.e.*, (7,5) and (7,10). Although we further performed the CAS-SCF calculations using other kinds of active spaces including π-electron effects, these calculations fail to obtain the sufficient converged results. These failures are presumed to be caused by cutting off the active space in an imbalanced manner.

Table 6.1 γ_{xxxx} values [a.u.] calculated by the CAS-SCF and CCSD(T) methods using 6-31G, 6-31G+*p*, 6-31G+*d* and 6-31G+*pd* basis sets.*)

Method	6-31G	6-31G+*p*	6-31G+*d*	6-31G+*pd*
CAS-SCF(7,5)	-1160000	-5360000	-6440000	-7350000
CAS-SCF(7,10)	-155000	not converged	-259000	-288000
UCCSD(T)	-21000	-67800	-75600	-65600

*) In the CAS-SCF(7,5), we choose the 5 π_y type molecular orbitals obtained by the restricted open-shell HF (ROHF) for 7 π-electrons as the active space, while in the CAS-SCF(7,10) we used further 5 π_y type valence orbitals arising from the outer *p* functions of split-valence basis sets.

In order to estimate the quality of the γ_{xxxx} by using the CAS-SCF calculations, we compare the γ_{xxxx} by the CAS-SCF methods with that by the CCSD(T) method, which are considered to provide the most reliable γ_{xxxx} value in this study. It is found that the CAS-SCF methods provide larger $|\gamma_{xxxx}|$ than those at CCSD(T) level. It is further found that the augmentation of diffuse and polarization functions enhance this negative contribution. As seen from the comparison of the $|\gamma_{xxxx}|$ obtained by the CAS-SCF(7,10) calculation with those by the CAS-SCF(7,5) calculation, the negative contributions decrease when larger active spaces are used. However, the larger active space, *i.e.*, (7,10), is considered to be still insufficient for providing the γ_{xxxx} at CCSD(T) level, since the $|\gamma_{xxxx}|$ obtained by CAS-SCF(7,10) calculations are much larger than those by CCSD(T) method. Therefore, a further expansion of the active space is considered to be necessary for providing reliable γ_{xxxx}. There are two approaches to the expansion of active space: the inclusion of only π orbitals and the inclusion of both π and σ orbitals. However, judging from computer resources we access to presently, it is difficult to perform the CAS-SCF calculations with such larger size of active space.

6.2.4. Analysis of spatial contributions to γ_{xxxx} by the hyperpolarizability density.

In order to elucidate the relationships among the spatial contributions of electrons, the basis set and electron-correlation dependencies of γ_{xxxx}, the γ_{xxxx} density ($\rho^{(3)}_{xxx}(\boldsymbol{r})$) plots were investigated. Fig.6.5 gives contour plots of $\rho^{(3)}_{xxx}(\boldsymbol{r})$ on the σ_v+1 a.u. plane of the NN radical shown in Fig.6.1.

From the plots of $\rho^{(3)}_{xxx}(\boldsymbol{r})$ by the HF method (Figs.6.5(a) and (b)), diffuse *p* and *d* functions are not shown to change the qualitative spatial contributions of electrons to the γ_{xxxx}, except for their size differences. As can be seen from all of the $\rho^{(3)}_{xxx}(\boldsymbol{r})$ plots, the $\rho^{(3)}_{xxx}(\boldsymbol{r})$ mainly contributing to the γ_{xxxx} are distributed along the bond region of the O-N-C-N-O unit. This implies that a charge fluctuation in the bond region of the O-N-C-N-O unit predominantly determines the features of γ_{xxxx}. This is in contrast to the usual case for a neutral closed-shell π-conjugated system, where the contributions to γ from expanded regions remote from the bond regions are dominant.

The tendency of the distribution of the $\rho^{(3)}_{xxx}(\boldsymbol{r})$'s at the HF and QCISD levels is found to be dramatically different from that at other levels, and therefore the distribution of $\rho^{(3)}_{xxx}(\boldsymbol{r})$ can be classified into two types. The first type (type A) includes the $\rho^{(3)}_{xxx}(\boldsymbol{r})$ by the HF and QCISD methods, and the second type (type B) includes the $\rho^{(3)}_{xxx}(\boldsymbol{r})$ by the MP2, MP3, MP4DQ, MP4SDQ and CCD methods. As shown in Fig.6.5, γ_{xxxx} of type A are negative, while those of type B are positive. A common feature of both types is that contributions from the vicinity of the (α-)carbon atom (in the O-N-C-N-O skeleton) are appreciably small, or can be negligible, so that the γ_{xxxx} are contributed primarily from the vicinity of the NO groups on the left- and right-hand sides. For type A, it is surprising that there is no difference between the feature of

distribution of $\rho^{(3)}_{xxx}(\boldsymbol{r})$ at the HF level and that at the QCISD level. The contributions from the $\rho^{(3)}_{xxx}(\boldsymbol{r})$ in the vicinity of the N atoms in both NO groups are shown to be positive, while those of the O atoms in both NO groups are shown to be negative. As can be seen from Eq. (2), the contribution from a pair of $\rho^{(3)}_{xxx}(\boldsymbol{r})$ is more significant when the distance of the pair of $\rho^{(3)}_{xxx}(\boldsymbol{r})$ is larger. In the present case, since the O-O distance is larger than the N-N distance, the total γ_{xxxx} is mainly determined by the contribution from both O atoms, and becomes negative. In contrast, for type B, which mainly include the D or Q effects, the contributions from $\rho^{(3)}_{xxx}(\boldsymbol{r})$ distributed over the vicinity of the N atoms in both NO groups are shown to be negative, while those of O atoms in both NO groups are shown to be positive, so that the total γ_{xxxx} becomes positive. As can be seen from the MP4DQ and MP4SDQ results, the S effects tend to decrease $|\rho^{(3)}_{xxx}(\boldsymbol{r})|$ in the O atom regions in both NO groups, so that γ_{xxxx} at the MP4SDQ level becomes smaller than that at the MP4DQ level. The distribution of γ_{xxxx} at the CCD level is shown to provide a positive γ_{xxxx} similarly to that at the MP4DQ level. In contrast, the S effects involved in the higher-order (beyond the fourth-order) perturbation methods are found to reverse the sign of $\rho^{(3)}_{xxx}(\boldsymbol{r})$ at the CCD level. As a result, an inclusion of the D and Q effects up to infinite-order cannot reproduce the qualitative features of the distributions of $\rho^{(3)}_{xxx}(\boldsymbol{r})$ at the QCISD level. It is also noteworthy for this system that the features of $\rho^{(3)}_{xxx}(\boldsymbol{r})$ at the HF level (Fig.6.5(b)) is very similar to that at the QCISD level (Fig.6.5(h)). This suggests that a cancellation among the S and DQ effects is qualitatively achieved at infinite-order. For this system, an incomplete or unbalanced consideration of electron correlations will lead to incorrect features of the sign and magnitude of the γ_{xxxx}.

We consider the quality of the $\rho^{(3)}_{xxx}(\boldsymbol{r})$ distributions calculated by the BLYP and B3LYP methods in comparison with those calculated by QCISD method. As shown in Fig.6.6, there are found to be two kinds of features in the $\rho^{(3)}_{xxx}(\boldsymbol{r})$ distributions obtained by the DFT approaches. First, large $|\rho^{(3)}_{xxx}(\boldsymbol{r})|$ regions by using the DFT approaches are much smaller than those by the QCISD method, while the distribution pattern of the sign of $\rho^{(3)}_{xxx}(\boldsymbol{r})$ in the π-bond regions are in good agreement with that by the QCISD method. This feature is considered to reflect the small $|\gamma_{xxxx}|$ obtained by the DFT approaches. Second, new $\rho^{(3)}_{xxx}(\boldsymbol{r})$ regions, which positively contribute to the γ_{xxxx}, appear at the outside of π-bond region. The positive contribution from the outside of the π-bond, where the electron density is very small, is not observed at the QCISD level. Therefore, we presume this positive contribution to be unreliable and to be an evidence of the disadvantage of BLYP and B3LYP methods. In the chapter 4, we pointed out that BLYP method cannot reproduce reliable $\rho^{(3)}_{xxx}(\boldsymbol{r})$ at the bond region of nitroxide radical. It is clear that this disadvantage of the DFT approach is not removed completely even in the B3LYP method. In the $\rho^{(3)}_{xxx}(\boldsymbol{r})$ plot obtained by B3LYP method, however, the large $|\rho^{(3)}_{xxx}(\boldsymbol{r})|$ regions of π-bond are shown to increase, while the $|\rho^{(3)}_{xxx}(\boldsymbol{r})|$ regions outside of π-bond are shown to decrease, compared to those by BLYP method. Since the B3LYP and BLYP methods provide the negative and positive γ_{xxxx}, respectively, the negative contribution originating in π-electrons is considered to overcome the positive contribution from outside

regions of π-bond. Consequently, the effect of novel exchange-functional in the B3LYP method is expected to improve the $\rho^{(3)}_{xxx}(\boldsymbol{r})$ distribution. If the disadvantages observed here are overcome, the DFT approach will be useful for providing the γ for large-size radicals.

(a) HF/6-31G γ_{xxxx} = -102000 a.u.

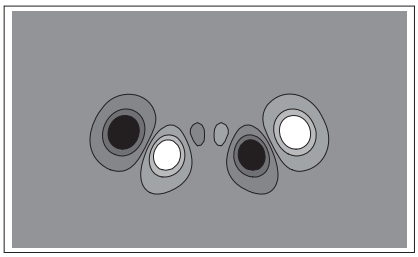

(b) HF/6-31G+pd γ_{xxxx} = -292000 a.u.

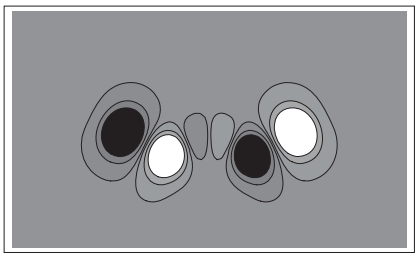

(c)MP2/6-31G+pd γ_{xxxx} = 1270000 a.u.

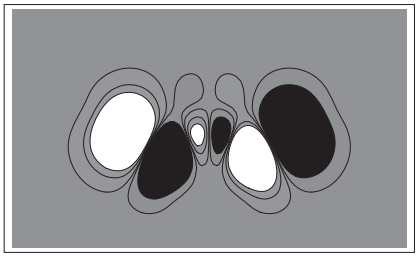

(d) MP3/6-31G+pd γ_{xxxx} = 886000 a.u.

(e) MP4DQ/6-31G+pd γ_{xxxx} = 921000 a.u.

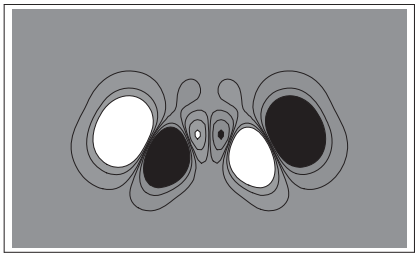

(f) MP4SDQ/6-31G+pd γ_{xxxx} = 390000 a.u.

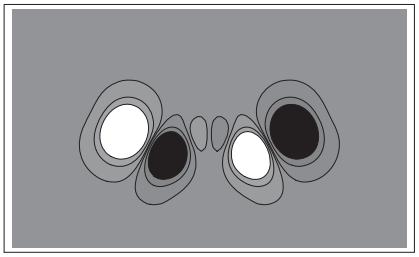

(g) CCD/6-31G+pd γ_{xxxx} = 834000 a.u.

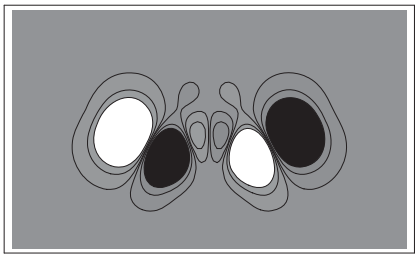

(h) QCISD/6-31G+pd γ_{xxxx} = -271000 a.u.

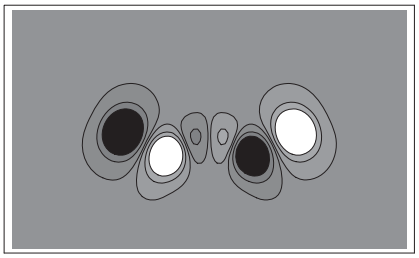

Fig.6.5. Contour plots of γ_{xxx} densities on the σ_v+1 a.u. plane of nitronyl nitroxide radical (Fig. 1) and γ_{xxx} for various calculation methods. Contours are drawn from -1250 to 1250 a.u. Lighter areas represent the spatial regions with larger $\rho^{(3)}_{xxx}(\boldsymbol{r})$ values. The white regions correspond to those with $\rho^{(3)}_{xxx}(\boldsymbol{r})$ larger than 1250 a.u., while the black regions correspond to those with $\rho^{(3)}_{xxx}(\boldsymbol{r})$ smaller than -1250 a.u.

(a) BLYP MP2/6-31G+pd γ_{xxxx} = 2110 a.u.

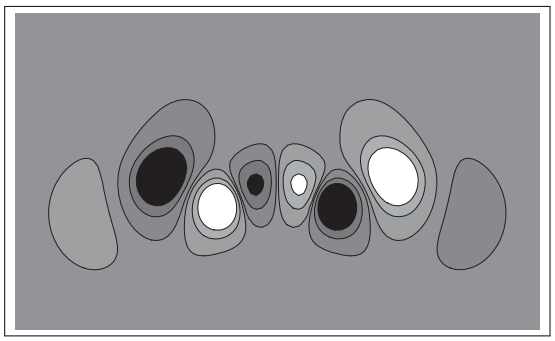

(b) B3LYP/6-31G+pd γ_{xxxx} = -666 a.u.

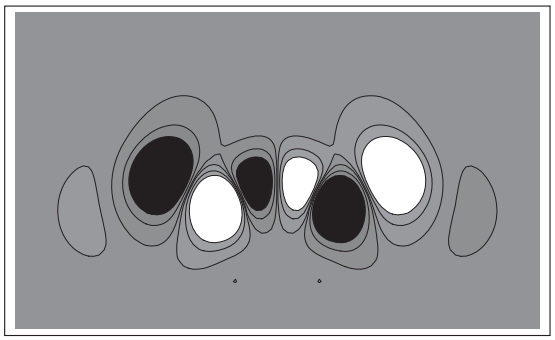

(c) QCISD/6-31G+pd γ_{xxxx} = -271000 a.u.

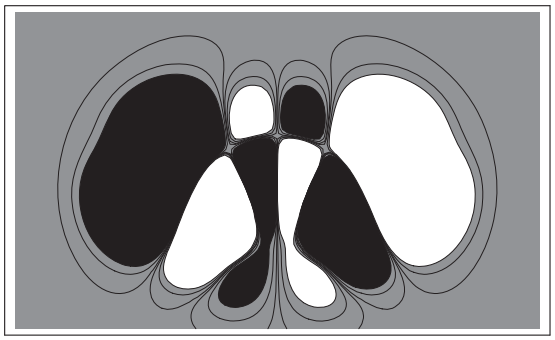

Fig.6.6. Contour plots of $\rho^{(3)}_{iii}(\boldsymbol{r})$ distribution on the σ_v + 1.0 a.u. plane of nitronyl nitroxide radical by using the BLYP, B3LYP and QCISD methods. Contours are drawn from -12.5 to 12.5 a.u. Lighter areas represent the spatial regions with larger $\rho^{(3)}_{xxx}(\boldsymbol{r})$ values. The white regions correspond to those with $\rho^{(3)}_{xxx}(\boldsymbol{r})$ larger than 12.5 a.u., while the black regions correspond to those with $\rho^{(3)}_{xxx}(\boldsymbol{r})$ smaller than -12.5 a.u.

6.3. Concluding remarks

It is found that there are some unique features of γ_{xxxx} for the NN radical. First, it is found that the neutral five-center radical, *i.e.*, NN radical, have large negative γ just we have expected. As mentioned in chapter 4, the neutral one- and three-center radicals, *i.e.*, CH_3 and $CH(CH_2)_2$, are shown to have positive γ, since the electronic polarized structure in SRIP is considered to scarcely contribute to the ground state. However, the electronic polarized structure of NN radical (See Fig.6.1) is expected to contribute to the ground state, since the electrons in nitroxide groups (NO•) tend to fluctuate. Second, it is found from the plots of $\rho^{(3)}_{xxx}(\boldsymbol{r})$ that γ_{xxxx} is primarily determined by the electron fluctuations in the bond region of the O-N-C-N-O unit. This feature is different from the usual case, where the extended spatial region remote from the bond region provides a dominant contribution to the γ. The third unique feature is the qualitatively good coincidence between $\rho^{(3)}_{xxx}(\boldsymbol{r})$ by the HF and QCISD methods. However, this does not immediately imply a good convergence of $\rho^{(3)}_{xxx}(\boldsymbol{r})$ by including low-order MP electron correlations. Actually, the MP2, MP3 and MP4 methods cannot sufficiently reproduce converged γ_{xxxx}, even in the sign. From a comparison among the MP4DQ, MP4SDQ, CCD and QCISD $\rho^{(3)}_{xxx}(\boldsymbol{r})$, a balanced inclusion of electron correlations with S and DQ effects beyond the fourth-order is essential for obtaining at least the correct sign of γ_{xxxx}. Judging from the qualitative coincidence of the spatial distributions of $\rho^{(3)}_{xxx}(\boldsymbol{r})$'s at the HF and QCISD methods, a cancellation among the S and DQ effects seems to be qualitatively achieved at the infinite-order.

By using the hyperpolarizability density analysis, a dominant contribution to γ_{xxxx} is found to be determined by the electron fluctuation in the O-N-C-N-O unit, where the SRIP largely contributes to the stability of the NN radical. As shown in the plot of the $\rho^{(3)}_{xxx}(\boldsymbol{r})$ at the QCISD level, the contributions from the vicinity of the N and O atoms on the left- and right-hand sides are different in sign. Since the magnitude of the positive contribution from the N atom regions both in NO groups is smaller than that of the negative contribution from the O atom regions both in NO groups, the total γ_{zzzz} is found to become negative.

Considering the sensitive electron fluctuation of the O-N-C-N-O radical unit, the high-order nonlinear optical responses would be dramatically changed by adding subtle chemical and physical perturbations. It is further expected from its attracting magnetic property that these systems with NN radicals would be one of the feasible candidates of high-order magnetic and optical systems in the future.

The multi-reference-based methods with small-size active space are found to be inferior to the single-reference-based high-order correlation methods in the calculation of γ for the system with SRIP. In the case of using small active spaces, the $|\gamma_{xxxx}|$ at the CAS-SCF level are considered to be much larger than that at CCSD(T) level. This indicates that the non-dynamical correlation corrections included in the CAS-SCF methods using small active spaces cannot remarkably improve the γ_{xxxx}, compared to the case of dynamical correlation correction included in the

CCSD(T) method. Although the $|\gamma_{xxxx}|$ become smaller in the case of larger active space, the use of a large active space reduces the advantage of the CAS-SCF method. Alternative methods including both high-order dynamical and non-dynamical correlation effects, *e.g.*, multi-reference-based coupled-cluster (MR-CC), will be necessary for providing correct γ_{xxxx} of larger-size SRIP systems with plural radical sites.

It is also found that the DFT approaches cannot well reproduce the $\rho^{(3)}{}_{xxx}(\boldsymbol{r})$ distribution at the QCISD level of NN radical particularly in the outside region with low electron density. However, the DF method has the advantage of treating large-size systems. If the improvement of the DFT approach is achieved by sophisticating the exchange and correlation functional, DFT approaches may be useful for the calculation of γ for these open-shell systems with SRIP. As a tentative attempt, a DFT approach with hybrid exchange functional will be effective for reproducing QCISD and CCSD(T) γ densities of a similar series of large size radical species.

Chapter 7 *Structure-property correlation in the second hyperpolarizabilities γ for phenyl nitronyl nitroxide radicals*

In the previous chapter, the main component of γ for nitronyl nitroxide radical (NN) is found to be large negative, and the main negative contribution is also found to originate in the electron fluctuation confined in the bond region of the NN unit from the γ density analysis. The mechanism of the electron fluctuation in the bond region also suggests a sensitivity of the γ to subtle changes in the structure.

The γ of these compounds with SRIP have a possibility of being controlled by subtle chemical and physical perturbations. The physical perturbation implies, for instance, an addition of external magnetic fields, while the chemical perturbation implies the chemical modification, *e.g.*, changes in the framework of the molecule and an introduction of substituent groups. In this chapter, the effects of the chemical perturbation on the γ for some phenyl nitronyl nitroxide radical (PNN) compounds are investigated [112]. First, we examine the effects of the rotation of the phenyl ring on the γ. Second, we introduce some donor or acceptor groups into the phenyl ring in the para position in order to investigate the variation in the electron fluctuation in the nitronyl nitroxide radical unit. The effects of the chemical perturbations on the γ are discussed in connection with the variations in the distributions of the charge and γ densities on the nitronyl nitroxide radical unit.

7.1. Calculated compounds

Figure 7.1 shows the structures of model compounds involving a symmetric nitronyl nitroxide radical unit. The symbol X represents donor (NH_2 and CH_3) and acceptor (CHO and CN) groups and H atom. The bond lengths and bond angles are determined from the substituted phenyl ring structures optimized by the semiempirical MO (PM3) method and the nitronyl nitroxide radical structure optimized by the ab initio unrestricted Møller-Plesset second-order (UMP2) method. The *x* direction of the compound is along the direction of the largest polarization in the nitronyl nitroxide radical unit. The γ_{xxxx} of PNN compounds considered to be primarily determined by the contribution from the NN unit. In this study, therefore, we confine our attention to the largest component γ_{xxxx}. In order to elucidate the effects of the electron delocalization on the γ_{xxxx}, the para-substituted phenyl ring is rotated from $\theta = 0°$ (corresponding to the largest π-electron delocalization) to 90° (corresponding to non π-electron delocalization).

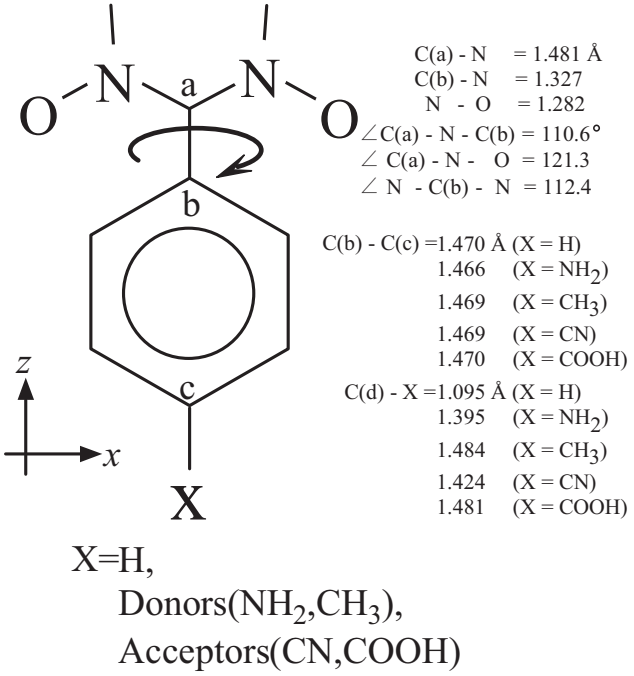

Fig.7.1. Structure of non- and para-substituted phenyl nitronyl nitroxide radicals (a) and the symmetric resonance structure with inversible polarization (SRIP) for nitronyl nitroxide radical unit (b). The X represents the substituent groups. The X = NH_2 and CH_3 are adopted as donor groups, while the X = CHO and CN are adopted as acceptor groups. The rotation angle of the substituted phenyl ring is depicted by the θ. The primarily bond lengths and bond angles optimized by PM3 and ab initio UMP2 using 6-311G** are also shown.

These γ are calculated by using the finite-field (FF) method in the INDO coupled Hartree-Fock (CHF) approximation. As concluded in the previous chapter, the NN radical have large SRIP contribution, therefore the γ of NN exhibit large electron-correlation dependency, though the basis set dependency of γ is relatively small. However, judging from the qualitative coincidence of the $\rho^{(3)}_{xxx}(\boldsymbol{r})$ distributions between at the HF and at the QCISD levels, a cancellation among the S and DQ effects seems to be qualitatively achieved at the infinite-order. Namely, the HF method is expected to reproduce the γ values of PNN compounds approximately at the QCISD level. In this study, INDO approximation is applied for calculation of γ for PNN compounds since the sizes of PNO compounds are too large to apply ab initio MO method. The INDO method has established reputation for calculation of radical species and can reproduce negative γ value for NN radical (γ_{xxxx}(HF/6-31G+*pd*) = -29200 a.u., γ_{xxxx}(QCISD/6-31G+*pd*) = -27100 a.u. and γ_{xxxx}(INDO) = -173000 a.u.), though the magnitude of γ_{xxxx} obtained by using INDO method is shown to be about six times as large as those using HF or QCISD methods. The results obtained by using INDO method are expected to be adequate for a qualitative study, particularly on sign of the γ.

7.2. Results and discussion

7.2.1. γ_{xxxx} versus rotation angle θ for non- and para-substituted phenyl nitronyl nitroxide radicals

Before investigating the γ_{xxxx}, we examine the γ_{zzzz} for all the compounds at the $\theta = 0°$. As shown in Table 7.1, all the γ_{xxxx} are negative against the positive γ_{zzzz}. For these compounds, as expected, the $|\gamma_{xxxx}|$ are found to be much larger than the $|\gamma_{zzzz}|$ and to be the largest components.

Table 7.1 γ_{xxxx} and γ_{zzzz} for all the substituted phenyl nitronyl nitroxide radicals at the $\theta = 0°$ calculated by using the INDO CHF method. The symbol X represents the substituent groups, *i.e.*, donor groups (NH_2 and CH_3) and acceptor groups (CHO and CN).

X	H	NH_2	CH_3	CHO	CN
γ_{xxxx}	-110000	-223000	-116000	-47900	-70600
γ_{zzzz}	3300	7400	6080	11700	8940

Variations in the γ_{xxxx} of non-, donor- and acceptor-substituted phenyl nitronyl nitroxide radicals for the rotational angle θ are shown in Fig.7.2. For the non-substituted phenyl nitronyl nitroxide radical, the γ_{xxxx} is shown to be negative in the whole range of the θ. As the θ increases from 0° to 90° the $|\gamma_{xxxx}|$ gradually declines and reaches the largest point at the $\theta = 90°$ where the largest $|\gamma_{xxxx}|$ is about 5 times as large as the $|\gamma_{xxxx}|$ at the $\theta = 90°$. This implies that a reduction of the π-electron delocalization over the nitronyl nitroxide radical unit and the phenyl ring causes the enhancement of the $|\gamma_{xxxx}|$.

For the phenyl nitronyl nitroxide radicals substituted by donor groups (X= NH_2 and CH_3), the γ_{xxxx} are also shown to be negative in the whole range of the θ. Similar increases in the $|\gamma_{xxxx}|$ with the increase in the γ_{xxxx} are observed. However, in the whole region of the θ, all the donor-substituted nitronyl nitroxide radicals are found to provide larger $|\gamma_{xxxx}|$ compared with those for non-substituted ones. The differences in the $|\gamma_{xxxx}|$ between for the non- and donor-substituted phenyl nitronyl nitroxide radicals are shown to be constant in the whole region of the θ, respectively, and are found to increase in order of the strength of the donating property ($NH_2 > CH_3$). This suggests that an increase in the electron density on the nitronyl nitroxide radical unit leads to the enhancement of the $|\gamma_{xxxx}|$.

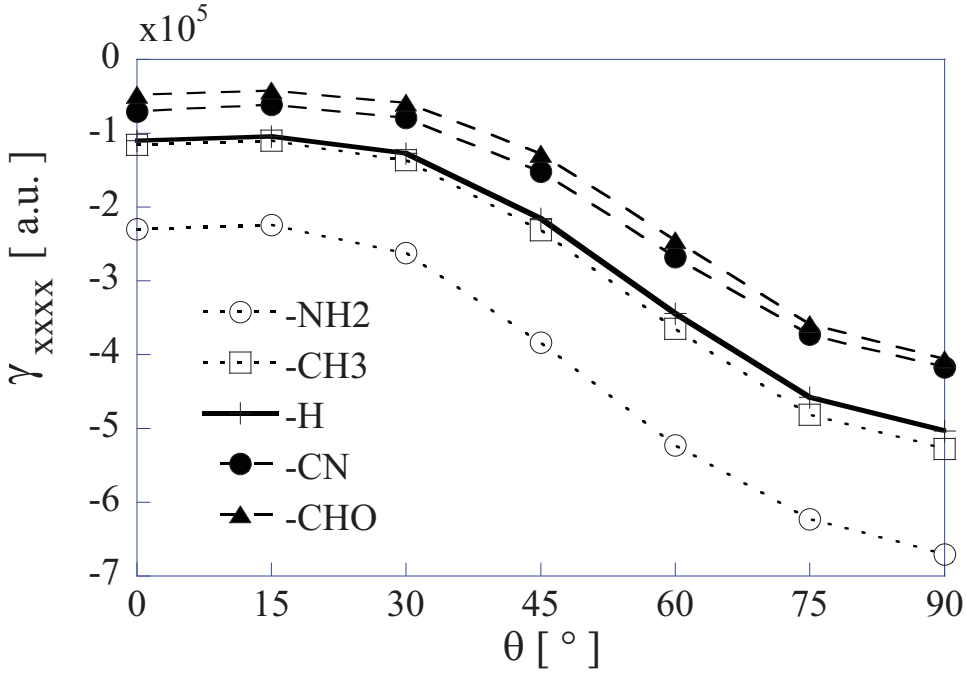

Fig.7.2. Variations in the γ_{xxxx} for the rotation angle θ. The solid, dotted and dashed lines represent the non-, donor- and acceptor-substituted phenyl nitronyl nitroxide radicals, respectively.

Similarly to the above two cases, the γ_{xxxx} for the phenyl nitronyl nitroxide radicals substituted by acceptor groups (X = CHO and CN) are also shown to be negative in the whole range of the θ and show increases in the $|\gamma_{xxxx}|$ with the increase in the θ. In contrast to the donor-substituted case, all the acceptor-substituted nitronyl nitroxide radicals are shown to provide smaller $|\gamma_{xxxx}|$ than non-substituted one does at the whole region of the θ. The differences in the $|\gamma_{xxxx}|$ between for non- and acceptor-substituted phenyl nitronyl nitroxide radicals are also shown to be constant in the whole range of the θ, respectively, and are found to increase in order of the strength of the accepting property (CHO > CN). This suggests that a decrease in the electron density on the nitronyl nitroxide unit leads to a decrease in the $|\gamma_{xxxx}|$.

7.2.2 γ_{xxxx} density analyses for non- and para-substituted phenyl nitronyl nitroxide radicals

Figure 7.3 shows the γ_{xxxx} densities on the nitronyl nitroxide radical units for the non- ((a)), donor- ((b) X = NH_2) and acceptor- ((c) X = CN) substituted phenyl nitronyl nitroxide radicals with the rotation angles θ = 0° and 90°.

(a) X = H

θ = 0° θ = 90°

(b) X = NH_2

θ = 0° θ = 90°

(c) X = CN

θ = 0° θ = 90°

Fig.7.3. Plots of γ_{xxxx} densities on the nitronyl nitroxide radical units for the non-(a), donor (X = NH_2)- and acceptor (X = CN)-substituted phenyl nitronyl nitroxide radicals, at the rotation angles θ = 0° and 90°. The dark circle indicates the position of atom.

For all the cases, the increases in the $|\gamma_{xxxx}|$ densities in the N-O regions are observed at the $\theta = 90°$ compared with the case at the $\theta = 0°$. This implies that the enhancement of the $|\gamma_{xxxx}|$ at the $\theta = 90°$ relates to the increase in the $|\gamma|$ densities since the contribution to the γ_{xxxx} from the N-O regions at the both ends of the nitronyl nitroxide radical units is found to provide a main negative contribution. Namely, a reduction of the π-electron delocalization over the nitronyl nitroxide radical unit and the phenyl ring is found to cause the enhancement of the $|\gamma_{xxxx}|$ density in the N-O regions.

It is found for the effects of the substituent groups on the γ_{xxxx} densities at the $\theta = 0°$ and 90° that the introduction of the donor group increases the $|\gamma_{xxxx}|$ densities in the N-O regions, while that of the acceptor group has an opposite effect. This feature suggests that the donating and accepting action on the phenyl ring primarily leads to the increase and decrease in the $|\gamma_{xxxx}|$ densities in the N-O regions, respectively, and then causes the changes in the γ_{xxxx}, as shown in Fig.7.2.

7.2.3 Relations between the distribution of charge density on the nitronyl nitroxide radical unit and the γ_{xxxx}

As mentioned in Sec.4.2, the increase and decrease in the charge density on the nitronyl nitroxide radical unit seem to determine the magnitude of the γ_{xxxx}. In this section, we examine the charge density on the nitronyl nitroxide radical units both at the $\theta = 90°$ and at the $\theta = 0°$ by reference to the charge density of the case for X = H at the $\theta = 0°$. As shown in Fig.7.4, the increase and the decrease in the charge densities on the O and N atom sites, respectively, are observed for these systems at the $\theta = 90°$. This indicates that a reduction of the π-electron delocalization over the nitronyl nitroxide radical unit and the phenyl ring causes the localization of electrons on the O atom sites due to the large electron negativity and then leads to the increase in the negative contributions to the γ_{xxxx}, as shown in Fig.7.3.

It is also found that the introduction of the donor group (X = NH_2) enhances the charge densities on the O atom sites, while the introduction of the acceptor group (X = CN) decreases the charge densities on the O atom sites. This feature is considered to lead to the remarkable changes in the γ_{xxxx} densities in the N-O regions for donor- and acceptor-substituted systems, as shown in Fig.7.3.

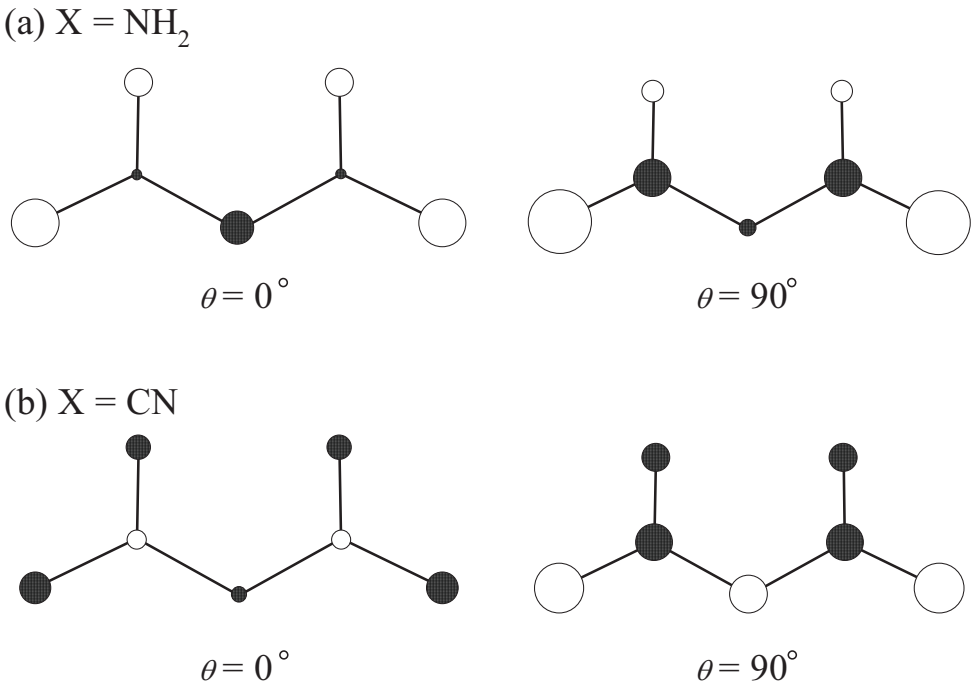

Fig.7.4. Plots of the charge densities on the nitronyl nitroxide radical units for the donor (X = NH_2)- and acceptor (X = CN)-substituted phenyl nitronyl nitroxide radicals both at the $\theta = 0°$ and at the $\theta = 90°$. These quantities are obtained by the charge density differences $\Delta\rho$ ($\equiv \rho$(X = NH_2 or CN, $\theta = 0°$ or 90°) - ρ(X = H, $\theta = 0°$)). The size of the circle represents the magnitude of the charge density difference. The white and black circles represent the positive and negative charge density differences, respectively.

7.3. Concluding remarks

The INDO CHF calculations and the γ_{xxxx} density analyses for some para-substituted phenyl nitronyl nitroxide radicals have been performed to elucidate the variations in the γ_{xxxx} by two chemical perturbations, *i.e.*, an introduction of donor or acceptor group, and a rotation of the substituted phenyl ring. For these compounds, the γ_{xxxx} are found to be negative and to be primarily contributed from the nitronyl nitroxide radical unit. From the results for the rotation of the phenyl rings, a reduction of π-electron delocalization over the nitronyl nitroxide radical unit and the phenyl ring is found to cause a localization of charges on the O atom sites and an enhancement of polarization in the N-O regions. The $|\gamma_{xxxx}|$ densities in the N-O regions are also found to enhance at the $\theta = 90°$. This can be explained by the enhancement of fluctuations of electrons in the N-O regions because of the increase and the decrease in charges on the O and N atom sites, respectively. As seen from the results for the introduction of donor or acceptor groups to the phenyl ring, the introduction of the donor group tends to increase the $|\gamma_{xxxx}|$, while

that of the acceptor group tends to decrease the $|\gamma_{xxxx}|$. This feature is also observed in the whole range of the θ. From the plots of the γ_{xxxx} densities and the charge differences on the nitronyl nitroxide radical units, the donating and accepting actions are found to cause respectively the increase and decrease in the polarization and $|\gamma_{xxxx}|$ densities in the N-O regions.

It is concluded that the $|\gamma_{xxxx}|$ of the phenyl nitronyl nitroxide radical is determined by the changes in the charge distributions in the N-O regions: the increase in the polarization in the N-O regions enhances the $|\gamma_{xxxx}|$, while the reduction of polarization in the N-O regions decreases the $|\gamma_{xxxx}|$. The charge densities on the O atom sites are predicted to be controlled by changing the degree of the π-electron delocalization over the nitronyl nitroxide radical unit and the phenyl ring, or by introducing donor or acceptor substituent group into the phenyl ring in para position. The reduction of the π-electron delocalization and the introduction of the donor group are found to increase and decrease in the charge densities on the O and N atom sites, respectively. As a result, the electron fluctuations in the nitronyl nitroxide radical unit is found to be sensitive to the subtle chemical perturbations.

After this theoretical study was reported, third-order nonlinear optical properties of 2-phenyl-4,4,5,5-tetramethylimidazoline-3-oxide-1-oxyl (PTIO), which is one of the phenyl nitronyl nitroxide radical, was reported by Kamada et al. [113]. The nonresonant values of second hyperpolarizabilities for PTIO measured by femtosecond Z-scan method at 780-857 nm are found to be negative. The observed absolute γ values for PTIO are in the order $10^{-35} \sim 10^{-34}$ e.s.u. These values are one or two order lager those of molecules with similar size unsaturated chain (2,5-dimethyl-2,4-hexadiene, $\gamma = 4.9 \times 10^{-36}$ e.s.u.; measured by THG method at 1908 nm) [114]. Although a comparison of γ obtained by different methods and in different wavelength is very difficult, the γ of PTIO is considered to support our prediction. Namely, this relatively large magnitude of γ is considered to originate in large charge fluctuation in NN group.

Chapter 8 *Theoretical study on the third-order nonlinear optical susceptibilities for β-phase crystal of p-NPNN*

In chapter 1, an approximate formula of γ and a classification rule based on the three-type analysis for sign and magnitude of γ is presented. Although it is well known that most organic molecules have positive γ, an existence of molecules with negative γ is predicted on the basis of the above analysis. Namely, the symmetric systems with large ground-state polarizabilities tend to exhibit negative γ. In chapter 6, we investigate the γ of the nitronyl nitroxide (NN) radical, whose structure conform to the guideline of negative γ, and found that NN radical has large negative γ at the higher-order electron-correlation levels. In chapter 7, we investigate the γ for several phenyl nitronyl nitroxide (PNN) radical species and found that PNN compounds also have negative γ.

In this chapter, the γ for para-nitrophenyl nitronyl nitroxide (*p*-NPNN), which is an open-shell system with two nitroxide radical groups nearly symmetrically arranged, is investigated[115,116]. On the basis of our classification rule, this molecule is expected to exhibit negative γ in the direction (x) of bond axis of the nitronyl nitroxide group. We also estimate the $\chi^{(3)}$ for the β-phase crystal of *p*-NPNN [117] by the oriented gas model [118,119]. In this crystal, the nitronyl nitroxide radicals align in a direction x, and hence the characteristics of γ_{xxxx} are considered to be reflected by those of γ of *p*-NPNN. Namely, the $\chi^{(3)}_{XXXX}$ is also expected to become negative in sign.

A combination of nonlinear optical and other functional properties is attracting for getting more profound understanding of the structure-property relationships. Recently, it was reported that the intercalated layered materials comprising an organic dye and inorganic MPS3 (M = Mn^{2+} or Cd^{2+}) exhibit both the second-order optical nonlinearity and permanent magnetization [120]. In contrast, the *p*-NPNN in the present study is known to construct a stable crystal (β-phase crystal), which is an organic ferromagnet below Tc = 0.6 K and is also a second-order nonlinear optical material [121]. Therefore, the β-phase crystal of *p*-NPNN has a possibility of being a fundamental system for high-order organic magneto-optical systems in the future.

For nitronyl nitroxide group involved in *p*-NPNN, which is nearly symmetric in the direction of x axis, the SRIP (shown in Fig.8.1) seem to largely contribute to the ground state, so that the γ_{xxxx} is expected to be negative.

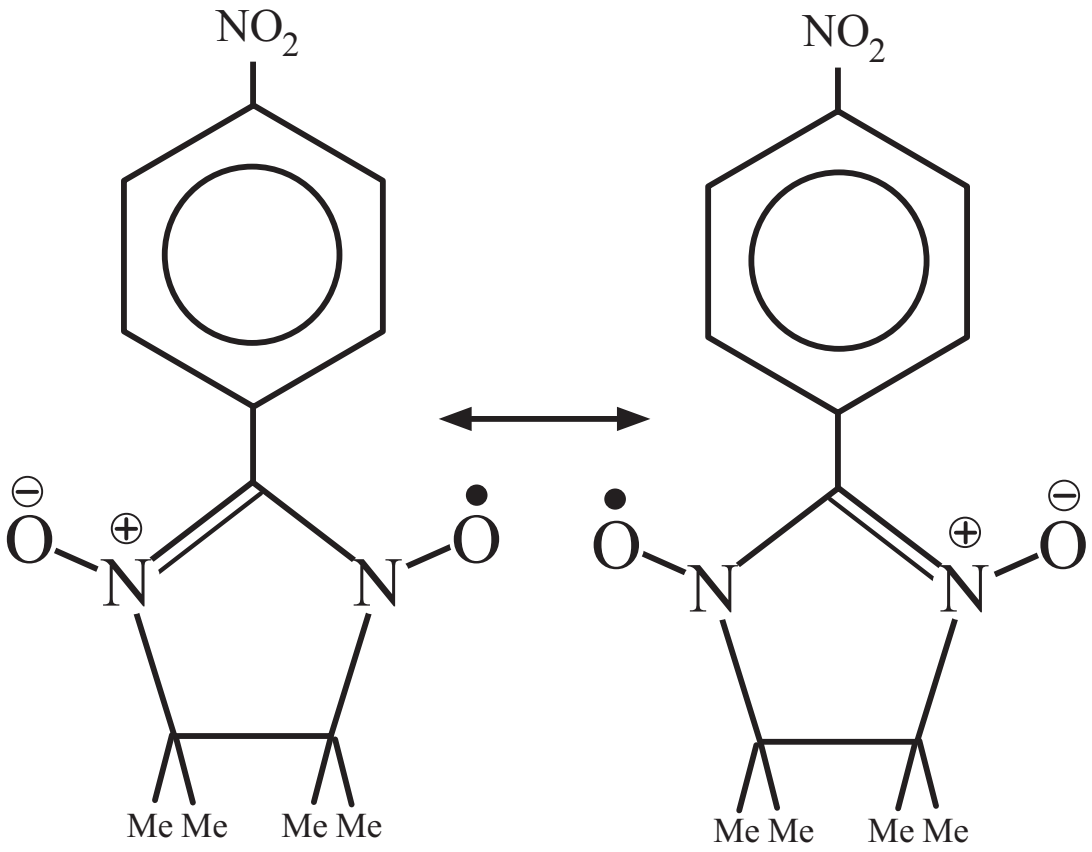

Fig.8.1. Symmetric resonance structures with inversible polarization (SRIP) for p-NPNN.

8.1. Calculation method and calculated systems

8.1.1. Monomer and cluster models in p-NPNN β-phase crystal

Figures 8.2 and 8.3 show the structures obtained from X-ray spectra [120] for *p*-NPNN monomer and its β-phase crystal. The *x* direction of the *p*-NPNN monomer is along the direction of the largest polarization in the nitronyl nitroxide radical group, O-N-C-N-O. The γ_{xxxx} of the nitronyl nitroxide radical group is expected to be negative based on our classification rule of γ. Further, the directions of the polarizations in the nitronyl nitroxide units nearly coincide with the direction of the *a* axis of the β-phase crystal of *p*-NPNN as shown in Fig.8.3. This structure suggests an emergence of negative $\chi^{(3)}$ in the direction of the *a* axis. Before the calculation of the macroscopic susceptibilities in the oriented gas model, we should consider the effects of intermolecular interactions on the γ since those effects are known to largely affect the γ. In this study, two types of main interaction paths along the *a* and *c* axes, respectively, (shown in Fig.8.4) are considered.

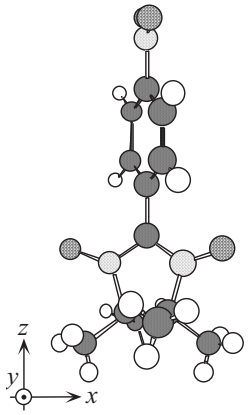

Fig.8.2. Structure of *p*-NPNN monomer obtained by the X-ray spectra.

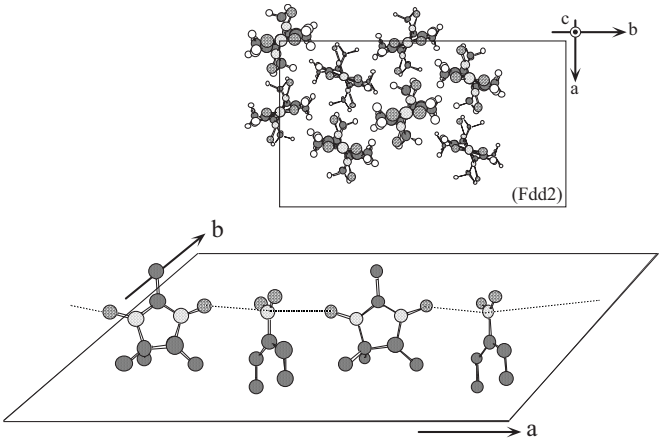

Fig.8.3. Configuration of *p*-NPNN in the β-phase crystal.

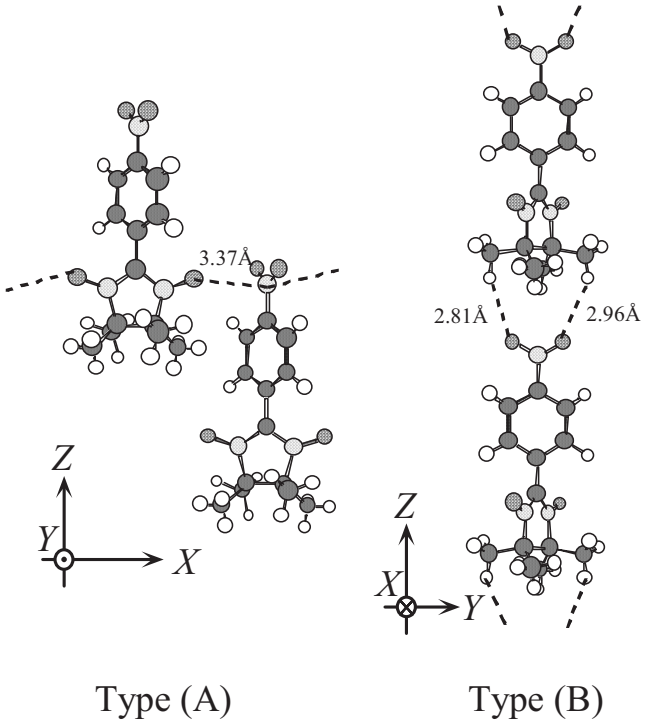

Fig.8.4. Two types of cluster models (types (A) and (B)), existing in *p*-NPNN β-phase crystal. The break lines represent the main intermolecular interaction paths.

For the calculation of γ for *p*-NPNN monomer and its cluster models, the INDO CHF method is employed. From a comparison between the experimental β [119] and the β calculated by the INDO CHF method, this method is considered to be adequate for a qualitative study, at least on sign of the γ.

8.1.2. Oriented gas model

In this section, we briefly explain a method for the calculation of nonlinear optical susceptibility on the basis of the oriented gas model [117]. The nonlinear optical susceptibilities for organic molecular crystals with weak intermolecular interactions are determined by the molecular hyperpolarizabilities. However, the molecular environment causes the changes of the molecular hyperpolarizabilities by the mutual polarization effects of neighboring molecules. On the macroscopic scale, this effect can be accounted for by a proper Lorentz local-field correction. A simple summation scheme can be adopted, whereby the hyperpolarizability tensor $\gamma(s)$ is related to the corresponding crystalline third-order nonlinear susceptibility $\chi^{(3)}$ (with components c^t_{IJKI} in crystalline frame), through the following relation. If the crystal point group γ allows for n(g) equivalent positions in the unit cell, then

$$\chi^{(3)}_{IJKL} = f_I(\omega_4) f_J(\omega_1) f_K(\omega_2) f_L(\omega_3) \sum_{t=1}^{P} N_t c^t_{IJKL} \tag{8.1}$$

$$c^t_{IJKL} = \frac{1}{n(\mathrm{g})} \sum_{\substack{s=1 \\ ijkl}}^{n(\mathrm{g})} \cos(I, i(s)) \cos(J, j(s)) \cos(K, k(s)) \cos(L, l(s)) \gamma_{ijkl} \tag{8.2}$$

where $f_I(\omega_4)$, $f_J(\omega_1)$, $f_K(\omega_2)$ and $f_L(\omega_3)$ represent local-field correlation, t is any of the P unequivalent positions and N_t is the actual number of molecules in one of the P nonequivalent subsets. Local molecular frames are fixed with respect to the molecules so that γ_{ijkl} in Eq. (8.2) is not dependent on either s or t.

Further, the summation in Eq. (8.2) initially running independently over all four molecular indices *ijkl* will be restricted to 24 components of the tensor γ_{ijkl} (allowing for Kleinman permutation symmetry).

Lorentz local field corrections used in Eq. (8.1) are calculated as follows. The factor a^t_{IJ}, which corresponds to c^t_{IJKL} in the third-order nonlinearity, is represented by

$$a^t_{IJ} = \frac{1}{n(\mathrm{g})} \sum_{\substack{s=1 \\ ij}}^{n(\mathrm{g})} \cos(I, i(s)) \cos(J, j(s)) \alpha_{ij} \quad . \tag{8.3}$$

The diagonal part a^t_{II} can be related to the refraction index n_I as

$$a^t_{II} = \frac{3}{4\pi N_A} \frac{n_I^2 - 1}{n_I^2 + 2} \quad , \tag{8.4}$$

where N_A is Avogadro number. Using Eq. (8.4), Lorentz local field correction is represented by the static a^t_{II}

$$f_I(0) = \frac{n_I^2 + 2}{3} = \frac{3}{3 - 4\pi N_A \alpha^t_{II}} \qquad (\mathrm{I} = \mathrm{X}, \mathrm{Y}, \mathrm{Z}), \tag{8.5}$$

where a^t_{II} can be calculated from α_{ij} by using Eq. (8.3).

8.2. Results and discussion

8.2.1. INDO CHF calculation of γ for p-NPNN monomer

Each component of γ for a monomer of *p*-NPNN calculated by the INDO CHF method is shown in Table 8.1. The largest component, γ_{xxxx}, is found to be negative. This feature is in

good agreement with our prediction based on our classification rule. Namely, a feasibility of electron fluctuation on the nitronyl nitroxide radical unit, O-N-C-N-O, seems to enhance the ground state polarizability and hence tends to provide negative γ_{xxxx}. In contrast, the second largest component, γ_{zzzz}, is shown to be positive. From our classification rule of γ, this seems to be ascribed to a predominant contribution from the charge transfer (CT) excitation between the ground and the allowed first excited states with noncentrosymmetric charge distributions.

8.2.2. Macroscopic $\chi^{(3)}$ in β-phase crystal of p-NPNN

In the β-phase crystal of *p*-NPNN shown in Fig.8.3, two types of main intermolecular interaction paths in the directions of the a and c axes exist. Fig.8.4 shows two types of cluster models, (A) and (B), of *p*-NPNN, corresponding to the two types of main interaction paths, respectively. To include this interaction effects, the *a* and *c* for monomer estimated by the calculations of the cluster models are used in the oriented gas model. Fig.8.5 shows variations in γ_{zzzz} per monomer and γ_{xxxx} per monomer with the increase in the size of the clusters in types (A) and (B). The increase in the size of the cluster in type (B) enhances the γ_{zzzz} per monomer, while that in type (A) decreases the γ_{zzzz} per monomer. As a result, the increases in the size of the clusters both in types (A) and (B) are expected to have only a small effect on the γ_{zzzz} per monomer. This is indicated by the γ_{zzzz} for a tetramer model in type (A)+(B). The increase in the size of the cluster in type (B) slightly changes the γ_{xxxx} per monomer, while that in type (A) largely enhance the magnitude of the γ_{xxxx} per monomer. As a result, in the β-phase crystal of *p*-NPNN, the magnitude of the γ_{xxxx} per monomer is expected to be considerably enhanced compared with that for a monomer model. In the oriented gas model, therefore, for γ_{xxxx} per monomer we use the value obtained from the tetramer model in type (A), while for γ_{zzzz} per monomer we use the value obtained from the monomer model.

Table 8.1 Microscopic γ values [a.u.] of *p*-NPNN calculated using the INDO CHF method.

γ_{xxxx}	γ_{yyyy}	γ_{zzzz}	γ_{xxyy}	γ_{yyzz}	γ_{xxzz}
-33900	-284	14700	-2350	41.1	4137

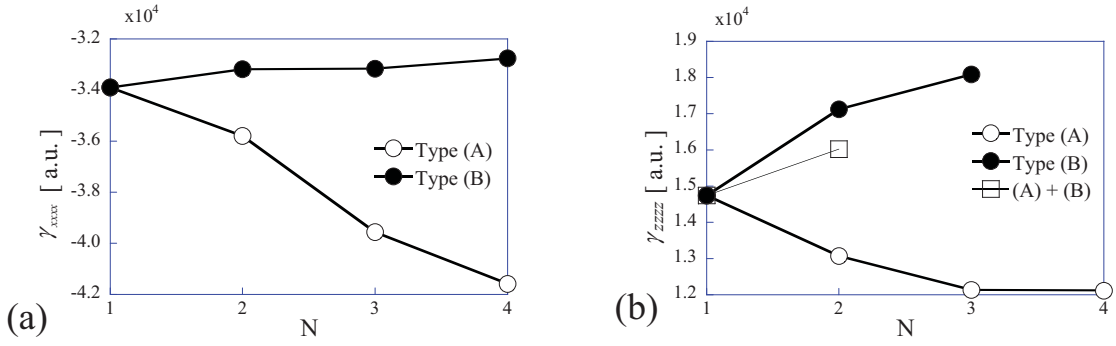

Fig.8.5. Variations in γ_{zzzz} per monomer and γ_{xxxx} per monomer with the increase in the size of the clusters in types (A) and (B) shown in Fig.3. The symbol N depicts the number of monomer. The γ_{zzzz} per monomer is shown to be sufficiently converged for tetramer models in types (A) and (B), though the γ_{zzzz} for the tetramer in type (B) was not obtained in sufficient precision.

Each component of $\chi^{(3)}$ for the β-phase crystal of *p*-NPNN calculated by the INDO CHF method are given in Table 8.2. As expected from the characteristics of γ_{xxxx} for the nitronyl nitroxide and alignment structure of *p*-NPNN in the β-phase crystal, the largest component, $\chi^{(3)}_{XXXX}$, is found to be negative, while the second largest component, $\chi^{(3)}_{ZZZZ}$, is found to be positive. From a comparison of relative magnitudes of these components between for *p*-NPNN monomer and for its crystal, the difference in magnitudes is more enhanced in the crystal than in the monomer. This feature seems to be caused by the differences in the contributions from intermolecular interactions, types (A) and (B), to the γ_{xxxx} and γ_{zzzz}.

Table 8.2 Macroscopic $\chi^{(3)}/10^{-14}$ values [esu/cm^3] for β-phase crystal of *p*-NPNN calculated using the INDO CHF method in the oriented gas model.

$\chi^{(3)}_{XXXX}$	$\chi^{(3)}_{YYYY}$	$\chi^{(3)}_{ZZZZ}$	$\chi^{(3)}_{XXYY}$	$\chi^{(3)}_{YYZZ}$	$\chi^{(3)}_{XXZZ}$
-15.27	-0.08	5.90	-0.77	0.01	1.59

8.3. Concluding remarks

The INDO CHF calculation is found to provide a large negative γ for *p*-NPNN, in which the nitronyl nitroxide radical structure is involved. It is also found that the main intermolecular interactions in types (A) and (B) existing in the β-phase crystal of *p*-NPNN enhance the magnitude of the γ_{xxxx} per monomer (negative) in contrast to the γ_{zzzz} per monomer (positive). This feature suggests that the negative contribution from the symmetric nitronyl nitroxide structure is considerably enhanced by the one-dimensional interaction path on the one-dimensional structure nearly symmetrically aligned in the direction of the *a* axis. Therefore, the $\chi^{(3)}_{XXXX}$ for the β-phase crystal of *p*-NPNN is expected to be a largely enhanced negative value. Actually, in the oriented gas model using the γ including the effects of intermolecular interactions, the $\chi^{(3)}_{XXXX}$ for β-phase crystal of *p*-NPNN is found to be the largest component with negative sign. It is also interesting that the ferromagnetic interaction path in the direction of the O-N-C-N-O axis is also essential for the realization of the large negative $\chi^{(3)}_{XXXX}$. In order to confirm the features obtained here, the ab initio electron correlation methods have to be applied to the evaluation of the γ for *p*-NPNN and for its clusters, since it is pointed out that open-shell systems exhibit large electron-correlation dependencies of γ.

Chapter 9 Conclusions

9.1. Summary

In the present study, the second hyperpolarizabilities for radical species and realization of the system with large negative second hyperpolarizability are investigated.

In chapter 1, a classification rule for molecular second hyperpolarizability based on virtual excitation process of a molecule is suggested. Based on the classification rule, it is possible to design novel systems with large negative γ. Namely, if the symmetric resonance structures with inversible polarization (SRIP) greatly contribute to the ground state, the system tend to exhibit large negative γ and the electron-correlation dependency of γ is predicted to be very large.

In chapter 3, the analysis method using hyperpolarizability density is developed. The hyperpolarizability is defined as the differentiation of charge density with respect to the external electric field. Therefore, we can estimate the spatial contribution of charges to hyperpolarizability by using hyperpolarizability density distributions. By using the second hyperpolarizability density distribution of ethylene, the variation of γ for ethylene in basis sets and electron-correlation levels are visualized.

In chapter 4, the large electron-correlation effects detected in nitroxide radical (H_2NO) by using hyperpolarizability density analysis. This feature of γ in nitroxide radical are considered to be caused by the remarkable fluctuation of charges on N-O group, the effects of which are found to be evaluated qualitatively by the infinite-order single excitation correlation involved in the CCSD and QCISD methods.

In chapter 5, it is found that the γ values of iso-electronic one- and three-canter radicals sensitively reflect the features of the charge distributions and the degree of SRIP contributions. In particular, the defect in charge for three-center cation radical ($NH(CH_2)_2^+$) is considered to enhance the SRIP contribution, so that $NH(CH_2)_2^+$ exhibits negative γ, though the magnitude of the γ is small.

In chapter 6, it is found that the neutral five-center radical, *i.e.*, nitronyl nitroxide (NN) radical, possess large negative γ just as we have expected. It is also found from γ density distribution that the γ of NN radical is primarily determined by the electron fluctuations in the bond region of the O-N-C-N-O unit.

In chapter 7, it is found that the $|\gamma_{xxxx}|$ of the phenyl nitronyl nitroxide (PNN) radical is determined by the changes in the charge distributions in the N-O regions: the increase in the polarization in the N-O regions enhances the $|\gamma_{xxxx}|$, while the reduction of polarization in the N-O regions decreases the $|\gamma_{xxxx}|$. The charge densities on the O atom sites are predicted to be

controlled by changing the degree of the π-electron delocalization over the NN unit and the phenyl ring, or by introducing donor or acceptor substituent group into the phenyl ring in para position.

In chapter 8, it is found that a real stable radical, para-nitro phenyl nitronyl nitroxide (*p*-NPNN) radical, has a large negative γ. It is also found that the main intermolecular interactions existing in the β-phase crystal of *p*-NPNN enhance the magnitude of the γ_{xxxx} (negative) per monomer in contrast to the γ_{zzzz} (positive) per monomer. Therefore, the $\chi^{(3)}_{XXXX}$ for the β-phase crystal of *p*-NPNN is expected to be enhanced. Actually, in the oriented gas model using the γ including the effects of intermolecular interactions, the $\chi^{(3)}_{XXXX}$ for β-phase crystal of *p*-NPNN is found to be the largest component with negative sign.

It is concluded from the present study that the radical species are expected to be important as nonlinear optical materials. The large negative second hyperpolarizability of small size neutral molecule, *i.e.*, NN radical, is considered to be caused by the electron fluctuation in radical species. Besides the nonlinear optical properties of radical species are expected to be controlled easily by chemical perturbations as observed in PNN compounds. The classification rule of γ based on virtual excitation process is found to be useful for predicting the nonlinear optical property of radical species, and the hyperpolarizability density analysis is considered to be useful for obtaining a "local view" of the nonlinear optical polarization.

9.2 Future extensions

In the present study, the calculations of hyperpolarizabilities for PNN compounds and p-NPNN are carried out by using INDO method, notwithstanding the importance of electron-correlation for describing the second hyperpolarizability. One reason is that the INDO approximation is expected to provide qualitative values of hyperpolarizabilities for PNN compounds and p-NPNN radical, since the γ value of NN radical obtained using INDO method give agreement with that using QCISD method. The other reason is that the higher-order electron-correlation methods, *e.g.*, QCISD and CCSD(T) methods, cannot be applied because of the large size of the molecules. Although, it is not impossible to apply DFT approaches, *e.g.*, BLYP and B3LYP methods, for the calculation of hyperpolarizabilities for PNN compounds, it is found that these methods cannot well reproduce γ of NN radical at the CCSD(T) level in chapter 6. Therefore, it is desirable to develop a new DFT approach, which can reproduce hyperpolarizabilities of systems with large SRIP contributions at the CCSD(T) level as soon as possible. For example, a hybrid exchange functional approach would be useful.

In chapter 8, the effect of interaction between p-NPNN molecules in the crystal on γ is estimated from the variations of γ per monomer obtained from the cluster calculations. In this approach, the effects of the intermolecular spin interaction on the nonlinear optical properties have not been investigated. However, this interaction is considered to be indispensable for studying magnet-optical phenomena in radical clusters. The author wishes to solve this

problem in future.

In the present study, the author investigates organic radicals alone. However, nonlinear optical properties of systems including metal atoms are very interesting, since the existence of electrons in d-orbital is expected to cause various effects on nonlinear optical phenomena. The author have already studied the hyperpolarizabilities of organometalic conjugated systems by using higher-order electron-correlation methods and hyperpolarizability density analysis [123,124]. The author plans to apply DFT approaches to calculations of various organometalic conjugated systems, which are expected to novel nonlinear optical phenomena.

References

Chapter 1

[1] N. Bloembergen, *Nonlinear Optics*, Benjamin, New York. (1965)

[2] J. Orr and J. F. Ward, *Mol. Phys.* **20**, 513 (1971).

[3] J. Z yss and G. Berthier, *J. Chem. Phys.* **77**, 3635 (1982).

[4] J. Zyss, *J. Chem. Phys.* **70**, 3333, 3341; *ibid*. **71**, 909 (1979).

[5] O. Zamani-Khamiri, E. F. McIntyre and H. F. Hameka, *J. Chem. Phys.* **72**, 1280, 5906 (1980).

[6] E. F. McIntyre and H. F. Hameka, *J. Chem. Phys.* **68**, 3481, 5534; *ibid*. **69**, 4814 (1978);, *ibid*. **70**, 2215 (1979).

[7] O. Zamani-Khamiri H. F. and Hameka, *J. Chem. Phys.* **71**, 1607 (1979).

[8] J. Yu, B. Freedman, P. R. Baldwin and W. P. Su, *Phys. Rev. B* **39**, 12814 (1989).

[9] H. F. Hameka and E. N. Svendsen, *Int. J. Quantum Chem.* **XI**, 129 (1977).

[10] X. Sun, Z. Shuai, R. Fu, K. Nasu, X. S. Li, D. L. Lin and T. F. George, *J. Phys. Condens. Matt.* 2, 9713 (1990).

[11] D. M. Mackie, R. J. Cohen and A. J. Glick, *Phys. Rev.* **39**, 3442 (1989).

[12] W. Wu, *Phys. Rev. Lett.* **61**, 1119 (1988).

[13] W. Wu and S. Kivelson, *Synt. Metals* **28**, D575 (1989).

[14] W. Wu and X. Sun, *Phys. Rev. B* **42**, 9736 (1990).

[15] Z. G. Soos and G. W. Hayden, *Phys. Rev. B* **40**, 3081 (1989).

[16] D. Li, M. A. Ratner and T. J. Marks, *J. Am. Chem. Soc.* **110**, 1707 (1988).

[17] C. W. Dirk, R. J. Twieg and G. Wagniere, *J. Am. Chem. Soc.* **108**, 5387 (1986).

[18] S. Ramasesha and I. D. L. Albert, *Phys. Rev. B* **42**, 8587 (1990).

[19] I. D. L. Albert, P. K. Das and S. Ramasesha, *Chem. Phys. Lett.* **168**, 454 (1990).

[20] Z. G. Soos and S. Ramasesha, *J. Chem. Phys.* **90**, 1067 (1989).

[21] I. D. L. Albert and S. Ramasesha, *Chem. Phys. Lett.* **182**, 351 (1991).

[22] J. O. Morley, P. Pavlides and D. Pugh, *J. Chem. Soc. Faraday Trans* 2 85, 1789 (1989).

[23] J. O. Morley, V. J. Docherty and D. Pugh, *J. Chem. Soc. Perkin Trans* 2 1351, 1361, 1357 (1987).

[24] J. O. Morley, *J. Am. Chem. Soc.* 110, 7660 1991;, *J. Chem. Soc. Faraday Trans*. 2 87, 3009, 3015, 3021 (1988).

[25] J. R. Heflin, K. Y. Wong, O. Zamani-Khamiri and A. F. Garito, *Phys. Rev. B* **38**, 1573 (1988).

[26] V. J. Docherty, D. Pugh and J. O. Morley, *J. Chem. Soc. Faraday Trans*. 2, 81, 1179 (1985).

[27] C. C. Teng and A. F. Garito, *Phys. Rev. B* **28**, 6766; *Phys. Rev. Lett.* **50**, 350 (1983).

[28] J. A. Morrell and A. C. Albrecht, *Chem. Phys. Lett.* **64**, 46 (1979).

[29] S. J. Lalama, K. D. Singer, A. F. Garito and K. N. Desai, Appl. Phys. Lett. **39**, 940 (1981).

[30] S. J. Lalama and A. F. Garito, *Phys. Rev. A* **20**, 1179 (1979).
[31] T. Tsunekawa, T. Gotoh and M. Iwamoto, *Chem. Phys. Lett.* **166**, 353 (1990).
[32] T. Tsunekawa, T. Gotoh, H. Mataki, T. Kondoh, S. Fukuda and M. Iwam oto, *Nonlinear Optical Properties of Organic Materials III*, SPIE. **1337**, 272 (1990).
[33] J. Wu, J. R. Heflin, R. A. Norwood, K. Y. Wong, O. Zamani-Khamiri and A. F. Garito, *J. Opt. Soc. Am. B* **6**, 707 (1989).
[34] B. M. Pierce, *J. Chem. Phys.* **91**, 791 (1989); *Mat. Res. Soc. Symp. Proc.* **109**, 109 (1988).
[35] W. A. Parkinson and M. C. Zerner, *J. Chem. Phys.* **90**, 5606 (1989); *ibid*. **94**, 478 (1991).
[36] T. Yoshimura, *Appl. Phys. Lett.* 55, 534 (1989); *Phys. Rev. B* **40**, 6292 (1989).
[37] T. Yasukawa, T. Kimura and M. Uda, *Chem. Phys. Lett.* **169**, 259 (1990).
[38] F. C. Spano and S. Mukamel, *Phys. Rev. A* **40**, 5783 (1989).
[39] M. E. Lines, *Phys. Rev. B* **41**, 3372, 3383 (1990).
[40] C. Cojian, G. P. Agrawal and C, Flytzanis, *Phys. Rev. B* **15**, 909 (1977).
[41] G. P. Agrawal, C. Cojian and C. Flytzanis, *Phys. Rev. B* **17**, 776 (1989).
[42] T. T. Rantala, M. L. Stockmann, D. A. Jelski and T. F. George, *J. Chem. Phys.* **93**, 7427, (1990).
[43] G. Senatore and K. R. Subbaswamy, *Phys. Rev. A* **35**, 2440 (1987).
[44] R. L. Martin, E. R. Davidson and D. F. Eggers, *Chem. Phys.* **38**, 341 (1979).
[45] T. Inoue and S. Iwata, *Chem. Phys. Lett.* **167**, 566 (1990).
[46] Y. Nomura, S. Miura, M. Fukunaga, S. Narita and T. Shibuya, *J. Chem. Phys.* **106**, 3243 (1997).
[47] D. Jacquemin, B. Champagne, J-M. Andre, *Chem. Phys.* **197**, 107 (1995).
[48] D. M. Bishop and B. Lam, *J. Chem. Phys.* **89**, 1571 (1988); *ibid*. **91**, 3549 (1989).
[49] G. H. Wagniere and J. B. Hutter, *J. Opt. Soc. Am. B* **6**, 693 (1989).
[50] D. N. Beratan, J. N. Onuchic and J. W. Perry, *J. Phys. Chem.* **91**, 2696 (1987).
[51] S. M. Risser and K. F. Ferris, *Chem. Phys. Lett.* **170**, 349 (1990).
[52] Nakano, M., Yamaguchi, K., and Fueno, T., in *Nonlinear Optics of Organic and Semiconconductors*, T. Kobayashi (Ed.), Springer Proceedings in Physics **36**, 98, 103 (1989).
[53] M. Nakano, M. Okumura, K. Yamaguchi and T. Fueno, *Mol. Cryst. Liq. Cryst.* **182A**, 1 (1990).
[54] M. Nakano, K. Yamaguchi and T. Fueno, *Computer Aided Innovation of New Materials*, Elsevier, Amsterdam, 259 (1991).
[55] M. Nakano and K. Yamaguchi, *Chem. Phys. Lett.* **206**, 285 (1993).
[56] R. G. Denning, *J. Mater. Chem.* **5**, 365 (1995).
[57] F. Kajzar, J. Messier in *Conjugated Polymers*, J. L. Brédas and R. Silbey (Eds.), 509, Kluwer, Dordrecht (1991).
[58] C. W. Dirk, L-T. Cheng and M. G. Kuzyk, *Int. J. Quantum Chem.* 43, 27 (1992).

[59] J. R. Heflin and A. F. Garito in *Electroresponsive Molecular and Polymeric Systems*, T. A. Skotheim (Ed.), Marcel Dekker, New York, Vol.2, 113 (1991).
[60] Y. R. Shen, *The Principles of Nonlinear Optics*, Wiley, New York (1984).
[61] D. J. Williams, *Angew. Chem. Int. Ed.* **23**, 690 (1984).
[62] D. P. Craig and T. Thirunamachandran, *Molecular Quantum Electrodynamics*, Academic Press, New York (1984).
[63] D. Jacquemin, B. Champagne, J-M. Andre, *Chem. Phys.* **197**, 107 (1995).
[64] M. Nakano, K. Yamaguchi, Y. Matuzaki, K. Tanaka and T. Yamabe, *J. Chem. Phys.* **102**, 2996 (1995).
[65] M. Nakano, S. Kiribayachi, S. Yamada, I. Shigemoto and K. Yamaguchi, *Chem. Phys. Lett.* **262**, 66 (1996).

Chapter 2

[66] Gaussian 94, Revision B.1, M. J. Frisch, G. W. Trucks, M. Head-Gordon, P. M. W. Gill, M. W. Wong, J. B. Foresman, B. G. Johnson, H. B. Schlegel, M. A. Robb, E. S. Replogle, R. Gomperts, J. L. Andres, K. Raghavachari, J. S. Binkley, C. Gonzalez, R. L. Martin, D. J. Fox, D. J. Defrees, J. Baker, J. J. P. Stewart and J. A. Pople, Gaussian, Inc., Pittsburgh PA (1995).
[67] M. Peng, *Proc. Soc. Lond. A* **178**, 449 (1941).
[68] J. Zyss, *J. Chem. Phys.* **70**, 3333 (1979).
[69] M. G. Papadopoulos, J. Waite and C. A. Nicolaides, *J. Chem. Phys.* **77**, 2527 (1982).
[70] J. Waite and M. G. Papadopoulos, *J. Chem. Phys.* **82**, 1427 (1985).
[71] C. P. deMelo and R. Silbey, *Chem. Phys. Lett.* **140**, 537 (1987).
[72] P. Chopra, L. Carlacci, H. F. King and P. N. Prasad, *J. Phys. Chem.* **93**, 7120 (1989).
[73] E. Perrin, P. N. Prasad, P. Mougenot and M. Dupuis, *J. Chem. Phys.* **91**, 4728 (1989).
[74] R.J. Bartlet and G.D. Purvis III, *Phys. Rev. A* **20**, 1313 (1979).
[75] B. Kirtman and M. Hasan, *Chem. Phys. Lett.* **157**, 123 (1989).
[76] H. D. Cohen and C. C. J. Roothaan, *J. Chem. Phys.* **S34**, 43 (1965).
[77] N. S. Hush and M. L. Williams, *Chem. Phys. Lett.* **5**, 507 (1970).
[78] J. E. Gready and G. B. Bacskay and N. S. Hush, *Chem. Phys.* **22**, 141 (1977).
[79] R. Feynman, *Phys. Rev.* **56**, 340 (1939); S. T. Epatein, *Am. J. Phys.* **22**, 613 (1954); R. E. Stanton,*J. Chem. Phys.* **36**, 1298 (1962).
[80] O. Sinanoglu, *J. Chem. Phys.* **36**, 706 (1962).
[81] O. Sinanoglu, *J. Chem. Phys.* **36**, 3198 (1962).
[82] O. Sinanoglu and D. F. Tuan, *J. Chem. Phys.* **38**, 1740 (1963).
[83] C. Møller and M. S. Plesset, *Phys. Rev.* **46**, 618 (1934).
[84] F. Coester, *Nucl. Phys.* **7**, 421 (1958).
[85] F. Coester and H. Kümmel, *Nucl. Phys.* **17**, 477 (1960).
[86] J. Cizek and J. Paldus, *Int. J. Quantum Chem.* **5**, 359 (1971).
[87] J. Paldus, J. Cizek and I. Shavitt, *Phys. Rev. A* **5**, 50 (1972).
[88] R. J. Bartlett and G. D. Purvis, *Int. J. Quantum Chem.* **16**, 561 (1978).

[89] R. J. Bartlett, *J. Phys. Chem.* **93**, 169 (1989)
[90] J. A. Pople and M. Head-Gordon, *J. Chem. Phys.* **87**, 5968 (1987).
[91] G. E. Scuseria and H. F. Schaefar III, *J. Chem. Phys.* **90**, 3700 (1989).
[92] P. Hohenberg and W. Kohn, *Phys. Rev. B* **136**, 864 (1964); W. Kohn and L. J. Sham, *Phys. Rev. A* **140**, 1133 (1965).
[93] A. D. Becke, *Phys. Rev. A* 38 3098 (1988); *Int. J. Quantum Chem. Symp.* **23**, 599 (1989).
[94] C. Lee, W. Yang and R. G. Parr, *Phys. Rev. B* **37**, 786 (1988)
[95] A. D. Becke, *J. Chem. Phys.* **96**, 2155 (1992).
[96] A. D. Becke, *J. Chem. Phys.* **97**, 9173 (1992).
[97] A. D. Becke, *J. Chem. Phys.* **98**, 5648 (1993).
[98] J. P. Perdew and Y. Wang, *Phys. Rev. B* **45**, 13244 (1992).
[99] N. Matsuzawa and D. A. Dixon, *J. Phys. Chem.* **96**, 6241, 6872 (1992).
[100] B. O. Roos, P. R. Taylor and P.E.M. Siegbahn, *Chem. Phys.* **48**, 157 (1980).
[101] B. O. Roos and A. J. Sadlej, *J. Chem. Phys.* **76**, 5444 (1982).
[102] J. A. Pople and D. L. Beveridge, *Approximate Molecular Orbital Theory*, McGraw-Hill, New York (1970).

Chapter 3

[103] M. Nakano, K. Yamaguchi and T. Fueno, *Nonlinear Opt.* **6**, 289 (1994)
[104] M. Nakano, K. Yamaguchi and T. Fueno, *Chem. Phys. Lett.* **185**, 550

Chapter 4

[105] S. Yamada, M. Nakano, I. Shigemoto and K. Yamaguchi, *Chem. Phys. Lett.* **254**, 158 (1996).
[106] N. Matsuzawa and D. A. Dixon, *J. Phys. Chem.* **98**, 2545 (1994).

Chapter 5

[107] S. Yamada, M. Nakano, M. Nishino and K. Yamaguchi, *Synt. Metals*, *in press* (1999)
[108] S. Yamada, M. Nakano and K. Yamaguchi, *Mol. Cryst. Liq. Cryst*, *in press* (1999)
[109] S. Yamada, M. Nakano, M. Nishino and K. Yamaguchi, *Opt. Rev. in press* (1999)

Chapter 6

[110] M. Nakano, S. Yamada and K. Yamaguchi, *Bull. Chem. Soc. Jpn.* **71**, 845 (1998)
[111] S. Yamada, M. Nakano and K. Yamaguchi, *Int. J. Quantum Chem.* **71**, 329(1999).

Chapter 7

[112] S. Yamada, M. Nakano and K. Yamaguchi, *Chem. Phys. Lett.* **276**, 375 (1996)
[113] K. Kamada, K.Ohta, J. Nakamura, S. Yamada, M. Nakano and K. Yamaguchi, *Mol. Cryst. Liq. Cryst.* **315**, 117 (1998)

[114] S. H. Stevenson, D. S. Donald and G. R. Meredith, *Mater. Res. Soc. Symp. Proc.*, **109**, 103 (1988).

Chapter 8

[115] M. Nakano, S. Yamada, I. Shigemoto, S. Kiribayashi, and K. Yamaguchi, *Mol. Cryst. Liq. Cryst.* **294**, 251 (1997)

[116] S. Yamada, M. Nakano, S. Kiribayashi, I. Shigemoto and K. Yamaguchi, *Synt. Metals* **85**, 1081 (1997)

[117] S. Yamada, M. Nakano, I. Shigemoto, S. Kiribayashi and K. Yamaguchi, *Chem. Phys. Lett.* **267**, 438 (1997)

[118] J. Zyss, G. Tsoucaris in *Structure and Properties of Molecular Crystals*, edited by M. Pierrot, Elsevier, Amsterdam, **Chapter 6**, 297 (1990).

[119] J. Zyss and J. L. Eudora, *Phys. Rev. A* **26**, 2028 (1982).

[120] P. G. Lacroix, R. Clement, K. Nakatani, J. Zyss, I. Ledoux, *Science* **263**, 658 (1994).

[121] J. F. Nicoud, C. Serbutoviez, G. Puccetti, I. Ledoux and J. Zyss, *Chem. Phys. Lett.* **175**, 257 (1990).

[122] K. Awaga, private communication.

Chapter 9

[123] I. Shigemoto, M. Nakano, S. Yamada, S. Kiribayashi and K. Yamaguchi, *Mol. Cryst. Liq. Cryst.* **286**, 159 (1996).

[124] I. Shigemoto, M. Nakano, S. Yamada, S. Kiribayashi, S. Yamanaka and K. Yamaguchi, *Synt. Metals* **86**, 2241 (1997).

Publish list

Papers

[1] "Theoretical Studies on Hyperpolarizabilities of Nitroxide Species I",
M. Nakano, S. Yamada and K. Yamaguchi, *Synt. Metals* **71**, 1691-1692. (1995)

[2] "Size-consistent approach and density analysis of hyperpolarizability: Second hyperpolarizabilities of polymeric systems with and without defects",
M. Nakano, I. Shigemoto, S. Yamada and K. Yamaguchi, *J. Chem. Phys.* **103**, 4175-4191 (1995).

[3] "Theoretical study on the geometry dependence of the second hyperpolarizability of allyl cation based on a numerical Liouville three-type analysis",
M. Nakano, S. Yamada, I. Shigemoto and K. Yamaguchi, *Chem. Phys. Lett.* **251**, 381-396 (1996).

[4] "Theoretical studies on nonlinear optical properties of organometallic conjugated systems I. Static third-order hyperpolarizabilities of first-transition-metal and metal-methylene cations",
I. Shigemoto, M. Nakano, S. Yamada, S. Kiribayashi and K. Yamaguchi, *Mol. Cryst. Liq. Cryst.* **286,** 159-164 (1996).

[5] "Static second hyperpolarizabilities γ of nitroxide radical and formaldehyde: evaluation of spatial contributions to γ by a hyperpolarizability density analysis",
S. Yamada, M. Nakano, I. Shigemoto and K. Yamaguchi, *Chem. Phys. Lett.* **254**, 158-164 (1996).

[6] "Theoretical study of the second hyperpolarizabilities of three charged states of pentalene. A consideration of the structure-property correlation for the sensitive second hyperpolarizability",
M. Nakano, S. Kiribayashi, S. Yamada, I. Shigemoto and K. Yamaguchi, *Chem. Phys. Lett.* **262**, 66-73 (1996).

[7] "Dynamic (hyper)polarizability density analysis based on virtual excitation processes: Visualization of dynamic electron fluctuatability of systems under time-dependent external electric fields",
M. Nakano, S. Yamada, I. Shigemoto and K. Yamaguchi, *Chem. Phys. Lett.* **250**, 247-254 (1996).

[8] "Intense electron correlation dependence of the first hyperpolarizabilities γ of a nitroxide radical and formaldehyde",
S. Yamada, M. Nakano, I. Shigemoto, S. Kiribayashi and K. Yamaguchi, *Chem. Phys. Lett.* **267,** 445-451 (1997).

[9] "Theoretical study of the third-order nonlinear optical susceptibilities for the β-phase crystal of p-NPNN",
S. Yamada, M. Nakano, I. Shigemoto, S. Kiribayashi and K. Yamaguchi, *Chem. Phys. Lett.* **267**, 438-444 (1997).

[10] "Structure-property correlation in the second hyperpolarizabilities γ for phenyl nitronyl nitroxide radicals",
S. Yamada, M. Nakano and K. Yamaguchi, *Chem. Phys. Lett.* **276**, 375-380 (1997).

[11] "Theoretical studies on hyperpolarizabilities of nitroxide species. III. Effects of intermolecular interactions of p-NPNN on the γ",
S. Yamada, M. Nakano, S. Kiribayashi, I. Shigemoto and K. Yamaguchi, *Synt. Metals* **85**, 1081-1082 (1997)

[12] "Theoretical studies for second hyperpolarizabilities of alternant and condensed ring conjugated systems II",
S. Kiribayashi, M. Nakano, S. Yamada, I. Shigemoto, H. Nagao and K. Yamaguchi, *Synt. Metals* **85**, 1163-1164 (1997).

[13] "Theoretical studies on nonlinear optical properties of organometallic conjugated systems III: second hyperpolarizabilities of Mn(I)-carbene systems",
I. Shigemoto, M. Nakano, S. Yamada, S. Kiribayashi, S. Yamanaka and K. Yamaguchi, *Synt. Metals* **86**, 2241-2242 (1997).

[14] "Theoretical studies on hyperpolarizabilities of nitroxide species II. Second hyperpolarizability of p-NPNN",
M. Nakano, S. Yamada, I. Shigemoto, S. Kiribayashi, and K. Yamaguchi, *Mol. Cryst. Liq. Cryst.* **294**, 251-254 (1997).

[15] "Negative Second Hyperpolarizability of the Nitronyl Nitroxide Radical",
M. Nakano, S. Yamada and K. Yamaguchi, *Bull. Chem. Soc. Jpn.* **71**, 845-850 (1998).

[16] "Third-order nonlinear optical properties of a stable radical species with nitronyl nitroxide group",
K. Kamada, K. Ohta, J. Nakamura, S. Yamada, M. Nakano and K. Yamaguchi, *Mol. Cryst. Liq. Cryst.* **315**, 117-122 (1998)..

[17] "Hyperpolarizabilities of one-dimensional H*n* systems: the second hyperpolarizability density analyses for regular and charged soliton-like linear chains",
M. Nakano, S. Yamada and K. Yamaguchi, *Int. J. Quantum Chem.* **70**, 269-282 (1998).

[18] "CAS-SCF and density functional calculations of second hyperpolarizabilities for a nitronyl nitroxide radical",
S. Yamada, M. Nakano and K. Yamaguchi, *Int. J. Quantum Chem.* **71**, 329-336 (1999)

[19] "Electron Correlation and Structure Dependences of the Second Hyperpolarizability of Ethylene",
S. Yamada, M. Nakano and K. Yamaguchi, *Int. J. Quantum Chem.* **71**, 177-183 (1999)

[20] " Second hyperpolarizabilities of 1-center radicals",
S. Yamada, M. Nakano, M. Nishino and K. Yamaguchi, *Synt. Metal*, *in press* (1999)

[21] "Theoretical Study on the Second Hyperpolarizabilities for Small Radical Systems",
S. Yamada, M. Nakano and K. Yamaguchi, *Mol. Cry. Liq. Cryst.*, *in press* (1999).

[22] "Theoretical Study on the Second Hyperpolarizabilities for Small Radical Systems",
S. Yamada, M. Nakano, M. Nishino and K. Yamaguchi, *Opt. Rev. in press* (1999)

Others

[23] "Theoretical studies of spin density populations on nitroxide and nitronyl nitroxide derivatives",
S. Yamanaka, T. Kawakami, S. Yamada, H. Nagao, M. Nakano and K. Yamaguchi, *Chem. Phys. Lett.* **240**, 268-277 (1995).

[24] "Theoretical and Experimental Studies of a Charge-Transfer Mechanism for Biomimetic Oxygenations of Phenol and Indol Derivatives",
Y. Yoshioka, S. Yamanaka, S. Yamada, T. Kawakami, M. Nishino, K. Yamaguchi and A. Nishinaga, *Bull. Chem. Soc. Jpn.* **69**, 2701-2722 (1996).

[25] "Theoretical calculation of effective exchange integrals for one- and two-dimensional poly(phenylenmethylene) systems: possibilities of organic ferro- and ferri-magnetic solids",
D. Yamaki, S. Yamada, G. Maruta, T. Kawakami, W. Mori and K. Yamaguchi, *Mol. Cryst. Liq. Cryst.* **279**, 9-18 (1996).

[26] " Many-Electron-Wavepackets Method",
H. Nagao, M. Nakano, S. Yamanaka, Y. Shigeta, S. Yamada, D. Yamaki, I. Shigemoto, S. Kiribayashi and K. Yamaguchi, *Int. J. Quantum Chem.* **60**, 79-89 (1996)..

[27] "Damping wave packets approach: a calculation method of intensity-dependent nonlinear optical susceptibilities including effects of nuclear motions at finite temperatures",
M. Nakano, Y. Matsuzaki, H. Nagao, S.. Yamada, I. Shigemoto and K. Yamaguchi, *Chem. Phys. Lett.* **258**, 307-315 (1996).

[28] Y. Yoshioka, S. Yamada, T. Kawakami, M. Nishino, K. Yamaguchi and I. Saito
Ab initio Molecular Orbital Studies of Singlet Oxygen Reactions of Olefins, Enol Ethers and Enamines, *Bull. Chem. Soc. Jpn.* **69**, 2683-2699 (1996).

[29] "Theoretical study on second hyperpolarizability of H_3^+ systems by path integral method",
H. Nagao, M. Nakano, S. Yamada, K. Ohta and K. Yamaguchi, *Synt. Metals* **85**, 1159-1160 (1997).